

ABSTRACT

RAWAT, PREETI. Morphology and Functionality of Polyvinyl Alcohol based Nanofibers. (Under the direction of Dr. Ericka Ford.)

Nanofibers are known for their exceptionally high surface area which is important in many applications such as tissue engineering, filtration, purification, sensors, and biotechnology devices. Nanofibers are produced by many techniques such as template synthesis, force-spinning, melt blowing, phase separation, and electrospinning. Electrospinning is a widely known technique for producing nanofibers because of its ability to control fiber size, morphology and pore dimensions. The functionalization of nanofibers is of interest for property enhancement, cost-effectiveness, and use as advanced materials. Nanofiber functionalization is achieved by modifying its surface or synthesizing novel polymers for electrospinning.

In this research, we have developed functional nanofibrous membranes from iodoacetylated polyvinyl alcohol for the covalent attachment of proteins. The conditions of thiol/thioether/amine reaction with iodoacetylated nanofibers were thoroughly studied. To achieve the overall research objective, copolymers of iodoacetylated polyvinyl alcohol (PVA) were synthesized for electrospinning. The percentage of iodoacetylation was found to influence the solubility of this copolymer in various solvents. Copolymers becomes less soluble in water and dimethyl sulfoxide as the percentage of iodoacetate groups increase. The self-assembly of like groups reduces their solubility.

The influence of acetate functional groups was also studied in polyvinyl alcohol/poly vinyl acetate (PVA/PVAc) blended fibers was also investigated in this research. The presence of acetate groups in the blend reduced the solution viscosity due to disruption of intramolecular hydrogen bonding. To compensate viscosity reduction the concentration of polymer solution is increased to achieve critical entanglement concentration which is necessary for beadless nanofiber formation.

It was found that solvents with high boiling such as DMSO (boiling point 183 °C) demands higher concentration than critical entanglement concentration due to slower evaporation. Longer tip to collector distance is also required with high boiling point solvents to allow enough time for fiber solidification. PVA/PVAc blended nanofibers were spun with two types of solvent -DMSO and Acetic acid/water (3:1) at 18 and 12 wt.% solution concentrations respectively. Finer fiber with reduced error was obtained with later case due to solution homogeneity.

Electrospun polyvinyl alcohol copolymers, having acetate, chloroacetate and iodoacetate groups, were compared to observe the influence of end group (-CH₃, Cl, I) on dope properties and nanofiber morphology. Percent acetylation affected solution viscosity as also found with PVA/PVAc blends. Solution conductivity increased with haloacetylation. However, this increase on the microsiemens/cm scale and did not significantly reduced the fiber diameter. Nanofibers of PVA copolymer were crosslinked with glutaraldehyde to prevent dissolution in water.

Iodoacetylation was performed to encourage protein attachment. Model compounds were used to understand mechanism of protein attachment onto crosslinked nanofibers: methionine, mercaptoethanol and glutathione. Infrared spectroscopy confirmed the pH-dependent attachment of model compounds through thiol, thioether, and amine that are common among proteins. Interestingly, unreacted glutaraldehyde end groups along the nanofibers reacted with thiol and amine groups. This study highlighted possible modes of macromolecular protein attachment to nanofibers.

Glucose oxidase (a catalyst for glucose to gluconic acid conversion), was chosen as a model protein for nanofiber attachment. Attachment of enzymatic protein to iodoacetylated nanofibers occurred under alkaline condition. The enzymatic activity glucose oxidase was observed for immobilized and free. Dye oxidation, as catalyzed by glucose oxidase in the presence of oxygen,

led to 29% dye decolorization. Dye decolorization doubled from 13 to 29% after enzyme immobilization along iodoacetylated nanofiber. Thus, iodoacetylation of PVA gives reactive nanofibers that can bind to enzymes without inhibiting their activity.

© Copyright 2018, Preeti Rawat

All Rights Reserved

Morphology and Functionality of Polyvinyl Alcohol based Nanofibers

by
Preeti Rawat

A dissertation submitted to the Graduate Faculty of
North Carolina State University
in partial fulfillment of the
requirements for the degree of
Doctor of Philosophy

Fiber and Polymer Science

Raleigh, North Carolina

2018

APPROVED BY:

Dr. Ericka Ford
Committee Chair

Dr. Ruben Carbonell

Dr. Terrence Gardner

Dr. Samuel Hudson

Dr. Wendy Krause

DEDICATION

I dedicate this work to my parents, my in-laws, my husband and my daughter for continuously supporting me and encouraging me to complete this work.

BIOGRAPHY

Preeti Rawat was born in Kanpur, UP, India. She grew up in UP, India and graduated from high school in 2002. She earned Bachelor of Technology (B. Tech) degree with focus on Man Made Fiber Technology from Uttar Pradesh Technical University in 2007. Then, she joined IIT, Delhi to pursue Master of Technology in Textile Engineering and graduated in 2009. After that she served in industry and the product development of home furnishings and automotive textiles. She also gained academic experience as an assistant professor, where she taught several textile related courses. She started her Ph.D. in Fall 2014 under the direction of Dr. Ericka Ford and investigated functional nanofibrous membranes.

ACKNOWLEDGMENTS

Firstly, I would like to express deep gratitude to my advisor Dr. Ericka Ford for providing me with the opportunity to work in her research group and for continuously supporting me throughout this study. I would also like to acknowledge my committee members- Dr. Ruben Carbonell, Dr. Terrence Gardner, Dr. Samuel Hudson and Dr. Wendy Krause for their valuable support throughout this research.

I really appreciate Dr. Nelson Vinueza and his Ph.D. student Yufei Chen for helping me with polymer characterization using Mass Spectrometry.

I would like to acknowledge The Nonwoven Institute (NWI) for supporting this research. I would like to thank Ms. Birgit Anderson, Lab Manager in Textile Engineering, Chemistry and Science (TECS) in the College of Textiles, for training in Fourier Transform Infrared (FTIR) and ultraviolet visible (UV-Vis) spectroscopy. I would also like to say thanks to Mr. Chuck Mooney, Lab Manager in Analytical Instrumentation Facility (AIF), for training me to use the Scanning Electron Microscope. I really appreciate Mr. Chris Pernell, in the Department of Food, Bioprocessing and Nutrition Sciences, for rheological measurements of my samples.

I would like to thank to my research team- Chunhong Lu, Charles Blackwell, Yaewon Park, and Rong Huang, for their suggestions and constructive comments on my research. I would also like to thank my friends Nadia Sultana, Nguyen Vu, and Hasan Shahariar for their continuous encouragement.

Finally, I would like to thank my family: including my parents for their continuous support and encouragement throughout my many years of academic endeavors; my husband and my daughter (Siddharth and Saanvi) for their love and patience, which made the completion of this dissertation possible.

TABLE OF CONTENTS

| | |
|--------------------------------------------------------------------|--------------|
| LIST OF TABLES | xv |
| LIST OF FIGURES | xvii |
| LIST OF ABBREVIATIONS | xx |
| LIST OF SYMBOLS | xxvi |
| CHAPTER 1 INTRODUCTION | 1 |
| 1.1 Functional Nanofibrous Membranes..... | 1 |
| 1.2 Types of Membranes..... | 2 |
| 1.2.1 Symmetric Microporous Membranes | 2 |
| 1.2.1.1 Irradiation | 2 |
| 1.2.1.2 Expanding Film | 3 |
| 1.2.1.3 Template Leaching..... | 3 |
| 1.2.2 Asymmetric Membranes | 4 |
| 1.2.2.1 Phase Inversion Method | 4 |
| 1.3 Electrospinning | 5 |
| 1.3.1 Fundamentals of Electrospinning | 5 |
| 1.3.2 Conventional Electrospinning vs Roller Electrospinning..... | 6 |
| 1.3.3 Parameters Affecting Fiber Morphology:..... | 7 |
| 1.3.3.1 Process Parameters | 7 |
| 1.3.3.1.1 Applied Voltage..... | 7 |
| 1.3.3.1.2 Tip to Collector Distance..... | 8 |
| 1.3.3.1.3 Feed Rate | 8 |
| 1.3.3.2 Solution Properties | 8 |
| 1.3.3.2.1 Solution Concentration | 9 |
| 1.3.3.2.2 Molecular Weight | 9 |
| 1.3.3.2.3 Viscosity | 9 |
| 1.3.3.2.4 Surface Tension | 9 |
| 1.3.3.2.5 Conductivity | 10 |
| 1.3.3.2.6 Ambient Conditions:..... | 10 |
| 1.4 Achievement of Surface Functionality in Electrospinning..... | 10 |
| 1.4.1 Core Shell Structure with Optimum Voltage..... | 11 |
| 1.4.2 Core Shell Structure with Appropriate Polarity:..... | 11 |
| 1.4.3 Core Shell Structure based on Dielectrophoretic Forces | 12 |
| 1.4.4 Core Shell Structure with Carbon Nanotubes | 13 |
| 1.5 Functional Nanofiber Membranes in Different Applications | 13 |
| 1.5.1 Chem-Bio Sensors by Nanofibrous Membranes..... | 13 |
| 1.5.2 Chem-Bio Deactivation by Nanofibrous Membranes..... | 14 |
| 1.5.3 Filtration through Nanofibrous Membranes | 16 |
| 1.5.3.1 Filtration Mechanisms | 17 |
| 1.5.3.1.1 Sieving/Straining | 17 |
| 1.5.3.1.2 Inertial Impaction | 17 |
| 1.5.3.1.3 Brownian Diffusion | 18 |
| 1.5.3.1.4 Interception..... | 18 |
| 1.5.3.1.5 Electrostatic Settling..... | 18 |
| 1.5.3.2 Size Exclusion through Nanofibrous Membranes..... | 19 |

| | | |
|-----------|------------------------------------------------------------------------|----|
| 1.5.1 | Particle Attachment through Functional Membranes for Purification..... | 21 |
| 1.5.1.1 | Chemical Separation..... | 22 |
| 1.5.1.1.1 | Chemical Separation by Ion Exchange Membranes..... | 22 |
| 1.5.1.1.2 | Chemical Separation by Molecular Inclusions Membranes..... | 23 |
| 1.5.1.1.3 | Chemical Separation by Adsorbing Membranes..... | 24 |
| 1.5.1.2 | Biological Separation by Adsorbing Membranes..... | 24 |
| 1.6 | Iodoacetate use with Biologicals..... | 25 |
| 1.6.1 | Iodoacetate for Characterization & Inactivation..... | 25 |
| 1.7 | Techniques used to Confirm Physical and Molecular Capture..... | 27 |
| 1.7.1 | Liquid Chromatography:..... | 27 |
| 1.7.2 | UV-Vis spectroscopy..... | 28 |
| 1.7.3 | Quartz Crystal Microgravimetry..... | 29 |
| 1.7.4 | Bicinchonic Acid Assay..... | 30 |
| 1.7.5 | X-Ray Photoelectron Spectroscopy..... | 31 |
| 1.7.6 | Fourier Transform Infrared Spectroscopy..... | 31 |
| 1.8 | Research Objectives:..... | 32 |

CHAPTER 2 EFFECT OF ACETATE MOIETIES ON THE MORPHOLOGY OF ELECTROSPUN POLYVINYL ALCOHOL BLENDS AND COPOLYMERS.....34

| | | |
|---------|-----------------------------------------------------------------|----|
| 2.1 | Introduction:..... | 34 |
| 2.2 | Materials and Methods:..... | 36 |
| 2.2.1 | Materials..... | 36 |
| 2.2.2 | Methods..... | 37 |
| 2.2.2.1 | Synthesis of PVA-co-PVClAc..... | 37 |
| 2.2.2.2 | Characterizing Degree of Acetylation..... | 37 |
| 2.2.3 | Synthesis of PVA-co-PVIAc..... | 38 |
| 2.2.4 | Electrospinning Solutions..... | 38 |
| 2.2.4.1 | Solution Characterization..... | 38 |
| 2.2.4.2 | Electrospinning..... | 39 |
| 2.2.4.3 | Scanning Electron Microscopy..... | 39 |
| 2.3 | Result and Discussion..... | 39 |
| 2.3.1 | PVA- <i>blend</i> -PVAc Fiber Morphology..... | 39 |
| 2.3.2 | Spectra of PVA- <i>blend</i> -PVAc Fibers..... | 41 |
| 2.3.1 | PVA- <i>blend</i> -PVAc Conductivity..... | 42 |
| 2.3.1 | Optimization of PVA/PVAc Blended Fiber Diameter Morphology..... | 43 |
| 2.3.2 | Spectral Characterization of PVA copolymers..... | 45 |
| 2.3.3 | PVA Copolymer Fiber Morphologies..... | 49 |
| 2.3.4 | PVA Copolymer Conductivity..... | 51 |
| 2.4 | Conclusion..... | 52 |

CHAPTER 3 MECHANISM OF PROTEIN ATTACHMENT ONTO PVA-PVIAc NANOFIBERS54

| | | |
|---------|----------------------------------------------------|----|
| 3.1 | Introduction..... | 54 |
| 3.2 | Materials and Methods..... | 55 |
| 3.2.1 | Materials..... | 55 |
| 3.2.2 | Methods..... | 56 |
| 3.2.2.1 | Synthesis of Functionalized Polyvinyl Alcohol..... | 56 |

| | | |
|------------------------------------------------------------------------------------------------------|----------------------------------------------------------------------------------------|-----------|
| 3.2.2.2 | Electrospinning of Functionalized PVA..... | 56 |
| 3.2.2.3 | Crosslinking of Nanofibers | 56 |
| 3.2.3 | Protein Attachment on Functionalized Nanofibers | 57 |
| 3.2.4 | Characterization of Protein Attachment on Functionalized Nanofibers | 58 |
| 3.3 | Result and Discussion | 59 |
| 3.3.1 | Morphology of Functional Nanofibers | 59 |
| 3.3.2 | Methionine Attachment on Membranes..... | 60 |
| 3.3.2.1 | UV-Vis Study of Membranes after Methionine Attachment | 60 |
| 3.3.2.2 | FTIR study of membranes after methionine attachment | 65 |
| 3.3.3 | Mercaptoethanol Attachment on Membranes | 70 |
| 3.3.3.1 | UV-Vis Study of Membranes after Mercaptoethanol Attachment..... | 70 |
| 3.3.3.2 | FTIR Study Of Membranes After Mercaptoethanol Attachment..... | 73 |
| 3.3.4 | Glutathione Attachment on Membranes | 75 |
| 3.3.4.1 | UV-Vis Study of Membranes after Glutathione Attachment..... | 75 |
| 3.3.4.2 | FTIR Study of Membranes after Glutathione Attachment..... | 79 |
| 3.4 | CONCLUSION..... | 81 |
| CHAPTER 4 IMMOBLIZATION AND ENZYMATIC ACTIVITY OF GOX ON FUNCTIONAL PVA BASED NANOFIBERS..... | | 83 |
| 4.1 | Introduction..... | 83 |
| 4.2 | Materials and Methods..... | 84 |
| 4.2.1 | Materials | 84 |
| 4.2.2 | Methods..... | 85 |
| 4.2.2.1 | Functionalization of PVA for Enzyme Attachment | 85 |
| 4.2.2.2 | Electrospinning of Functional Nanofibers | 85 |
| 4.2.2.3 | Morphology of Electrospun Nanofibers..... | 85 |
| 4.2.2.4 | Crosslinking of Electrospun Nanofibers | 85 |
| 4.2.2.5 | Attachment of Glucose oxidase (GOx) on Iodoacetate Functionalized Nanofibers | 86 |
| 4.2.2.6 | GOx Activity of Enzyme Immobilized Functional Membrane for Dye Decolorization | 87 |
| 4.3 | Result and Discussion | 88 |
| 4.3.1 | Morphology of Electrospun and Crosslinked Nanofibers | 88 |
| 4.3.2 | Enzyme Attachment on Functional Nanofibers..... | 88 |
| 4.3.3 | UV-Vis Study to Confirm Concentration Change After Reaction | 89 |
| 4.3.4 | FTIR study to Confirm Glucose Oxidase Attachment on Functional Nanofibers Surface..... | 92 |
| 4.3.4.1 | Dye Decolorization with GOx without Immobilization..... | 93 |
| 4.3.4.2 | Dye Decolorization with GOx Immobilized Nanofibers | 94 |
| 4.4 | Conclusion | 98 |
| CHAPTER 5 CONCLUSION AND RECOMMENDATIONS | | 99 |
| 5.1 | Conclusions..... | 99 |
| 5.1.1 | Influence of Degree of Iodoacetylation on Polymer Solubility | 99 |
| 5.1.2 | Influence of Crosslinking of PVA based Membranes with Glutaraldehyde..... | 99 |
| 5.1.3 | Identification of Covalent Attachment vs Absorption of Proteins: | 100 |
| 5.1.4 | Immobilization and Activity of GOx towards Dye Decolorization..... | 100 |

| | |
|------------------------------------------------------------------------------------------------------------------|------------|
| 5.2 Recommendation for Future Work | 101 |
| APPENDICES..... | 111 |
| Appendix A. XPS Study of Covalent Capturing of Methionine through Functional PVIAC Nanofibrous Membrane | 111 |
| Appendix B. Enzymatic Activity of Nanofibers towards Glucose Oxidation..... | 114 |
| REFERENCES..... | 107 |

LIST OF TABLES

| | | |
|-------------------|------------------------------------------------------------------------------------------------|----|
| Table 2.1. | Conductivity and fiber diameters from PVA-Blend-PVAc in DMSO. | 41 |
| Table 2.2. | Electrospun fiber diameters from PVA-Blend-PVAc in Acetic Acid: Water-3:1 | 45 |
| Table 2.3. | Spectral determination of polymer acetylation among commercial polymers and modified PVA | 48 |
| Table 2.4. | Solution conductivity and electrospun fiber diameter of PVA and its Copolymers. | 51 |
| Table 3.1. | Change in UV absorbance after Methionine attachment on membranes..... | 61 |
| Table 3.2. | Change in UV absorbance after Mercaptoethanol attachment on membranes | 71 |
| Table 3.3. | Change in UV absorbance after Glutathione attachment on membranes | 75 |
| Table 4.1. | Glucose Oxidase attachment on PVIAC membrane..... | 89 |
| Table 4.2. | Absorption vs covalent attachment of Glucose Oxidase on PVIAC Membranes..... | 90 |
| Table 4.3. | Dye decolorization of GOx without immobilization. | 93 |
| Table 4.4. | Samples used for dye decolorization. | 95 |
| Table 4.5. | Dye decolorization of GOX-PVIAC nanofibers..... | 95 |

LIST OF FIGURES

| | |
|-----------------------------------------------------------------------------------------------------------------------------------------------------------------------------------------------------------------------------------------------------------------------------------------------------|----|
| Figure 1.1. Schematic showing the two-step fabrication of microporous membranes by irradiation. (a) Polycarbonate film was exposed to charged particles within a nuclear reactor. (b) Holes formed by charged particles and corrosive liquid leave behind uniform pores ⁷ | 3 |
| Figure 1.2. Schematic of expanded polypropylene film and scanning electron micrograph of its structure ⁷ | 4 |
| Figure 1.3. Schematic of conventional electrospinning (horizontal Set up). | 6 |
| Figure 1.4. Schematic of roller electrospinning. | 7 |
| Figure 1.5. Schematic diagram illustrating the formation of core-shell PVA/BSA nanofibers during the electrospinning process (a) and (b) ²⁴ | 11 |
| Figure 1.6. Schematic diagram, highlighting the reorientation of polymer chains, shows the effect of electrospinning under (a) positive applied voltage and (b) negative applied voltage ²⁵ | 12 |
| Figure 1.7. Hydrolysis of PNA and paraoxon by electrospun biohybrids of PVA/BSA/SWNTs ²⁷ | 16 |
| Figure 1.8. Schematic of filtration through filter media ³⁶ | 16 |
| Figure 1.9. Filtration mechanisms as depicted by the single fiber filtration theory ³⁷ | 17 |
| Figure 1.10. Membranes process classification based on particle size ³⁸ | 18 |
| Figure 1.11. Alkylation of Methionine residue of SEB. | 26 |
| Figure 1.12. The predicted reaction scheme between iodoacetic acid and L-Cysteine based on the result of MS ⁶⁸ | 27 |
| Figure 1.13. Purplish color is observed when BCA and cuprous ions complex ⁷⁰ | 30 |
| Figure 2.1. PVA-co-PVClAc was synthesized from PVA and then converted into and PVA-co-PVIAc. | 37 |
| Figure 2.2. Fiber morphology of PVA-blend-PVAc blends (w/w) at (a)100/0 (b) 75/25 (c) 50/50 (d) 25/75 (e) 0/100, solution concentration of 18wt%, and DMSO as the solvent. | 40 |
| Figure 2.3. IR spectra confirm differences between the chemical compositions of PVA-co-PVAc blends as noted by change in –C=O peak intensity.. | 41 |
| Figure 2.4. Solution of PVA/PVAc in blends at 12 wt. % concentration in Acetic Acid/Water. | 44 |

| | |
|---------------------------------------------------------------------------------------------------------------------------------------------------------------------------------------------------------------------------------------------------------|----|
| Figure 2.5. Fiber morphology of PVA-blend-PVAc blends (w/w) at (a)100/0 (b) 75/25 (c) 50/50 (d) 25/75 (e) 0/100, solution concentration-12wt%, solvent: Acetic Acid: Water-3:1.. | 44 |
| Figure 2.6. IR spectra of commercial powers (PVA, PVA-co-PVAc, and PVAc) and copolymers of PVA-co-PVClAc are shown in (a). The calibration curve determining chloroacetylation were based upon commercial polymers, which were used as-received. | 47 |
| Figure 2.7. Electrospinning dope of PVA copolymers. | 49 |
| Figure 2.8. Fiber morphology of PVA and its copolymers. (a) Pure PVA, (b) PVA Co PVAc, (c1) PVClAc 11%, (c2) PVClAc 12%, (c3) PVClAc 16%, (C4) PVClAc 17% (d1) PVClAc 11%, (d2) PVIAc 12%, (d3) PVClAc 16% (d4) PVIAc 17..... | 50 |
| Figure 3.1. Functionalization of PVA for protein attachment. | 56 |
| Figure 3.2. Crosslinking of functionalized nanofibers and PVA with GA. | 57 |
| Figure 3.3. Protein attachment on Iodoacetate Functionalized nanofibers. | 58 |
| Figure 3.4. Morphology of functionalized nanofibers before crosslinking (a) PVA and (b) PVA-Co-PVIAc and after cross linking (c) PVA and (d) PVA-Co-PVIAc.Methionine Attachment on Membrane | 59 |
| Figure 3.5. Capture with PVIAc membrane under acidic (a ₁ &a ₂), neutral (b ₁ &b ₂), and alkaline (c ₁ &c ₂) condition. | 61 |
| Figure 3.6. Methionine attachment on PVIAc membranes under acidic condition. | 62 |
| Figure 3.7. Decomposition product of carboxymethyl sulphonium salt ⁶⁹ | 63 |
| Figure 3.8. Reaction of amine and aldehyde under alkaline pH ¹¹⁴ . | 64 |
| Figure 3.9. Methionine Attachment on PVA membrane under neutral and alkaline condition. | 64 |
| Figure 3.10. Methionine Attachment on PVIAc membrane under neutral and alkaline condition. | 65 |
| Figure 3.11. Study of change in PVIAc membrane chemistry after methionine attachment under (a) acidic pH, (b) neutral pH, and (c) alkaline pH | 67 |
| Figure 3.12. Mercaptoethanol capture with PVIAc membrane under acidic condition (a1&a2), neutral condition (b1&b2) and alkaline condition (c1&c2). | 70 |
| Figure 3.13. Mercaptoethanol attachment on PVA membranes. | 71 |
| Figure 3.14. Mercaptoethanol oxidation in the presence of Iodide ion ¹¹⁸ | 72 |

| | |
|------------------------------------------------------------------------------------------------------------------------------------------------------------------------|----|
| Figure 3.15. Mercaptoethanol attachment on PVIAC membranes. | 72 |
| Figure 3.16. Study of change in PVIAC membrane chemistry after mercaptoethanol attachment under (a) acidic, (b) neutral, (c) alkaline conditions. | 73 |
| Figure 3.17. Glutathione Capture with PVIAC membrane under acidic (a1&a2), neutral and (b1&b2, and alkaline (c1&c2) condition.. | 76 |
| Figure 3.18. Glutathione attachment on PVA membranes under neutral and alkaline pH..... | 77 |
| Figure 3.19. Glutathione oxidation under mild conditions | 77 |
| Figure 3.20. Glutathione attachment on PVIAC membranes under acidic pH..... | 78 |
| Figure 3.21. Glutathione attachment on PVIAC membranes under neutral and alkaline pH.. | 78 |
| Figure 3.22. Study of change in PVIAC membrane chemistry after Glutathione attachment under (a) acidic pH, (b) neutral pH, (c) alkaline pH. | 79 |
| Figure 4.1. Reaction Scheme for PVA functionalization with iodoacetate functionality..... | 85 |
| Figure 4.2. Crosslinking of functionalized nanofibers with glutaraldehyde solution..... | 85 |
| Figure 4.3. Protein Capture through functional nanofibers having iodoacetate functionality.. | 87 |
| Figure 4.4. Morphology of functionalized nanofibers before crosslinking (a) PVA and (b) PVA-Co-PVIAC and after crosslinking (c) PVA and (d) PVA-Co-PVIAC.. | 88 |
| Figure 4.5. Glucose Oxidase attachment on PVIAC nanofibers (a) acidic (b) neutral (c) alkaline conditions (d) calibration curve of Glucose oxidase. | 91 |
| Figure 4.6. Spectra of GOx attached PVA and functionalized PVIAC after subtraction under alkaline pH. | 92 |
| Figure 4.7. Dye Decolorization with GOx-PVIAC nanofibers and calibration curve..... | 95 |
| Figure 4.8. Dye decolorization of GOx-PVIAC nanofibers. | 98 |

LIST OF ABBREVIATIONS

| | |
|------------------------|--------------------------------------|
| AFM | Atomic Force Microscopy |
| Ag | Silver |
| ATRP | Atom Transfer Radical Polymerization |
| Au | Gold |
| BCA | Bicinchoninic Acid Assay |
| BSA | Bovine Serum Albumin |
| C=O | Carbon Oxygen double bond |
| C=O | Carbonyl Group |
| CA | Cellulose Acetate |
| Ca ⁺⁺ | Calcium Ion |
| CAGR | Compound Annual Growth Rate |
| CB | Cibacron Blue |
| C-C | Carbon - Carbon Single Bond |
| CD | Cyclodextrin |
| C-H | Carbon Hydrogen Bond |
| -CH ₃ | Methyl Group |
| CH ₃ COOH | Acetic Acid |
| -CHO | Aldehyde group |
| ClCH ₂ COOH | Chloroacetic Acid |
| CMC | Carboxy Methyl Cellulose |
| C-N | Carbon Nitrogen Bond |
| CNF | Cellulose Nanofibrils |

| | |
|------------------------|---------------------------------------------|
| C-O | Carbon Oxygen Single Bond |
| -COOCH ₂ I | Iodoacetate Group |
| -COOCH ₂ Cl | Chloroacetate Group |
| -COOCH ₃ | Acetate Group |
| -COOH | Carboxyl Group |
| CPS | Count per Second |
| C-PVCs | Carboxylated Poly Vinyl Chloride |
| Cu ⁺ | Cuprous Ion |
| Cu ⁺⁺ | Cupric Ion |
| DEA | Diethylamine |
| DH | Degree of Hydrolysis |
| DMSO | Dimethyl Sulfoxide |
| DNT | Di-Nitro Toluene |
| DP | Degree of Polymerization |
| ED | Effective Dose |
| FESEM | Field Emission Scanning Electron Microscopy |
| FITC | Fluorescein Isothiocyanate |
| FTIR | Fourier Transform Infrared |
| FUMA | Furfuryl Methacrylate |
| GA | Glutaraldehyde |
| Glu. | Glutathione |
| GOx | Glucose Oxidase |
| H ⁺ | Protons |

| | |
|---------------------------------|-------------------------------------------------------------------------------|
| H ₂ SO ₄ | Sulphuric Acid |
| HI | Hydroiodic Acid |
| HOMO | Highest Occupied Molecular Orbital |
| IAA | Iodoacetic Acid |
| IgG | Immunoglobulin |
| KI | Potassium Iodide |
| LC | Liquid Chromatography |
| LD | Lethal Dose |
| LUMO | Lowest Unoccupied Molecular Orbital |
| Mer. | Mercaptoethanol |
| Met. | Methionine |
| MF | Microfiltration |
| Mg ⁺⁺ | Magnesium Ion |
| MMA | Methyl Methacrylate |
| Na ⁺ | Sodium Ion |
| Na ₂ CO ₃ | Sodium Carbonate |
| NF | Nanofiltration |
| NFs | Nanofibers |
| NH | Secondary Amine Group |
| NH ₂ | Primary Amine Group |
| NIPAAm- <i>co</i> - NHMAAm | <i>N</i> Isopropylacrylamide- <i>co</i> - <i>N</i> hydroxyl-methyl-acrylamide |
| O ⁻ | Oxide Ion |
| O ¹⁸ | Oxygen Isotope with molecular weight of 18 Da |

| | |
|-----------------------------|-------------------------------------------------------------------------------|
| O ₂ ⁻ | Superoxide Ion |
| OD | Optical Density |
| OH | Hydroxyl Groups |
| PA | Poly Amine |
| PAA | Poly Acrylic Acid |
| PAN | Poly Acrylo Nitrile |
| PBI | Poly Benzyl Imidazole |
| PBT | Poly Butylene Terephthalate |
| Pd | Palladium |
| PDA | Poly Dopamine |
| PEGMEMA | Poly(Ethylene Glycol Monomethyl Ether Methacrylate) |
| PEI | Poly Ethylene Imine |
| PEK | Poly Ether Ketone |
| PES | Poly Ether Sulphone |
| PET | Poly Ethylene Terephthalate |
| PGMA | Polyglycidyl Methacrylate |
| PI | Poly Imide |
| pI | Isoelectric Point |
| PM | Pyrene Methanol |
| PMMA | Poly Methyl Metha Acrylate |
| PNA | Para-Nitrophenol Acetate |
| poly-AMA-Co-HEMA | Poly (2-Aminoethyl Methacrylate Hydrochloride-co-2-Hydroxyethyl Methacrylate) |

| | |
|-------------------------|--------------------------------------------------------------|
| PP | Poly Propylene |
| PPh | Poly Phenylene |
| PPz | Poly Phosphazene |
| PRNP | Prion Protein |
| PS | Poly Sulphone |
| PSt | Poly Styrene |
| PU | Polyurethane |
| PVA | Poly Vinyl Alcohol |
| PVA- <i>blend</i> -PVAc | Blend of Poly Vinyl Alcohol and Poly Vinyl Acetate |
| PVAc | Poly Vinyl Acetate |
| PVA- <i>co</i> -PVAc | Copolymer of Poly vinyl alcohol and poly vinyl acetate |
| PVA- <i>co</i> -PVCIAc | Copolymer of Poly vinyl alcohol and poly vinyl Chloroacetate |
| PVA- <i>co</i> -PVIAC | Copolymer of Poly vinyl alcohol and poly vinyl Iodoacetate |
| PVC | Poly Vinyl Chloride |
| PVCIAc | Chloroacetylated Poly Vinyl Alcohol |
| PVDF | Poly Vinylidene Fluoride |
| PVIAC | Iodoacetylated Poly Vinyl Alcohol |
| QCM | Quartz Crystal Microgravimetry |
| SEB | Staphylococcus Enterotoxin B |
| Ser | Serine |
| SH | Thiol Group |
| SWNTs | Single Wall Carbon Nanotubes |
| TMP | Trans Membrane Pressure |

| | |
|--------|--------------------------------|
| UF | Ultrafiltration |
| UV | Ultraviolet |
| UV-Vis | Ultraviolet-Visible |
| XPS | X-Ray Photoelectron Microscopy |
| ZnO | Zinc Oxide |

LIST OF SYMBOLS

| | |
|--------------------|----------------------------------------------------|
| \sim | \sim Means Approximately |
| \$ | Price in Dollars |
| % | % Means Percentage |
| = | = Means Equal |
| > | > Means Greater than |
| \pm | \pm Means Plus or Minus |
| $^{\circ}$ | $^{\circ}$ Mean Degree of Angle |
| $^{\circ}\text{C}$ | $^{\circ}\text{C}$ Means Degrees Celsius |
| μg | μg Means Microgram |
| μ_q | μ_q Means Shear Modulus of Quartz |
| A | A Means Area |
| A_b | A_b Means Absorbance |
| A_s | A_s Means Surface Area |
| C_i | C_i Means Initial Concentration |
| cm | cm Means Centimeters |
| cm^{-1} | cm^{-1} Means Per Centimeters; Wavenumber |
| C_t | C_t Means Concentration at time t |
| DP | DP Means Degree of Polymerization |
| Fc | Crystallizable Region |
| f_o | f_o Means Fundamental Frequency |
| g | g Means Grams |
| g/mol | g/mol Means Gram per Mol |

| | |
|--------------------------------|----------------------------------------------------------------------------|
| $\text{gcm}^{-1}\text{s}^{-2}$ | $\text{gcm}^{-1}\text{s}^{-2}$ Means Gram per centimeter per square second |
| gcm^{-3} | gcm^{-3} Means Gram per Cubic Centimeter |
| h | h Means Time in Hour |
| hv | hv Means Energy |
| I | I Means Intensity of Incident Light |
| I_0 | I_0 Means Intensity of Transmitted Light |
| kDa | kDa Means Kilo Dalton, Molecular Weight Units |
| kV | kV Means Kilovolts |
| m | m Means percentage of hydroxyl groups in PVA Copolymer |
| M | M means Molar Concentration |
| mA | mA Means Milliampere |
| M_d | M_d Means Dry Mass |
| mg | mg Means Milligrams |
| mg/25ml | mg/25 ml Means Milligrams in 25 milliliters |
| mg/L | mg/L Means Milligrams per Liter |
| mg/m^2 | mg/m^2 means Milligram per Square meter |
| min | min Means Minutes |
| mL | mL Means Milliliters |
| mm | mm Means Millimeters |
| ms | ms Means Milliseconds |
| mS/cm | mS/cm Means millisiemens per Centimeter |
| N | N means Normal Concentration |
| n | n means percentage of Acetate derivative in PVA Copolymer |

| | |
|------------------|--------------------------------------------------------------------------------|
| ng/ml | nm/ml Means Nanogram per Milliliter |
| ng/person | ng/person Means Nanogram per Person |
| nM | nM means Nanomolar |
| nm | nm Means Nanometers |
| nm/min | nm/min Means Nanometers Per Minute |
| q | q Means Absorptive Capacity |
| R | R means Hydrogen, Chlorine or Iodine Atom in Acetate Group |
| s | s Means Second |
| S/cm | S/cm Means Siemens per Centimeter |
| V | V Means Volume |
| v/v | v/v Means Volume by Volume |
| w/v | w/v Means Weight by Volume |
| wt. % | wt%. Means Weight percentage |
| x | x Means Overtone Number |
| ΔA | ΔA Means Change in Absorbance |
| Δf | Δf Means Change in Frequency |
| ΔM_s | ΔM_s Means Change in Mass |
| η^* | η^* Means Complex Viscosity |
| λ | λ Means Wavelength |
| λ_{\max} | λ_{\max} Means Wavelength at which Maximum Absorption occurs in UV-Vis |
| μm | μm Means Micrometers |
| ρ_q | ρ_q Means Density of Quartz |

CHAPTER 1

INTRODUCTION

1.1 Functional Nanofibrous Membranes

The use of nanofibers is growing in various applications such as tissue engineering, filtration, protective textiles, and environmental engineering. The market for nanofibers is very promising. Over the next five years, it is expected to grow. Currently, the overall market for nanofibers is above \$390 million. Further, it is expected to grow at a compound annual growth rate (CAGR) of 38.6%¹. The share of polymeric nanofibers leads the overall nanofiber market due to their low raw materials cost and accessibility of synthetic and natural polymers. The polymers as raw materials market segment for nanofiber applications is expected to grow at an annual CAGR of 25.3 % from 2016 to 2024¹. Techniques for nanofiber production include magnetic spinning, force spinning, rotary jet spinning, phase separation², melt-blowing, solution blowing and electrospinning^{2,3}. Electrospinning is the most common technique used producing nanofibers at large scale⁴. Major manufacturers of nanofibrous webs are Revolution Fibers, FibeRio, Donaldson, Finetex EnE, Elmarco, and Nanopareil. In 2014, the market segment for nanofiltration was \$215.6 million and will be 445.1 million by 2019 (i.e. CAGR of 15.6)^{5,6}.

Functionality among nanofibers is the ability to perform specific functions. Functionality is imparted by the intrinsic characteristics of base polymer, addition of active compounds during fiber formation, or by treatment with surface active agents. There exist other types of membranes to be used in these applications. However, nanofibrous membranes have the advantage of high surface area and functionality towards a surface specific application; such as sensing and tissue engineering.

1.2 Types of Membranes

Membranes are generally classified as being porous or nonporous. Porous membranes filter fluids by sieving. Most ultrafiltration (UF) and microfiltration (MF) fall under this classification as membranes that function by sieving. Nonporous membranes- also called dense membranes- filter according to molecular diffusion, which is influenced by pressure, concentration gradient(s), and electrical potential. These dense, nonporous membranes are employed in applications for gas separation, pervaporation and reverse osmosis. In terms of their structure, membranes are classified as being symmetric or asymmetric⁷.

1.2.1 Symmetric Microporous Membranes

Symmetric membranes are porous or nonporous and have one structure throughout its thickness. The porosity of symmetric membranes is induced by three different methods: a) irradiation, b) expanding film, and c) template leaching.

1.2.1.1 Irradiation

Polymer films are etched by the irradiation of ions and free radicals. Film pore density is impacted by the film's exposure to radiation. After irradiation, films are etched in corrosive solutions, as shown in Figure 1.1. Emersion time within those solutions affect pore diameter. Uniform pores are created throughout the film's thickness, and yet these membranes have low porosity when compared to other techniques⁷.

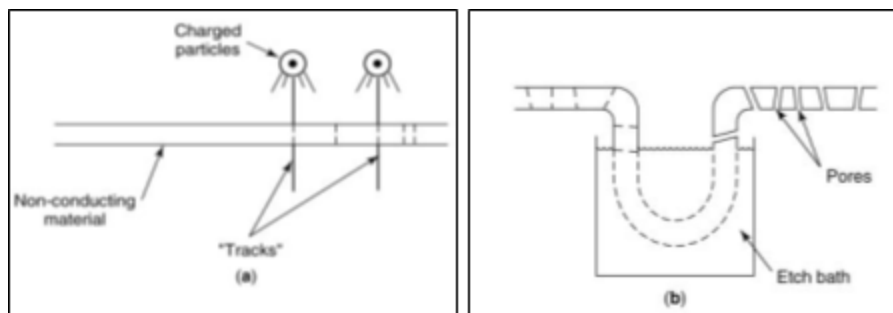


Figure 1.1 Schematic showing the two-step fabrication of microporous membranes by irradiation. (a) Polycarbonate film was exposed to charged particles within a nuclear reactor. (b) Holes formed by charged particles and corrosive liquid leave behind uniform pores⁷.

1.2.1.2 Expanding Film

A melt extruded film is uniaxially drawn in the machine direction to orient polymer chains. Afterwards, the same film is stretched in the transverse direction by 300%. As a result, slit-like micron-sized pores form in the film, as shown in Figure 1.2. This technique is only applicable to semi-crystalline polymers. Membranes formed by film expansion have poor tear strength in the machine direction. Although these porous films are not recommended for use as MF membranes, they are suitable for use as battery separators and in some medical devices⁷.

1.2.1.3 Template Leaching

This technique is applicable to membranes made from chemically inert polymers that are difficult to dissolve. The process of template leaching begins with introducing a soluble reagent within an insoluble film. As the soluble reagent is washed from the insoluble matrix, micropores form within the membrane.

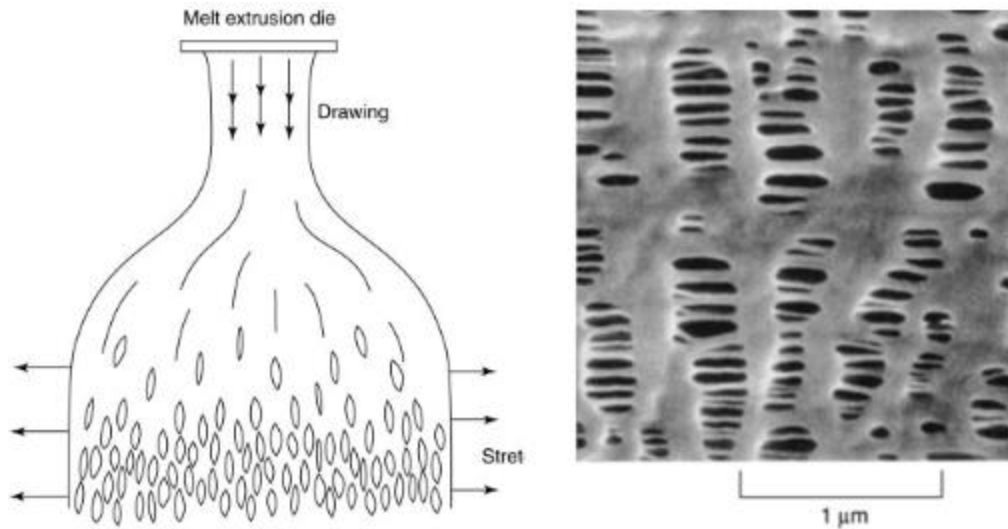


Figure 1.2. Schematic of expanded polypropylene film and scanning electron micrograph of its structure⁷.

1.2.2 Asymmetric Membranes

Asymmetric membranes are composite structures, wherein a thin layer overlays a thicker support membrane. Asymmetric membranes are common for commercial filtration. Layering helps to improve membrane mobility, reduce costs associated with filtration, impart mechanical integrity, and withstand the high pressures needed for filtration⁸. Each of the two layers is prepared in a single step or from different process. Asymmetric membranes are formed by the phase inversion method or the layering of solution-blowing nonwovens⁹, melt extruded fibers^{10,11}, melt-blowing nonwovens¹², and electrospinning nanofibrous webs^{8,13} onto a support. Herein, we will discuss two of the most common techniques to manufacture asymmetric membranes: phase inversion and electrospinning.

1.2.2.1 Phase Inversion Method

This is the most common technique for the commercial preparation of microporous membranes for use in UF and MF^{8,14–16}. Large membranes are rapidly produced. Initially, a film is cast from a polymer solution. Next, solvent extraction from the film is induced by

cooling, evaporation, or immersing the film into a non-solvent⁷. Each technique for solvent removal imparts unique membrane characteristics. Membranes prepared by phase inversion have closed pores throughout their structures; these can adversely affect flux and lead to fouling. Particulates can accumulate along the membrane surface during filtration, as the result of closed pores. Pore blockage leads to higher trans-membrane pressures (TMP), which describes the pressure difference between the feed and permeate sides), and flux will decrease with time. The application of external pressure is typically needed to maintain constant flux during filtration. High TMP will necessitate more energy for filtration. High flux during filtration is ideal to reduce filtration time and lower energy consumption^{17,18}.

The use of fibrous membranes could overcome some of the challenges associated with filtration by membranes prepared by phase inversion. Fibrous membranes have interconnecting pores, and surface area is a characteristic of membrane porosity. By forming nanofibers, high surface area membranes can be achieved.

1.3 Electrospinning

Electrospinning can yield fiber on the order of a few nanometers in diameter. By electrospinning, surface area, pore size distribution, interconnectivity between pores are influenced by fiber diameter^{8,16}. However, the electrospinning process is limited commercially by low production rates.

1.3.1 Fundamentals of Electrospinning

Electrospinning is a well-known technique for nanofiber production. Fibrous membranes are formed by the application of high voltage potential on a polymeric fluid¹⁹. The schematic of

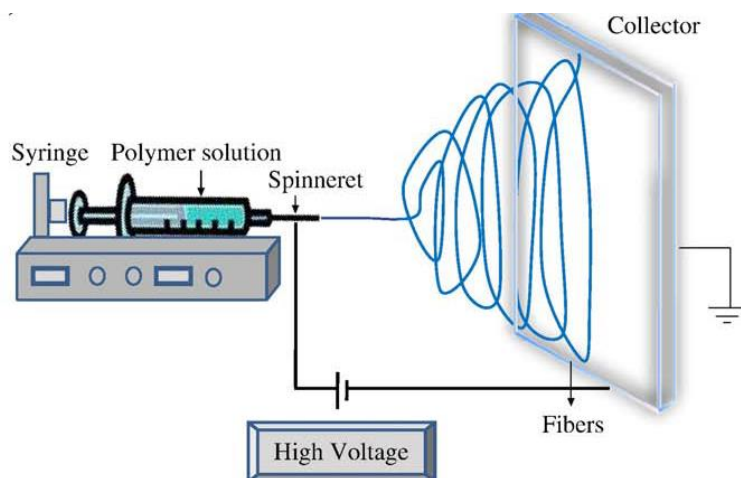


Figure 1.3. Schematic of conventional electrospinning (horizontal Set up).

the conventional electrospinning set up is shown in Figure 1.3. During electrospinning, polymer at the needle's tip is subjected to high voltage (Figure 1.3). In turn, the polymer droplet at the needle's tip transforms into an elongated Taylor cone. When the charge density exceeds a critical value, the surface tension of the polymer solution is overcome, and fine fibers are ejected from the needle tip and onto a conductive collector. Solvent evaporates from the polymer solution as the fiber transverses onto the collector. Chain entanglements within the polymer solution are necessary for fiber formation. In general, fiber diameters are produced in the range of $0.05\text{--}5\text{ }\mu\text{m}$ ^{20,21}.

The conventional method of electrospinning nanofibers from needle(s) have serious limitations; such as lower nanofiber production rates, the need to frequently change needles clogged with polymer, absence uniaxial orientation among nanofibers, and two-dimensionality²². Several technologies have led to greater productivity by electrospinning. Roller electrospinning is among those techniques¹⁹.

1.3.2 Conventional Electrospinning vs Roller Electrospinning

In 2005, Jirsak et al. invented roller electrospinning, as shown in Figure 1.4. This set-up was first commercialized by Elmarco Co. under the trade name of NanospiderTM ¹⁹. It is a

vertical and needleless approach to electrospinning- where fiber formation occurs against gravity. A rotating roller is used to form multiple jets for nanofiber spinning opposed to the use of a static needle. The rotating roller is partially immersed in polymer solution to yield droplets on the roller's surface. Under high voltage, multiple, fiber-forming jets transverse the air gap onto the grounded collector that is placed above the charged roller. The morphology of electrospun nanofibers depends on several parameters that fit into three categories: process parameters, solution properties, and c) ambient conditions

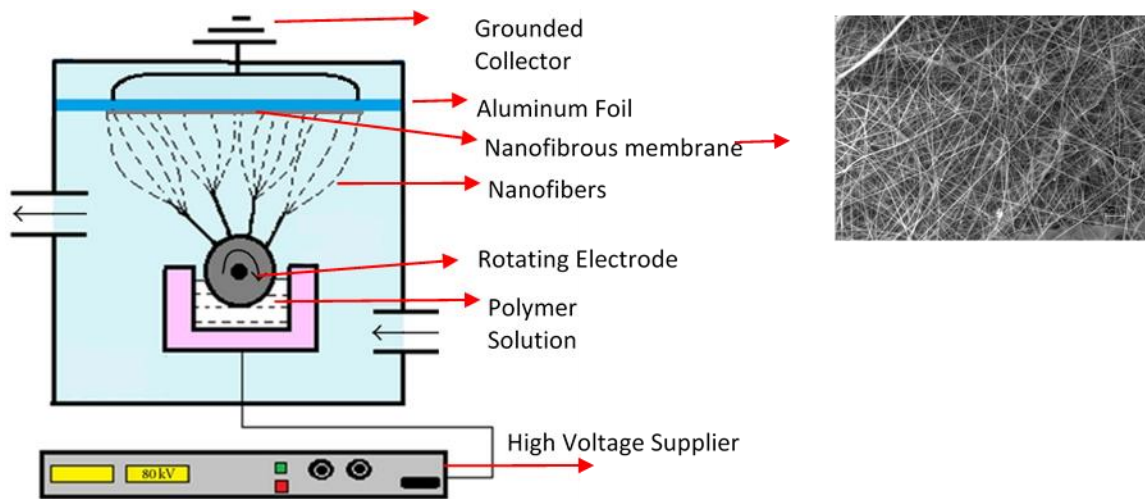


Figure 1.4. Schematic of roller electrospinning.

1.3.3 Parameters Affecting Fiber Morphology:

1.3.3.1 Process Parameters

Electrospinning process parameters are further divided into the following categories: applied voltage, tip to collector distance, and feed rate.

1.3.3.1.1 Applied Voltage

The process parameter identified as applied voltage is of great importance. Fiber formation only occurs when the applied voltage overcomes the surface tension of the polymer solution. This minimum voltage for electrospinning is called the threshold voltage. Applied

voltage depends upon the inherent properties of the polymer solution and tip to collector distance^{4,19}. Studies have differed in their views of how applied voltage affects fiber diameter. In 2010, Bhardwaj et al. states higher values of applied voltage may not decrease fiber diameter, because higher applied voltages can increase the amount of polymer ejected from the tip⁴. As the applied voltage increases, electrostatic repulsion can abound, which inevitably results in finer fibers⁴. The later explanation seems more plausible since the amount of polymer discharged from the syringe needle may also depend upon solution viscosity and surface tension.

1.3.3.1.2 Tip to Collector Distance

The tip to collector distance should suffice for solvent evaporation. Circular nanofibers form at optimum tip to collector distance. When tip to collector distance is too short, flat fibers are observed and solvent evaporation from the collected nanofibers is incomplete. However, longer distances may require higher voltage potentials for fiber formation^{4,19}.

1.3.3.1.3 Feed Rate

This parameter affects fiber diameter. A lower feed rates provide enough time for solvent evaporation, as fiber transverse onto the collector. Higher feed rates increases the fiber diameter due to less stretching time^{4,19}. In addition to that, it also causes fiber flattening due to insufficient evaporation time⁴.

1.3.3.2 Solution Properties

The solution properties are further defined by solution concentration, molecular weight, viscosity, surface tension, and conductivity.

1.3.3.2.1 Solution Concentration

The concentration of polymer in solution affects electrospinning. Concentrations below the critical value for chain entanglements causes bead formation. At higher polymer concentrations for chain entanglements, coarser fibers are observed, and continuous nanofibers are spun. Solution viscosity increases with higher amounts of polymer in solution concentration

1.3.3.2.2 Molecular Weight

Polymer molecular weight affects the viscosity, surface tension, conductivity and dielectric strength of polymer solutions^{19,23}. Higher molecular weights can provide critical amounts of chain entanglements for spinning fiber at lower concentrations of polymer in solution⁴. As molecular weight increases, chain entanglements cause solution viscosity to increase.

1.3.3.2.3 Viscosity

Low values of solution viscosity lead (below the critical concentration for chain entanglements) to the formation of discontinuous beads. As solution viscosity increases, fibers are discharged from the Taylor cone and onto the collector. When solution viscosity is too high, stress relaxation of the polymer droplet occurs at the Taylor cone. Polymer relaxation inhibits jet formation and discharge. Solution viscosity depends upon the molecular weight and concentration of the polymer in solution^{4,23}. Optimal values of polymer viscosity range between 1-20 poise⁴.

1.3.3.2.4 Surface Tension

Surface tension also influences fiber shape, whether they will be round or flat. Generally, lower surface tension will not require high values of applied voltage for fiber

production than at higher surface tension values. When surface tension is high, smooth beadless fibers may not form. The surface tension of polymer solutions is reduced when surfactants are added to the polymer solution.

1.3.3.2.5 Conductivity

Solution conductivity depends on the solvent, polymer type and the availability of ionizable groups. As solution conductivity increases, fiber size decreased, and fiber size distributions of those diameters broadened. At optimum values of solution conductivity, uniform fibers were obtained. Beads may form if conductivity values are too low. The addition of salt in a polymer solution can be used to control the uniformity of fiber diameters by electrospinning.

1.3.3.2.6 Ambient Conditions:

Apart from process parameters and solutions properties, ambient conditions such as temperature and humidity can affect fiber morphology. Control over humidity and ambient temperature are needed to optimize the morphology of nanofibers spun from polymer solutions⁴. Relative humidity affects solvent evaporation. When humidity is high, solvent is retained by the electrospun fibers. As a result, the fibers may appear flattened or beaded. High relative humidity leads to the clogging of needles.

1.4 Achievement of Surface Functionality in Electrospinning

The functionalization of nanofibers is important for applications in bio sensing and the fabrication of affinity membranes. Functional groups at the fiber surface must facilitate interactions between nanofibers and target molecules. Several approaches are used to functionalize the nanofiber surface; such as those described below.

1.4.1 Core Shell Structure with Optimum Voltage

In 2012, Won et al. studied the role of applied voltage on the migration of bovine serum albumin (BSA) proteins towards the surface of electrospun poly(vinyl alcohol)/bovine serum albumin (PVA/BSA) fibers²⁴. Different blend ratios of PVA/BSA were electrospun at 15, 22 and 29 kV. At optimum voltage, the majority of BSA migrated towards the fiber surface. As shown in Figure 1.5, phase separation occurred between PVA and BSA under the applied electric field. At 22 kV, BSA molecules ionized towards the fiber surface, Core shell structure, due to the preferential migration of charged additives, only occurs at optimum voltage.

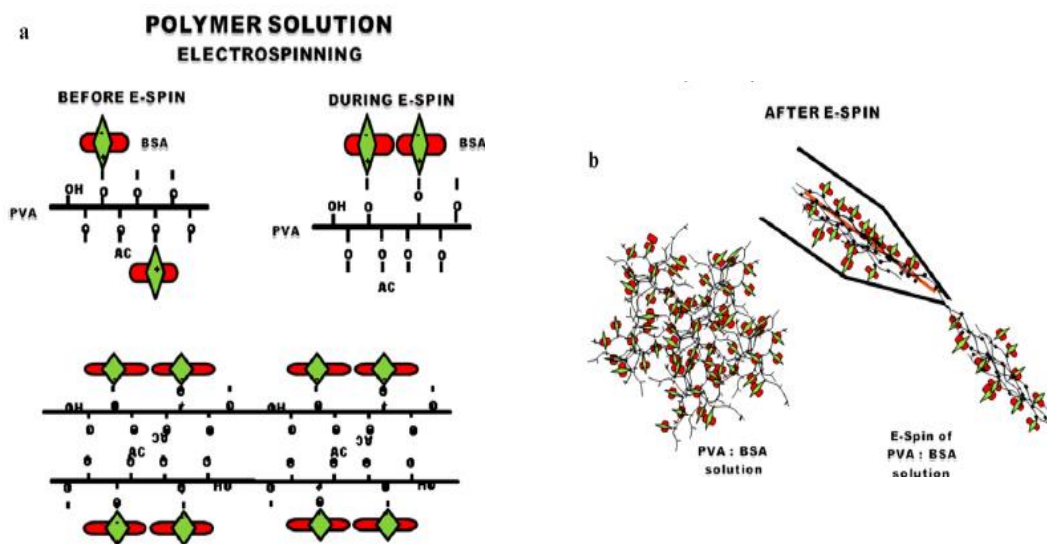


Figure 1.5. Schematic diagram illustrating the formation of core-shell PVA/BSA nanofibers during the electrospinning process (a) and (b)²⁴.

1.4.2 Core Shell Structure with Appropriate Polarity:

Core shell structure among functionalized nanofibers is induced by changing the polarity of applied voltage. In 2012, Stachwicz et al. electrospun nylon 6 nanofibers in binary solvents- of acetic acid and formic acid- under positive and negative voltage polarities²⁵. Polymers having electronegative groups oriented themselves towards the surface of nanofibers

spun under positive polarity. Electronegative groups directed towards the nanofiber core when negative polarity was applied during electrospinning. Functional group orientation depended on voltage bias, as shown in Figure 1.6. X-ray photoelectron spectroscopy (XPS) and water contact angle measurements were used to confirm changes in the surface chemistry of nanofibers subsequent spinning under different voltage biases. Under negative polarity, the nanofiber surface was nitrogen rich. Under positive polarity, the nanofiber surface was oxygen rich.

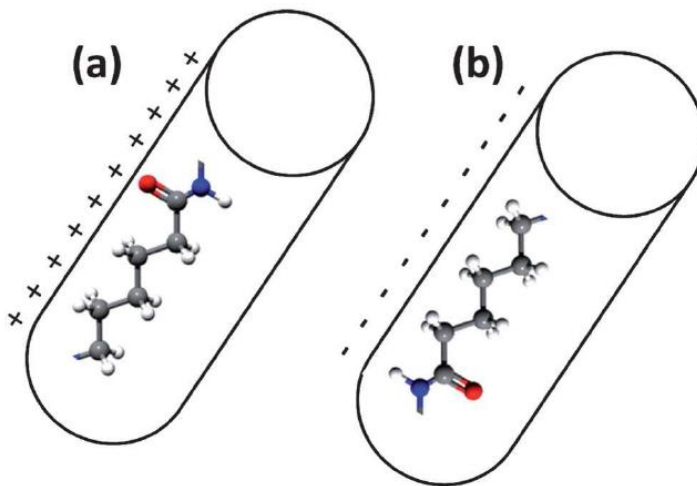


Figure 1.6. Schematic diagram, highlighting the reorientation of polymer chains, shows the effect of electrospinning under (a) positive applied voltage and (b) negative applied voltage²⁵.

1.4.3 Core Shell Structure based on Dielectrophoretic Forces

In 2012, Tang et al. studied phase separation among core-shell nanofibers²⁶. Dielectrophoresis- which governs the motion of charged particles under electric field- was attributed to core shell structure among PVA/BSA nanofibers. Nanofibers were electrospun at different values of pH. At the isoelectric point (pI) of BSA (pI=5.0), BSA migrated towards the nanofiber surface when $\text{pH}=\text{pI}\pm 2$. At those values of pH, BSA was negatively charged and

core-shell structure was achieved by electrospinning. The authors concluded phase separation occurs when electric polarizability of protein additives and polymer chains differ.

1.4.4 Core Shell Structure with Carbon Nanotubes

In 2014, Ford et al. demonstrated carbon nanotubes can induce core-shell structures among electrospun nanofibers²⁷. Biohybrids of PVA/BSA/SWNTs had shown the preferential migration of BSA towards the nanofiber surface. Atomic Force Microscopy (AFM) adhesion studies confirmed the locale of BSA to be at the nanofiber surface. Further, protein assays revealed the enzymatic decomposition of paraoxon by esterase nanofibers was enhanced by the core-shell morphology of hybrid nanofibers.

1.5 Functional Nanofiber Membranes in Different Applications

Functional nanofiber membranes have wide applications. Herein we will discuss applications physical and molecular attachment.

1.5.1 Chem-Bio Sensors by Nanofibrous Membranes

Functional membranes have potential use as sensors. Membrane surface area will influence its ability to interact with target molecules and the resolution of its sensing capabilities²⁸. In 2002, Wang et al. developed optical sensors based on the quenching of fluorescent signals. They electrospun membrane of polyacrylic acid (PAA) were modified with electron rich pyrene methanol (PM) and electron poor di-nitrotoluene (DNT) (i.e. fluorescence indicators) at their surface^{29,30}.

In 2008, Wang et al. electrospun zinc oxide (ZnO) membranes to sense toxic, combustible gases. First, ZnO was dispersed into PVA prior to electrospinning. Next, electrospun fibers underwent calcination to remove PVA while leaving ZnO³¹. When ZnO nanofibers were exposed to air, oxygen molecules adsorbed onto the nanofiber. This led to

generation of oxygen species (O_2^- , $O^{\cdot -}$) along the surface of ZnO, which affected the ZnO conductance band. ZnO conductance decreased in the presence of oxygen species, but organic gases reduced oxygen species along ZnO, thereby improving its conductance for sensing.

In 2008, Senecal et al. developed biological sensors for the staphylococcus enterotoxin B (SEB) toxin by attaching SEB capture antibodies onto electrospun nanofibers³². They used nanofibrous membranes of polyamine (PA), polyurethane (PU), and carboxylated polyvinylchlorides (C-PVCs). The researchers used C-PVC to mimic carboxyl terminus (C) of proteins. Primary rabbit anti-SEB and primary goat anti-SEB antibodies were crosslinked onto membrane surfaces. Then, secondary antibodies conjugated to horse radish peroxidase sandwiched SEB antigens that were captured by primary antibodies. Secondary antibody sources needed to complement primary antibodies (from rabbit and goat) to render strong chemiluminescent signals. In this way, SEB detection was achieved in the range of 1-100 ng/ml.

1.5.2 Chem-Bio Deactivation by Nanofibrous Membranes

Functional nanofibers can deactivate infectious pathogens and harmful toxins through molecular interaction or by disabling pathogens. In 2007, Jeong et al. developed cationic polyurethane-based nanofibers³³. The capture efficiency of nanofibers against *Staphylococcus aureus* and *Escherichia coli* was tested. Target bacteria propelled towards the nanofibrous mats by electro-kinetic attraction and were destroyed upon exposure to quaternary ammonium compounds. The negatively charged microorganisms were attracted to positively charged nanofibers.

In 2007, Lala et al. electrospun membranes of cellulose acetate (CA), PVC and polyacrylonitrile (PAN) that were coated with silver (Ag) nanoparticles to test against

microorganisms³⁴. Silver nanoparticles were generated along the surface of nanofibers containing silver nitrate. Upon exposure to UV radiation, silver nitrate reduced to silver nanoparticles. Antimicrobial performance was measured as the ratio of bacterial colonies before and after exposure to silver-coated nanofibers.

In 2013, Huang et al. electrospun polysulphone (PS) membranes having L-Serine (Ser) functionality on its surface, which could be used to capture endotoxins³⁵. Endotoxins in human plasma were exposed to membranes having different amounts of surface area. Endotoxin levels in human plasma decreased among nanofibers having more surface area.

In 2014, Ford et al. reported the molecular decomposition and deactivation of paraoxon organophosphate and *p*-nitrophenol acetate (PNA). BSA within PVA nanofibers caused the enzymatic hydrolysis of paraoxon and PNA,²⁷ as shown in Figure 1.7. Electrospun bio-hybrids of poly (vinyl alcohol)/bovine serum albumin/single-walled carbon nanotubes (PVA/BSA/SWNTs) enhanced the enzymatic hydrolysis of substrate molecules relative to PVA/BSA nanofibers. During electrospinning, BSA preferentially migrated towards the surface of SWNT containing nanofibers. Dielectrophoresis was the cause of molecular separation, which lead to core-shell nanofibers.

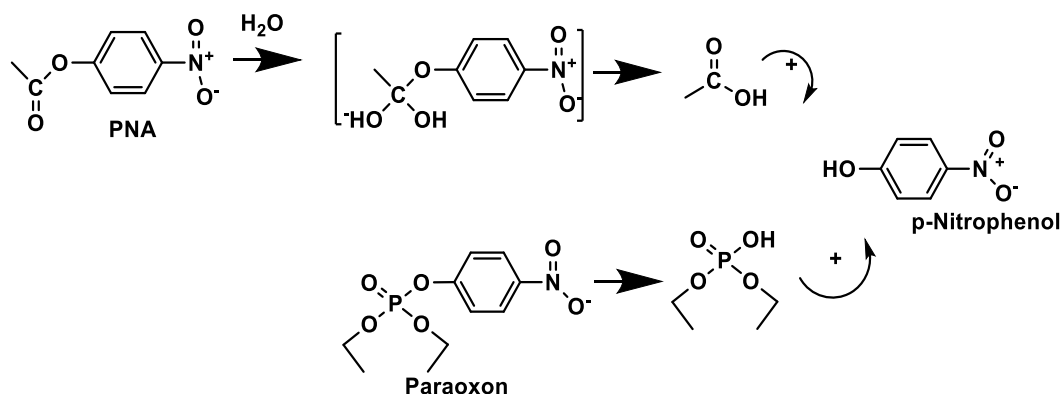


Figure 1.7. Hydrolysis of PNA and paraoxon by electrospun biohybrids of PVA/BSA/SWNTs²⁷.

1.5.3 Filtration through Nanofibrous Membranes

Environmental pollution is of great concern. Filtration is used to remediate pollution by separating of solids from fluids. As shown in Figure 1.8, fluid have a unidirectional pass through the pores of filter media. The average pore size and pore size distribution of filter media varies. These properties affect the appropriateness of filter media used in different application.

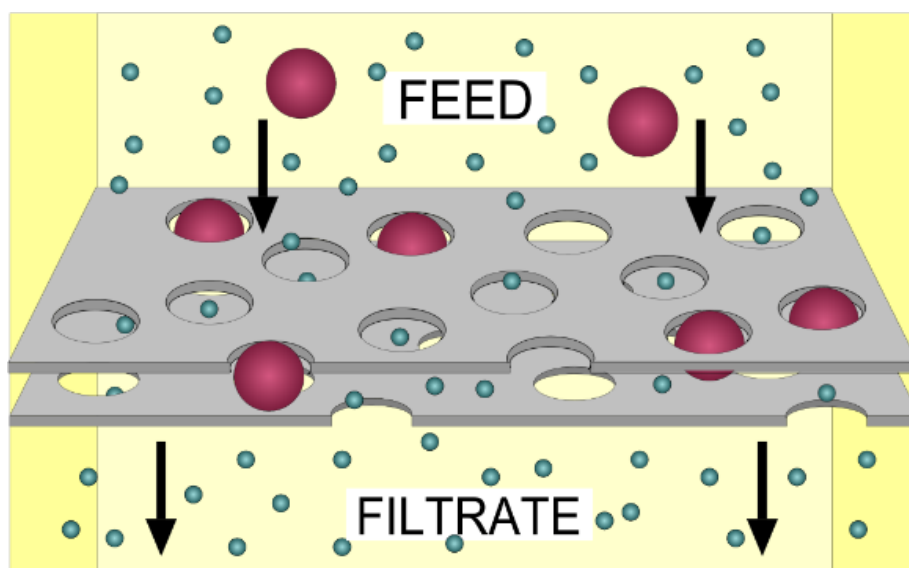


Figure 1.8. Schematic of filtration through filter media³⁶.

1.5.3.1 Filtration Mechanisms

As particles interact with filter media through static attachment to its surface. Mechanisms of filtration is explainable with the help of single fiber theory (shown in Figure 1.9.)

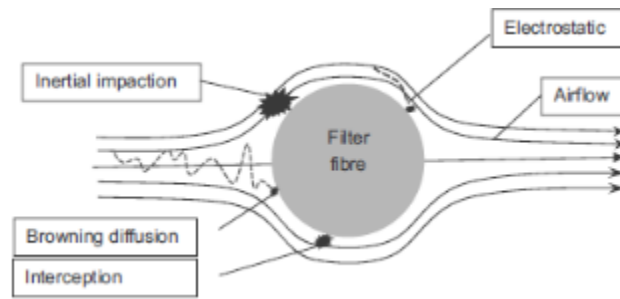


Figure 1.9. Filtration mechanisms as depicted by the single fiber filtration theory³⁷.

1.5.3.1.1 Sieving/Straining

Filtration by sieving and straining are mechanistically similar. Sieving is performed by filter media that possess constant pore size, but straining occurs among filter media having a distribution of pore sizes. In sieving, particle size must be smaller than pore size. To capture particles by straining, the largest pores of filter media should be smaller than all particles. Particle flow is hindered by small pore sizes.

1.5.3.1.2 Inertial Impaction

Particles in laminar flow fluids are size excluded by filter media. Large particles, having more inertia than small particles, separate from the flow stream after colliding with fibers in the filter.

1.5.3.1.3 Brownian Diffusion

Particles in the fluid stream collide with fibers in the filter media as the result of Brownian motion. Brownian motion is used to separate particles that are smaller than $0.1\mu\text{m}$ in size.

1.5.3.1.4 Interception

Small particles (less than one micron) are separated from the contaminated fluid stream. As particles in the flow stream engage the fiber surface, they lose kinetic energy upon collision and at rest along the filter's surface.

1.5.3.1.5 Electrostatic Settling

Charge carrying particles that are oppositely charged in respect to filter media are electrostatically attracted to the filter's surface.

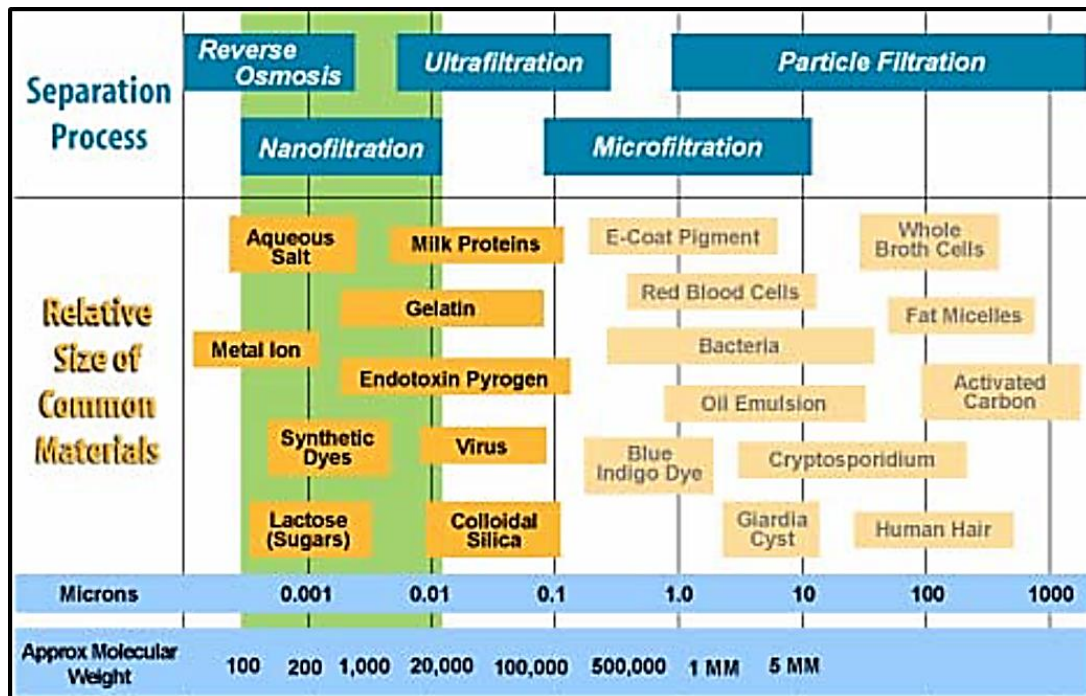


Figure 1.10. Membranes process classification based on particle size ³⁸.

Separation based upon particle size is classified into four categories of filtration- microfiltration, ultrafiltration, nanofiltration, and reverse osmosis. Particle size ranges are shown for each category in Figure 1.10.

1.5.3.2 Size Exclusion through Nanofibrous Membranes

Filtration is an energy-driven processes because fluid is forced through filter media under high pressures. Pressure drops must overcome resistance to flow along both sides of filter media. Flux (which is the flow rate per unit area) is an important membrane property. During filtration, particles are deposited along the filter surface and throughout the membrane's structure. Those deposits block pores thereby increasing the TMP. Flux will subsequently diminish with time. To maintain a constant flux during filtration, external pressure must exceed TMP. When TMP is high, higher values of external pressure are required for filtration. High flux will achieve rapid filtration and low energy consumption^{17,18}, because less pressure is required to push fluid through filter media.¹⁶

Conventional membranes for MF, UF and NF- nanofiltration- are produced by the phase inversion method^{8,14-16}. These composite membranes possess bilayers, where the top layer consists of asymmetric pores for filtration. The support layer is a nonwoven that provides mechanical strength and structural integrity⁸. The morphology and pore size distribution of phase inversion membranes have relatively lower low flux and more fouling. Additionally, macro voids exist throughout the thickness of conventional membranes. Electrospun webs of nanofibers can overcome these limitations that are associated with conventional filtration membranes, because nanofibrous webs have high surface area, tunable fiber diameter and pore size distribution and interconnected pores^{8,16}. Issues associated with the use of nanofibrous filters include low mechanical strength, static charge which makes web handling a challenge,

and mild interfiber cohesion¹⁶. Research have endeavored to overcome these drawbacks that are associated with nanofiber use. In 2012, Wang et al. developed a composite membrane by electrospinning PAN on nanofibers onto poly (ethylene terephthalate) (PET). The mechanical strength of the membranes improved within the composite, and the composite's flux was suitable for microfiltration. When nanofibers are layered onto the substrate, pore size decreases and pore size distribution is narrower (both occurrences are favorable to achieve high flux). The flux of the PAN/PET membrane was 2-3 times greater than that of conventional MF membranes. Nanofibers afforded structural advantages, such as high porosity and pore interconnectivity³⁹.

Annealing polymer below the melting point helps to improve the structural integrity nanofibrous membranes. In 2006 and 2012, Gopal et al. reported the development of self-supporting, nanofibers that had used in MF without adding any support. Membranes of polyvinylidene fluoride (PVDF) and polyether sulfone (PES) were electrospun for microfiltration. Thermal annealing caused interfiber bonding and structural integrity. Nanofibers achieved >90% particle rejection against polystyrene (PSt) beads that were 1-10 μm in diameter, even though nanofibers were not supported. Further, TMP was comparable to commercially available MF membranes^{16,40}

The strength of nanofibrous membranes is also improved by chemical modification. The aim of chemical modification is to bonds at fiber cross over points. In 2014, Huang et al. developed electrospun membranes of PAN and PS that were treated with dopamine- a hydrophilic monomer that is used as an adhesive for organics, inorganics and chemically inert materials⁴¹. Dopamine formed polydopamine (PDA) and helped to adjoin neighboring nanofibers (NFs) together. In turn, the tensile strength and Young's modulus improved by

100% for PAN, and tensile strength and Young's modulus increased by 80% and 210%, respectively for PS treated with polydopamine. PDA/PS membrane also improved in terms of their hydrophilicity. Contact angle decreased from 145° to 79° after PDA treatment. However, pore volume and flux were slightly compromised upon PDA modification. The PDA/PS membrane was also used without any support.

Membrane fouling is of great concern as it relates to filtration. Biofouling reduces flux due to pore blockage. More energy is required to supply the pressure needed for filtration. High porosity nanofibers favor higher values of flux. However, high porosity can cause irreversible fouling⁸. Researchers have overcome biofouling by covering filtration media with a layer of nonporous, hydrophilic particles, which acts as a physical barrier for particulates in the fluid stream. Only water can permeate through the membrane. In 2006, Yoon et al. developed a three-tier membrane- chitosan coated, PET nonwoven as a support for electrospun PAN. Flux values were suitable for UF and NF applications. Chitosan was impervious to particulates and helped to minimize fouling. Initially, high flux was achieved because of pore interconnectivity. Membrane performance was studied in response to coat thickness. Thin chitosan coatings gave high flux values, because water required less time to permeate through the thinner layer. After 20 h of operation, flux values were one order of magnitude higher than those obtained for conventional UF/NF membranes⁸. Hydrophilic coatings and polymer blends can yield higher flux with less fouling.⁴²

1.5.1 Particle Attachment through Functional Membranes for Purification

Purification is defined as the removal of impurities from material. Filtration is a type of purifying process that is governed by the size of impurities and separation of the desired chemistry. Purification also relies on chemical affinity, electrostatic attraction, ion exchange,

complexation and molecular interactions. Mechanisms of chemical association are based on either primary or secondary bonding. Primary bonding occurs irreversibly and is classified as ionic, covalent or coordinate. Interactions through secondary bonding are weaker than by primary bonding. Ion exchange, hydrogen bonding, and electrostatic adsorption occurs by secondary bonding. Reversible binding between molecules occurs by secondary bonding.

1.5.1.1 Chemical Separation

1.5.1.1.1 Chemical Separation by Ion Exchange Membranes

Ion exchange membranes are widely used for electrodialysis, recovery of chemicals and desalination. Ion exchange membranes contain cations on the membrane surface for separation. Ion exchange membranes are classified as being cation or anion exchange membranes for separation⁴³.

Cation exchange membranes selectively allow cations to permeate through. Usually these membranes are functionalized with anionic sulphonic acid, phosphoric acid, sulphonamides, and carboxylic acid groups⁴⁴. Polymers such as polyether sulfone (PES), polyether ketone (PEK), polybenzylimidazole (PBI), polyimide (PI), polyphenylene (PPh), polyphosphazene (PPz) and polyvinylidene fluoride (PVDF) are widely used matrixes⁴⁴. Cation exchange membranes prepared via the sulphonation of styrene copolymer, having divinyl benzene modified with chlorosulfonic acid or sulphuric acid, provide nanoscale separation^{43,44}. These membranes are used in electrodialytic separation, ionic dye removal, etc. Chakravarty et al (2010) developed electrospun cation exchange membranes from poly(ether ether ketone) and reported the ability to separate monovalent cations (Na^+) from divalent cations (Mg^{++} and Ca^{++})⁴⁵. Wu et al (2008) recovered nearly all of the cationic dye from waste

water using cations exchange membranes which were prepared with sulphonated groups on nonwoven polyester⁴⁶.

Anion Exchange membranes are typically made from polyelectrolytes containing positively charged groups and can selectively allow anions to permeate through. These membranes comprise cationic groups; such as quaternary ammonium, imidazole or guanidium, and diethyl amine. Usually, anion exchange membranes are produced from the triethyl amination of chloromethyl styrene and divinyl benzene copolymers⁴³.

Amphoteric (bipolar) membranes that have cation and anion exchange groups can separate cationic and anionic permeants⁴³. Most bipolar membranes comprise three layers; wherein the cation exchange and anion exchange layers are placed on either side of a (mildly acidic or basic) catalytic interlayer. At the catalytic interlayer, cations dissociate to protons (H^+) and anions to $-OH$ groups. Further, water dissociation at the interlayer depends upon catalyst concentration⁴³.

1.5.1.1.2 Chemical Separation by Molecular Inclusions Membranes

Water soluble contaminants (namely heavy metals, dyes, and industrial waste products) are difficult to filter from stationary water. Water soluble contaminants are confined to the membrane's surface by chemical interactions. Functionalized nanofibers, having ligands attached, are capable of removing water soluble impurities. Cyclodextrin (CD) are polysaccharide capsules or organic compounds. CD's hydrophilic surface and hydrophobic cores enables encapsulation and dissolution in water. CD can interact with target compounds by forming noncovalent inclusion complexes. In 2011, Zhang et al. electrospun blends of beta (β)-CD and polyvinyl alcohol that could capture ferrocene. β -CD's hydrophilic surface is

suitable for PVA blending and its hydrophobic cavity forms inclusion complexes with ferrocene⁴⁷.

1.5.1.1.3 Chemical Separation by Adsorbing Membranes

In 2008, Bessbouse et al. developed PVA//Polyethyleneimine (PEI) membranes to capture lead (Pb), cadmium (Cd), and copper (Cu) ions from aqueous solutions^{48,49}. PVA hydroxyl groups formed weak complexes with metal ions. Polyelectrolytes within the blends improved the efficiency of heavy metal removal. PVA /PEI membranes could also separate mercury (Hg) ions at different pH⁴⁹. In general, the removal of metal ions from solution was based upon molecular interactions between metal ions and functional groups along the polymeric membranes. Interactions include electrostatic attraction and complexation⁵⁰.

1.5.1.2 Biological Separation by Adsorbing Membranes

The transfusions bodily fluids are forms of therapy. Prior to fluid transfer from donor to acceptor, purification is required to prevent the transfer of infectious diseases to human patients. Affinity chromatography is used to purify bodily fluids of serum, antibodies and blood⁵¹. Affinity membranes provide several advantages over affinity chromatography; Flow rates and operation speeds are faster⁵². Affinity chromatography uses microporous, polymeric beads for chemical separation. In contrast, affinity membranes are more porous and possess higher surface area.

Immunoglobulin (IgG) antibody is an immunoprotein found in humans. Affinity membranes were developed to purify IgG antibodies for external use. Ma and Ramakrishna (2008) developed affinity membranes using cellulose acetate (CA) as the matrix polymer and protein A/G (fusion hybrid of proteins A and G) as the capture ligand for IgG⁵³. Protein A/G binds to the fragment crystallizable region (Fc) region of IgG. BSA is a model protein that is

used to evaluate the sorptive properties of affinity membranes. In 2005, 2006, 2008, and 2009, Ma et al. electrospun nanofibrous membranes of CA and polysulphone (PS) that were surface functionalized with Cibacron Blue F3GA (CB) and A/G protein (both were capable of binding with BSA and bilirubin through electrostatic adsorption⁵³⁻⁵⁶.

In 2010, Herigstad et al. modified polypropylene (PP) nonwoven membranes with hydroxylated polymethyl methacrylate (PMMA) and surficial amino groups- that were capable of biological separation⁵⁷. Modified nonwovens behaved as ion exchange membranes in the chromatography column⁵⁷. The interstices of fibrous nonwovens permitted the passage of cells and debris within contaminated fluid but captured target chemistries by ion exchange. In 2013, Liu et al. developed a nonwoven membrane from polybutylene terephthalate (PBT) that was surface functionalized with polyglycidyl methacrylate and a proprietary ligand- grafted by ultra-violet (UV) radiation. The capture of PRion protein (PRNP) onto PBT fibers occurred through anion exchange^{58,59}.

In 2013, Zhang et al. developed bioactive, cellulose nano-fibrils (CNF) in a two-step process⁶⁰. Initially, CNFs were modified by atomic-transfer radical-polymerization (ATRP) with poly(2-aminoethyl methacrylate hydrochloride-co-2-hydroxyethyl methacrylate) (poly-AMA-Co-HEMA)⁶⁰. The binding of IgG to cellulosic nano-fibrils was confirmed, but the specific mechanism of binding is unknown.

1.6 Iodoacetate use with Biologicals

1.6.1 Iodoacetate for Characterization & Inactivation

Iodoacetic acid (IAA) is used in thiol/ thioether containing protein quantification. Wang et al. developed a new strategy for cysteine containing protein quantification that was based on differential, stable isotope labeling for mass spectroscopy⁶¹. They labeled IAA with

O¹⁸ by incubating IAA in O¹⁸ enriched water at 50 °C for one day. Cysteine residues were capped with O¹⁸. IAA and were observed under mass spectrometry.

The chemical inactivation of SEB toxin after modified with IAA was reported by Chu et al. (see Figure 1.11)⁶². SEB, a major cause of food poisoning, is secreted from staphylococcus aureus. SEB triggers severe fever, headaches, and gastro-intestinal effects (such as vomiting, diarrhea, and respiratory illness). SEB is resistant to thermal and enzymatic degradation and deactivation in the gastrointestinal system^{63,64}.

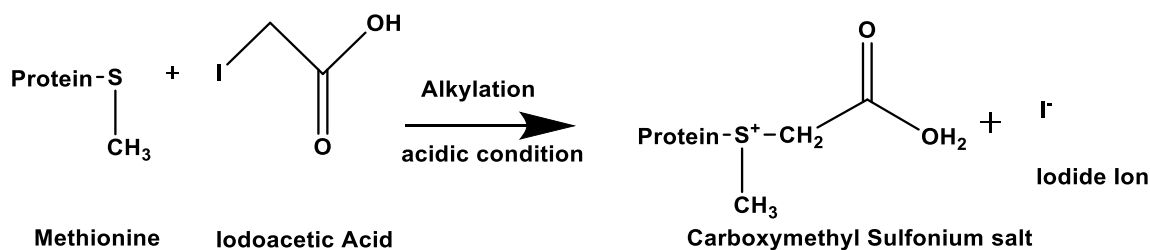


Figure 1.11. Alkylation of Methionine residue of SEB.

SEB is a single-chain polypeptide. It consists of (238-267) amino acid residues^{65,66} and has a molecular weight of 28.4 kDa⁶³. SEB is a super antigen that stimulates nonspecific T-cell proliferation and gastrointestinal toxins. As a result, cytokine release and inflammation occurs^{63,65}. Toxicity depends upon the frequency and dose of SEB. In case of ingestion, symptoms may appear after 4 h of exposure and last up to 12 h. At 30 ng/person, symptoms of food poisoning may occur⁶⁴. The effective dose (ED50 affecting 50% of the human population) for aerosol exposure is 0.0004 µg. Lethal dose (LD50 sufficient to kill 50% of the human population) is 0.02 µg. SEB is a potential agent for bio-warfare that is spread on battlefields as an aerosol⁶⁴. Hence, the deactivation and confinement of SEB are of interest.

Researchers confirmed SEB inactivation upon IAA reaction by feeding monkeys modified SEB. The emetic response to SEB antigen was lost when 5-7 methionine residues

were chemically modified with IAA. Conformational changes in SEB's structure upon IAA alkylation was proposed as a plausible mechanism of inactivation.

Thus, iodoacetylated polymer may also affect the biological response of biomacromolecules. In 2013, Ina et al. investigated the hemostatic performance of iodoacetylated chitosan. Iodoacetate groups formed covalent crosslinks with blood proteins via iodoacetate-thiol reactions. This accelerated blood clotting by one order of magnitude in comparison to unmodified chitosan over 2 h of exposure⁶⁷. The reaction between iodoacetate and cysteine amino acids occurred under alkaline conditions (pH=8.5). Hydroiodic acid (HI) and cystine were reaction products Figure 1.12

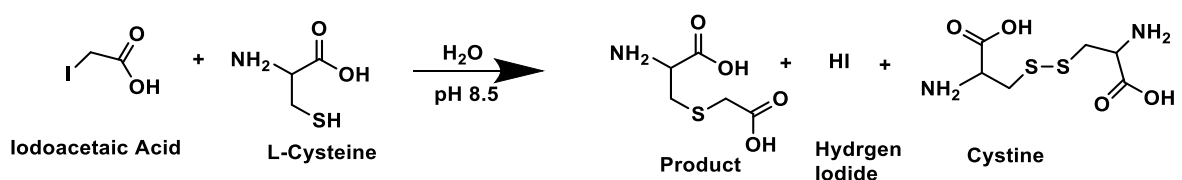


Figure 1.12. The predicted reaction scheme between IAA and L-Cysteine is based on mass spectrometry results.

1.7 Techniques used to Confirm Physical and Molecular Capture

1.7.1 Liquid Chromatography:

Liquid chromatography (LC) is used to separate complex mixtures. LC distinguishes between chemical constituents based on differences in their elution from chromatography columns. A typical LC set up consist of mobile phase, pump, stationary phase and a detector. In the mobile phase, a common solvent dissolve each component of the mixture. Using a pump, the mobile phase is injected though the stationary phase- a column filled silica gel, porous beads or alternate medium that can separate constituents by their molecular size or chemical affinity with the column media. Mechanisms of physical and chemical separation further divides LC techniques: size exclusion, ion exchange, reverse phase and affinity

chromatography are examples. The analyte constituent having the weakest (chemical and/or physical) interactions with the column elutes first from the column, but constituents that strongly interact with the column elutes last. The detector monitors the concentration of each component relative to the overall analyte volume.

In 1959, Gundalch et al. studied the reaction of methionine with IAA using ion exchange chromatography⁶⁸. In 1969, Chu et al. also studied the alkylation of SEB's methionine residues using liquid chromatography (LC)⁶². The fully modified SEB strongly adsorbed onto the carboxy methyl cellulose (CMC) column, but unmodified and partially modified SEB eluted at faster times from the column.

1.7.2 UV-Vis spectroscopy

This is a type of absorbance spectroscopy. Electromagnetic radiation is absorbed by π electrons or nonbonding electrons (n) of molecules; then, electrons are excited from the highest occupied molecular orbital (HOMO) to the lowest unoccupied molecular orbitals (LUMO). The energy difference between HOMO and LUMO is called band gap energy. Since energy is inversely proportional to wavelength, higher band gap energy necessitates longer absorbance wavelengths for excitation and vice versa. Molecular absorbance is compared in terms maximum absorbance wavelength (λ_{max}). Absorbance is modeled by Beer Lambert's law; thus UV-vis is quantitative analytical technique. Molecules absorbing electromagnetic radiation in the range of 200-800 nm are comparable by UV-Vis spectroscopy.

In 2013, Huang et al. studied the absorbance of endotoxins on a PS based affinity membrane which was immobilize by L-Serine with UV-Vis spectroscopy. The affinity membrane was immersed in a solution of endotoxin at 37 °C for 2 h under shaking. Endotoxin content was determined from absorbance measurements at 585 nm³⁵. In 2015, Liu et al. also

studied the dynamic binding of BSA on poly butylene terephthalate (PBT)/ polyglycidyl methacrylate (PGMA)/ diethylamine (DEA) membrane⁵⁸ BSA concentration was measured before and after binding to affinity membranes using absorbance intensities at 280 nm⁵⁸.

Optical density measurements by UV-Vis spectroscopy are used to characterize cell growth, biomass production and changes in cell morphology in bioassays. Absorbance intensity is converted into optical density (OD) by the Equation 1.1:

$$OD = \frac{A_b}{l} \quad 1.1$$

where OD is the optical density of the solution, l is sample thickness, and A_b is absorbance. A_b is determined from $A = -\log \frac{I}{I_0}$. In 2014, Ford et al. used this technique to confirm the hydrolysis of paraoxon and *p*-nitrophenol acetate by BSA²⁷.

1.7.3 Quartz Crystal Microgravimetry (QCM)

Using a quartz crystal microbalance, micrograms of specimen mass per unit area is determinable. Quartz crystal is an acoustic resonator that is sandwiched between electrodes. As mass is added or removed from the microbalance, resonance of the quartz crystal changes according to Sauerbrey's Equation 1.2:

$$\Delta f = \frac{-2\Delta M_s x f_o^2}{A_s \sqrt{\mu_Q \rho_Q}} \quad 1.2$$

where Δf is frequency change, ΔM_s is mass change, x is the overtone number, f_o is the fundamental frequency of the quartz oscillator, A_s is surface area, $\mu_Q = 2.947 \times 10^3 \text{ gcm}^{-1}\text{s}^{-2}$ is the shear modulus of quartz, $\rho_Q = 2.648 \text{ gcm}^{-3}$ is the density of quartz. This technique is accurate for mass change less than 2% of the quartz crystal⁶⁹. In 2013, Zhang et al. used QCM to study the binding of human IgG peptide with bioactive CNFs⁶⁰. Shifts in

resonating frequencies, at different overtones, were measured to quantitatively model the binding of IgG with a solidified liquid layer. Using this model, the mass of adsorbed IgG (15.1 mg/m²) was determined.

1.7.4 Bicinchoninic Acid Assay

The concentration of protein in solution is measured by bicinchoninic acid assay (BCA). A stock solution of sodium salt, bicinchoninic acid and copper salt is used to drive color changes- from green to purple- in direct proportion to protein concentration. First the peptide bond of protein reduces Cu⁺⁺ to Cu⁺. Secondly, two BCA molecules chelate Cu⁺ ions to give a purple color (see Figure 1.13)^{70,71}.

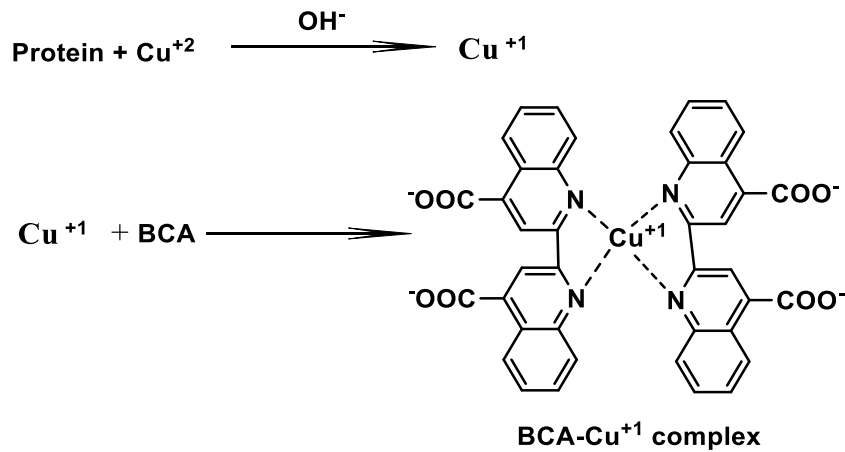


Figure 1.13. Purplish color is observed when BCA and cuprous ions complex⁷⁰.

In 2003, Ma et al. studied BSA adsorption onto CB-regenerated cellulose membranes using this BCA assay⁵⁴. BSA adsorption capacity was measured by the following Equation 1.3:

$$q = \left(\frac{C_i - C_t}{M_d} \right) * V \quad 1.3$$

where C_i and C_t are the concentrations at time $t=0$ and t , V is the volume, M_d is the dry mass of the membrane and q is the adsorptive capacity in mg/gm. In 2015, Liu et al. studied the static binding of BSA on anion exchange membrane using the same technique⁵⁸.

1.7.5 X-Ray Photoelectron Spectroscopy

X ray photoelectron spectroscopy (XPS) is a surface analytical technique. In XPS, photoemission occurs upon electron ejection from core shells as the material's surface is bombarded with photons having energy $h\nu$. The spectrometer analyzes the binding energy of emitted electrons versus signal intensity (i.e. counts of ejected electrons)⁷². In addition, surface chemistry analysis, XPS is used to quantify the relative amounts of element on a surface. Also, spectral images can be used to differentiate between chemical species to produce reactivity maps. The cleanliness of sample surfaces can be identified, and forms of molecular bonding are determinable. For instance, C-C, C-O, and C=O bonds are differentiable. Lastly, XPS can provide depth profiles of a surface.

In 2012, Min et al. studied the adsorption capacity of PES/PEI membranes for anionic dyes and heavy metals adsorption using XPS⁷³. They compared changes in binding energies along PES/PEI membranes before and after dye and heavy metal adsorption²⁷.

1.7.6 Fourier Transform Infrared Spectroscopy

Fourier transform infrared (FTIR) spectroscopy is a widely used characterization technique. The chemistry of materials can be analyzed for solid powder, solid thin film, paste, and liquids^{74,75}. FTIR is used to identify unknown samples by its functional groups, compare materials before and after chemical reaction, and analyze degrees of chemical modification among samples. This is an excellent tool for qualitative and quantitative analysis. Other data provided by FTIR includes polymer crystallinity and the extent of hydrogen bonding^{76,77}.

1.8 Research Objectives:

Mostly, protein attachment to surfaces mostly occurs with nonspecific binding that results from hydrogen, ionic and weak Van der Waals bonding forces. The reversibility of this form of binding makes membranes reusable. If the captured agent is SEB, the subsequent release of the protein remains a concern and risk upon disposal. The covalent attachment of proteins onto membrane surfaces gives a feasible solution to the problem. However, capturing the toxin alone is not enough because it can contaminate other surfaces upon contact. Deactivation is needed to prevent exposure to super antigen effects. Reactive nanofibers have potential use to immobilize proteins and toxins for a variety of applications. The surface chemistry and morphology of nanofibrous membranes are important because these can directly affect protein immobilization and potentially their deactivation.

IAA is known for its alkylation reaction with sulfhydryl and thioethers. Also, IAA is widely used in protein chemistry for purification and characterization. However, iodoacetic acid is carcinogenic and corrosive. We hypothesized the covalent attachment of proteins onto nanofibers functionalizing these high surface area membranes with reactive iodoacetate groups. In this regard, the iodoacetylation of polymer is safer for use.

The overall objective of this research was to fabricate functional nanofibrous membrane for irreversible protein attachment. Functional nanofibers PVA modified with pendant iodoacetate groups were electrospun. Thus, there is potential for these iodoacetylated PVA nanofibers to react with thioether residues along proteins. There is a need to test whether functional proteins (enzymes for example) will retain their activity. This research is divided into three sub-goals as follows:

1. Study the effect of acetate moieties (COOCH_3 , $\text{COOCH}_2\text{-Cl}$, $\text{COOCH}_2\text{-I}$) along PVA copolymers on the morphology of electrospun fibers
2. Understand mechanisms of protein attachment along poly (vinyl iodoacetate), PVIAC, nanofibers using amino acid residues
3. Immobilize enzymes onto PVIAC membranes and evaluate the enzymatic activity of immobilized enzymes

CHAPTER 2.

EFFECT OF ACETATE MOIETIES ON THE MORPHOLOGY OF ELECTROSPUN POLYVINYL ALCOHOL BLENDS AND COPOLYMERS

2.1 Introduction:

Polymer blends and copolymers yield performance properties that commercially available homopolymers may lack. Polymer blending has resulted in property enhancements, in relation to mechanical strength⁷⁸, hydrophilic/hydrophobic character^{79,80}, temperature resistance^{81,82} and chemical stability⁸², sustainability⁸³, and functionality (i.e. molecular capture or adsorption)^{47,84}. Halogenation is often used to synthesize functional polymers that are inherently flame retardant, chemically resistant and non-corrosive⁸⁵. To avoid the absorption of small halogenated compounds by human skin or mucous membranes, their confinement onto the surface of macromolecules provides safer alternatives. Further, molecular functionalization has led to development of active polymers, which have use in chemical and biological separation^{86,87,58}. For instance, Huang et al performed the chloromethylation of PS to ultimately cause L-serine attachment onto the hollow fibers³⁵. In turn, L-serine amino acids are capable of binding within endotoxins found in human plasma³⁵. Kenawy et al. chloroacetylated polyvinyl alcohol (PVCIAc) to attach ammonium and phosphonium salts for antimicrobial effects against gram- negative bacteria⁸⁸.

Electrospinning enables the formation of high surface area nanofibers^{20,89,22,90,91} that can exhibit functionality. Kim et al. fabricated nanofibers for the controlled drug release of fluorescein isothiocyanate (FITC)-dextran from electrospun polymers of *N* isopropylacrylamide-co- *N* hydroxyl-methyl-acrylamide (NIPAAm-co-NHMAAm)⁹². In 2015, Atlan et al. spun functional nanofibers for biotin-mediated streptavidin (protein) capture

via nonspecific binding using furfuryl methacrylate (FuMA), poly(ethylene glycol monomethyl ether methacrylate) (PEGMEMA), and methyl methacrylate (MMA)⁹³.

Processing and solution parameters affect the morphology of electrospun fibers. Examples of process parameters are applied voltage, voltage bias, tip to collector distance, collector type, flow rate and atmospheric conditions (namely ambient temperature and relative humidity)⁹⁴.

The viscosity, conductivity, and surface tension of polymer solutions are influenced by polymer/solvent chemistry^{4,91,95}. Polymer molecular weight will influence its minimum concentration for electrospinning⁹⁶. Functional groups along the polymer will influence its solubility in different solvents.

Zhang et al (2004) studied the effect of voltage, tip to collector distance, concentration, salt amount, and degree of hydrolysis in case of PVA⁹⁴. They showed that increasing concentration of polymer solution caused increase in fiber diameter because of rise in solution viscosity, which works against fiber stretching. They reported that with concentration more than 8.3% (MW- 81,400 g/mol. and DH 98%) and fibers can't be spun because of high viscosity⁹⁴. However, researchers have spun higher concentration with higher molecular. In this, 11 wt. % solution concentrations with the higher molecular weight were spun. In 2004, Son et al. had shown salt addition increases solution conductivity and then leads to finer fibers⁹⁷. As degree of hydrolysis (DH) increases from 80% to 99%, fiber morphology changed from flattened, collapsed fibers to circular fibers⁹⁴. Higher DH values relate to higher viscosity and conductivity values. In 2010, Park and et al. studied the effect of DH on the morphology of electrospun PVA fibers⁹⁸. PVA fiber size increased with DH% and the rise in solution viscosity⁹⁸. In 2005, Son et al had shown the effects of pH on the morphology of electrospun PVA⁹⁹. They observed trends using acidic and basic solutions. Solution conductivity increased

under basic conditions, which caused fiber diameters to reduce and straightened fibers to appear. Under acidic conditions, dis-continuous beaded fibers were observed in consequence to -OH protonation⁹⁹.

Since polymer blending and functionalization are used to electrospin active fibers, this study is interested in understanding the effects of acetate moieties on nanofiber morphology and spinnability. PVA has hydroxyl groups that are amendable to synthetic functionalization. Esterification, azido-acetylation, acetylation is commonly used synthetic routes. Therefore, blends and copolymers in this study are based on PVA. Quite notably, PVA is semi-crystalline even in its atactic form. Hydrogen bonding between PVA's hydroxyl groups are responsible for crystallization, hydrogen bonding, and solubility. And its thermal stability is up to 300 °C. Commercially available forms of atactic PVA are hydrolyzed from polyvinyl acetate (PVAc) at various degrees. By halo-acetylation of PVA, copolymers can have chloroacetate and iodoacetate groups^{100,101,88,102,103,104}. The morphologies of electrospun PVA blends (PVA-*blend*-PVAc) were investigated, as well as PVA copolymers having acetate and halogenated acetate groups.

2.2 Materials and Methods:

2.2.1 Materials

Pure PVA and PVAc polymers were purchased from Sigma Aldrich. Chloroacetic acid (ClCH_2COOH from Sigma Aldrich), potassium iodide (KI from Fisher Scientific), glacial acetic acid (CH_3COOH from BDH), 2.5 N sulfuric acid (H_2SO_4 from BDH), and dimethyl sulfoxide (DMSO from Alfa Aesar) were employed in the synthetic functionalization of PVA. Sodium carbonate Na_2CO_3 (from Brenntag Inc), isopropanol (>99% purity from BDH) and deionized water were used to purify polymers.

PVA polymers having 88 and 99% hydrolysis are termed PVA-*co*-PVAc and PVA, respectively. Polymer molecular weights were 89-98 kDa for PVA, 130 kDa for PVA-*co*-PVAc, and 100 kDa for PVAc. PVA-*co*-PVClAc is the product of PVA functionalized with chloroacetate groups. PVA-*co*-PVIAc is the product of PVA functionalized with iodoacetate groups.

2.2.2 Methods

2.2.2.1 Synthesis of PVA-*co*-PVClAc

40.00 g PVA was dissolved in DMSO at 80°C. Chloroacetic acid and 8 ml H₂SO₄ were added to the PVA/DMSO solution. Afterwards, the reaction was run for 4 h. at 85±5°C. The solids content of the chloroacetic acid in the reaction flask was maintained at 20%. PVA-*co*-PVClAc copolymers were neutralized by aqueous solutions of Na₂CO₃. Mixtures of 80/20 (v/v) isopropanol/water were used to precipitate polymer at room temperature. Acetylation of PVA was determined quantitatively from infrared spectra. The reaction scheme is shown in Figure

2.1

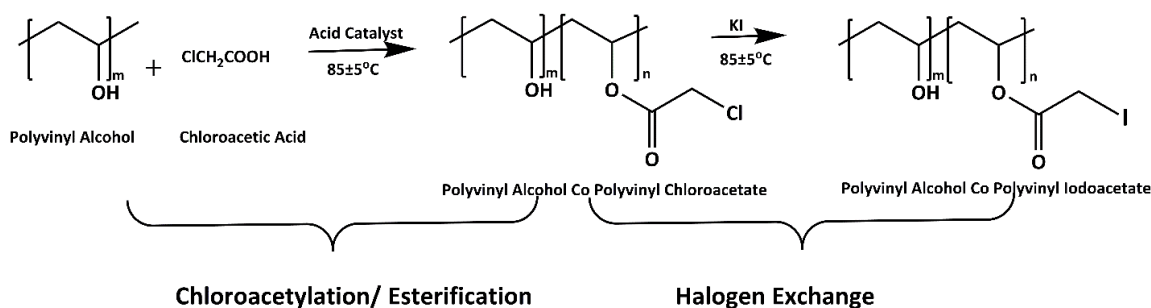


Figure 2.1. PVA-*co*-PVClAc was synthesized from PVA and then converted into and PVA-*co*-PVIAc.

2.2.2.2 Characterizing Degree of Acetylation

Spectra of PVA and PVA copolymers were collected with 64 scans and a resolution of 4 cm⁻¹ on the attenuated total reflectance Fourier transform infrared (ATR-FTIR)

Thermoelectron spectrometer. Baseline corrections were automatically applied. Each absorbance spectra were normalized according to the C-H bending peak at 1425 cm^{-1} . Calibration of polymer acetylation was based on carbonyl (C=O) peak intensities from commercial PVA, PVAc and PVAc-co-PVAc powders. Using the calibration curve, the degree of acetylation was calculated for PVClAc polymers that were derived from PVA.

2.2.3 Synthesis of PVA-co-PVIAc

PVA-co-PVClAc polymers in DMSO were reacted with 1.5 Eq. KI at $85\pm 5\text{ }^{\circ}\text{C}$ for 5 h. Afterwards, PVA-co-PVIAc polymers were precipitated from room temperature solutions using isopropanol/water. The halogen exchange reaction between chloroacetate groups and KI was repeated and again precipitated from solution.

2.2.4 Electrospinning Solutions

Five blends at weight ratios (w/w) of 100/0, 75/25, 50/50, 25/75, and 0/100 PVA-*blend*-PVAc were prepared. PVA-*blend*-PVAc were dissolved in DMSO at $85\text{ }^{\circ}\text{C}$ under constant stirring. The overall concentration of polymer in solution was 18 weight percent (wt. %). Aqueous solutions of 11 wt.% polymer was prepared from PVA, PVA-co-PVAc, PVA-co-PVClAc, and PVA-co-PVIAc dissolved in water at 80°C .

2.2.4.1 Solution Characterization

The conductivity of electrospinning solutions was measured. A minimum of three conductivity measurements were obtained with the Oakton ECTestr conductivity meter. In case of PVA copolymers, the solution was precipitated-re-precipitated four times after PVA modification and solution conductivity was measured each time to insure the residual salt removal.

2.2.4.2 Electrospinning

PVA-*blend*-PVAc were electrospun at 35 kV using a vertical tip to collector distance of 16 cm on the Elmarco Nanospider. PVA homo and copolymers were electrospun at 20 kV, with a horizontal tip to collector distance of 12 cm. Electrospinning was performed at 24-26 °C and 30-40 % RH.

2.2.4.3 Scanning Electron Microscopy

The morphology of electrospun fibers were imaged with the Verios Field Emission Scanning Electron Microscope (FESEM) at an accelerating voltage of 2 kV and current of 13 mA. Fibers were sputter coated with 60/40 Au/Pd for 1 min at 0.7 nm/min before imaging. Image J software was used to measure the diameters of at least 25 fibers per sample.

2.3 Result and Discussion

2.3.1 PVA-*blend*-PVAc Fiber Morphology

The morphology of PVA-*blend*-PVAc blended nanofibers is shown in Figure 2.2. The diameter of PVA fiber was ~1 μm . As PVAc content increased to 75%, fiber diameters decreased to 730 nm. PVAc (0/100 PVA-*blend*-PVAc) in DMSO was not spinnable. Intermolecular bonding between polymers within the blends is believed to affected blend properties in solution. Changes in intermolecular bonding between polymers were observed in Figure 2.3- IR spectra of solution cast PVA-*blend*-PVAc films. Conductivity measurements of the polymers solutions are given in Table 2.1. These were analyzed to understand the effects of blending and solution properties on fiber morphology.

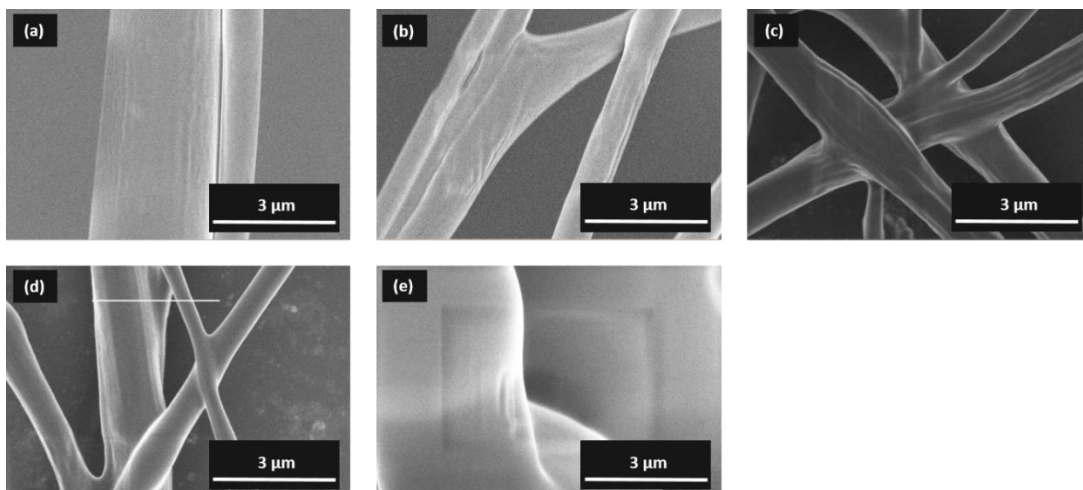


Figure 2.2. Fiber morphology of PVA-blend-PVAc blends (w/w) at (a)100/0 (b) 75/25 (c) 50/50 (d) 25/75 (e) 0/100, solution concentration of 18wt%, and DMSO as the solvent.

Table 2.1.Conductivity and fiber diameters from PVA-Blend-PVAc in DMSO.

| S.NO | PVA- <i>blend</i> -PVAc ratio (w/w) | Conductivity ($\mu\text{S/cm}$) | Fiber Diameter (nm) |
|------|-------------------------------------|-----------------------------------|---------------------|
| 1 | 100/0 | 56 ± 1 | 1164 ± 640 |
| 2 | 75/25 | 42 ± 1 | 890 ± 370 |
| 3 | 50/50 | 38 ± 1 | 790 ± 390 |
| 4 | 25/75 | 21 ± 1 | 730 ± 180 |
| 5 | 0/100 | 0 ± 0 | Not Applicable* |

* Fibers were not spun under these conditions. Coalesced droplets of polymer were found on the collector. Fiber were electrospun on the stainless-steel mesh.

2.3.2 Spectra of PVA-*blend*-PVAc Fibers

Changes in the blend compositions are reflected by changes in IR absorbance peaks for PVA –OH groups, acetate carbonyl groups, and PVA conformation (Figure 2.3). As PVAc content increased, the peak intensity for acetate carbonyl groups increased. The absorbance intensity for crystalline polymer of pure PVA (at 1151 cm^{-1}) is milder among 25/75 PVA-*blend*-PVAc.

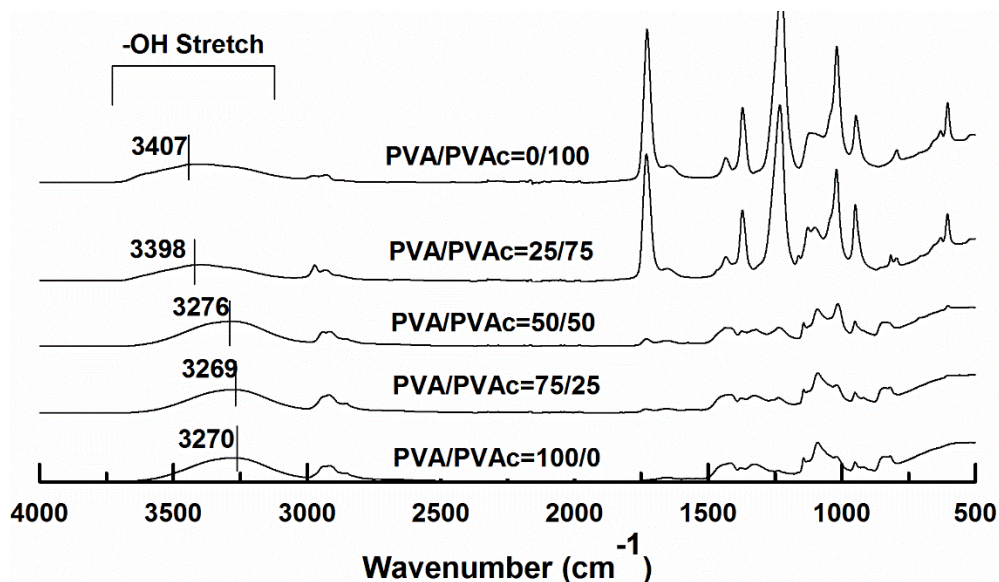


Figure 2.3. IR spectra confirm differences between the chemical compositions of PVA-co-PVAc blends as noted by change in –C=O peak intensity.

PVA-*blend*-PVAc composition affected inter- and intramolecular hydrogen bonding, as observed from IR frequency shifts in –OH peak intensities (as shown in Figure 3). The -OH

peak shifted towards higher wavenumbers as the ratio of PVAc increased. A similar effect has been observed among PVA-*co*-PVAc polymers with varying degrees of acetate group hydrolysis. In 2001, Ping et al. reported -OH peak shifted toward lower wavenumber with higher degrees of acetate hydrolysis¹⁰⁵. In 2003, Kubo et al. have also reported -OH peaks shifted toward lower wavenumbers when lignin was added to PVA from 3422 to 3414 cm⁻¹⁷⁸. Thus, this shift in -OH peak towards higher frequencies are associated with intramolecular hydrogen bonding between PVA molecules, whereas lower frequencies are associated with intermolecular hydrogen bonding between PVA molecules. Table 2.1 shows trends in solution conductivity and viscosity that can be attributed to changes in hydrogen bonding among PVA-*blend*-PVAc compositions.

2.3.1 PVA-*blend*-PVAc Conductivity

In electrospinning, fiber diameters are typically finer as solution conductivity increases. Adding low weight percentages of salt, having electron donating groups, and using ionic polymers can increase solution conductivity. In 2004, Son et al. reduced the averaged fiber diameter of PEO upon adding 0.1 wt. % of an polyelectrolyte poly(allyl amine hydrochloride) (PAH) or poly(acrylic acid sodium salt) (PAA)⁹⁷. Blend conductivities of PVA-*blend*-PVAc gradually decreased with PVAc content. Hydrogen bonding between PVA's electron donating hydroxyl groups are expected to become less prevalent as the ratio of PVA decreased. The conductivity of PVAc in DMSO was negligible because DMSO is an aprotic solvent that can only accept protons from polymer. The lack of electron donating hydroxyl groups diminishes the charge in the solution as the concentration of PVAc surpassed PVA in blends. The conductivity of PVA in DMSO is less than values reported for PVA in water. But, having

solution conductivities on the same order of magnitude did little to increase the overall size of electrospun fibers.

2.3.1 Optimization of PVA/PVAc Blended Fiber Diameter Morphology

Solvent selection is an important parameter for electrospinning because it affects surface tension and solvent evaporation from the dope. Applied voltage must overcome surface tension for continuous fiber formation. High surface tension leads to jet instability and bead formation during electrospinning⁴. Secondly, the boiling point of solvents influences the ease of evaporation during fiber formation. Higher boiling point solvents need longer air gaps for evaporation. Residual solvent leads to flattened fibers and film formation among nanofibers. To explore the effect of solvents on fiber morphology, we have used PVA/PVAc blends at fiber different blends ratio - 100/0, 75/25, 50/50, 25/75, 0/100 using two different solvents (DMSO and 3:1(v/v) acetic acid: water)-. Polymer concentrations between 12-20% were tried to spin the blends successfully.

DMSO has a boiling point of 183 °C and requires longer evaporation times during electrospinning. Fibers were electrospun using 10 cm tip to collector distance (TCD). All the fibers collapsed and turned into film because of incomplete solvent evaporation. To increase evaporation time, TCD was increased from 10 - 16 cm. At 16 cm TCD, fibers were spun from 16 wt% solutions and more concentrated solutions. A TCD=16cm provided sufficient time for solvent to evaporate from the 16 wt% solution. The addition of PVA to PVA-*blend*-PVAc increased fiber size. Nanofibers were obtained as shown in Figure 2.5

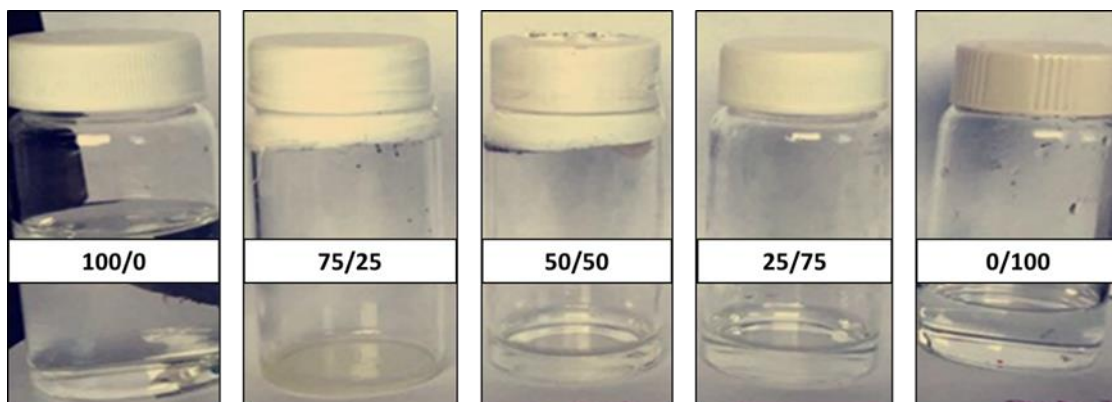


Figure 2. 4. Solution of PVA/PVAc in blends at 12 wt. % concentration in Acetic Acid/Water.

Acetic acid/water is a lower boiling point solvent system in comparison to DMSO. PVA at 88% hydrolysis was soluble in water; and PVAc was soluble in the acetic acid: water mixture. Polymers were dissolved in each solvent system separately before mixing each doped according to a desired polymer-to-polymer ratio. Initially, a cloudy gel was obtained, but the gel became transparent after placing the blended dopes inside the 80 °C oven for 4 h (see dopes in Figure 2.4). These blends of 12 wt% polymer was electrospun. Nanofibers in the range of 70-150 nm in size were observed (see Figure 2.5 and Table 2.2)

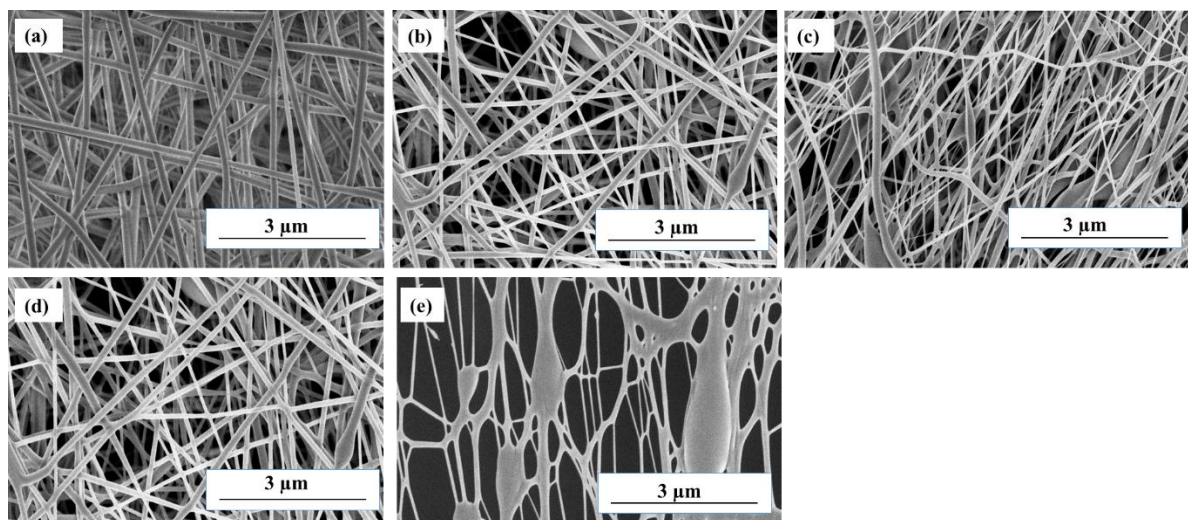


Figure 2.5. Fiber morphology of PVA-blend-PVAc blends (w/w) at (a)100/0 (b) 75/25 (c) 50/50 (d) 25/75 (e) 0/100, solution concentration-12wt%, solvent: Acetic Acid: Water-3:1.

Table 2.2 Electrospun fiber diameters from PVA-Blend-PVAc in Acetic Acid: Water-3:1

| S.NO | PVA- <i>blend</i> -PVAc ratio (w/w) | Fiber Diameter (nm) |
|------|-------------------------------------|---------------------|
| 1 | 100/0 | 164±32 |
| 2 | 75/25 | 111±64 |
| 3 | 50/50 | 78±38 |
| 4 | 25/75 | 63±32 |
| 5 | 0/100 | Not Applicable* |

* Fibers were not spun under these conditions. Coalesced droplets of polymer were found on the collector. Fiber were electrospun on the stainless-steel mesh.

2.3.2 Spectral Characterization of PVA copolymers

PVA was converted into copolymers of PVA-*co*-PVClAc and PVA-*co*-PVIAc, according to the scheme shown in Figure 2.1. IR spectra and calibration curve shown in Figure 2.6 were used to quantify the acetylation of PVA among copolymers of PVA-*co*-PVClAc and PVA-*co*-PVIAc. Commercial powders (PVA, PVAc, and PVA-*co*-PVAc) were used as received. Copolymers derived from PVA were cast as films from aqueous solutions. Chloroacetylation of PVA was expected to enhance the peak intensity of acetate carbonyl groups and reduced peak intensities due to hydroxyl groups. Peak height ratios of OH:C=O did decrease with chloracetylation, as shown in Table 2.3. Although the ratios OH:C=O can provide evidence of acetylation,¹⁰⁴ adsorped moisture can distort their representation of acetylation. Thus, the peak height of acetate carbonyl groups were used to determine acetylation. This technique was previously reported by Baschetti et al- to quantify dilation among polycarbonate, polyvinyl acetate, polyester and urethane carbonyl groups using IR spectra. Diffusion of acetonitrile swelled carbonyl groups of polymer and decreased the intensity of carbonyl -C=O groups within the spot size of IR radiation ¹⁰⁶. IR spectra in Figure 2.6 show sharp peaks at 1733 cm⁻¹ thus confirming PVA acetylation. The calibration curve for

PVA acetylation was based on commercial powders. A C=O peak with negligible intensity were observed for PVA sample as it was 99% hydrolyzed. Acetylation ranged between 11-17%, as reported in Table 2.3. Since copolymers having chloroacetate groups were converted into copolymers having iodoacetate groups, acetylation values for iodo polymers were implicit from the values of chlorinated polymers.

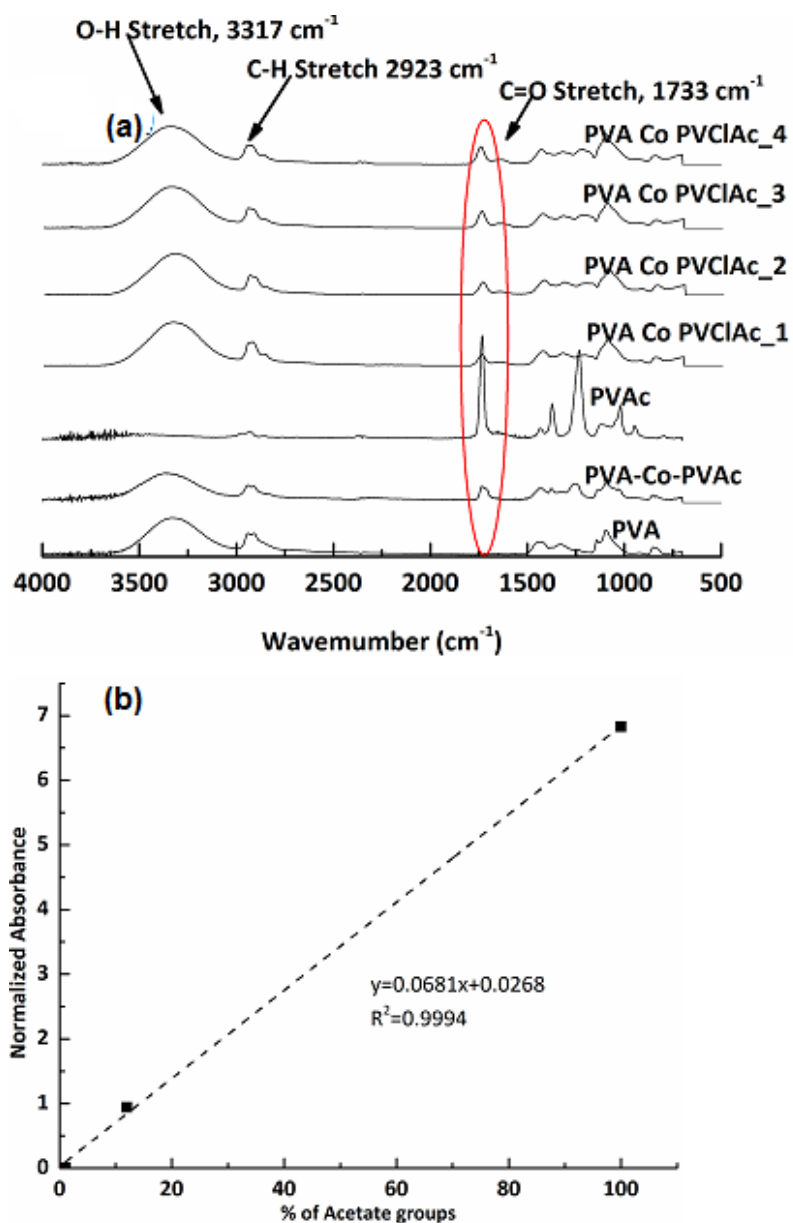


Figure 2.6. IR spectra of commercial polymers (PVA, PVA-co-PVAc, and PVAc) and copolymers of PVA-co-PVClAc are shown in (a). The calibration curve determining chloroacetylation was based upon commercial polymers, which were used as-received.

Table 2.3. Spectral determination of polymer acetylation among commercial polymers and modified PVA

| Sample # | Polymer | -OH Peak Height | -C=O Peak Height | -OH: -C=O Peak Height | Acetylation (%) |
|-----------------|------------------------|------------------------|-------------------------|------------------------------|------------------------|
| 1* | Pristine PVA | 2.23 | 0.01 | 223 | 1 |
| 2* | PVA <i>Co</i> PVAc | 1.52 | 0.94 | 1.61 | 12 |
| 3* | PVAc | 0.19 | 6.84 | 0.03 | 100 |
| 4 | PVA <i>Co</i> PVClAc_1 | 2.93 | 0.75 | 3.90 | 11 |
| 5 | PVA <i>Co</i> PVClAc_2 | 2.77 | 0.84 | 3.29 | 12 |
| 6 | PVA <i>Co</i> PVClAc_3 | 2.80 | 1.09 | 2.56 | 16 |
| 7 | PVA <i>Co</i> PVClAc_4 | 2.58 | 1.16 | 2.22 | 17 |

* Samples 1, 2 and 3 were obtained commercially and used as received.

2.3.3 PVA Copolymer Fiber Morphologies

Aqueous spinning dopes of sample 1-7 in Table 2.3 were prepared in water and subsequently electrosun. Photographs of those spining dopes are shown in Figure 2.7

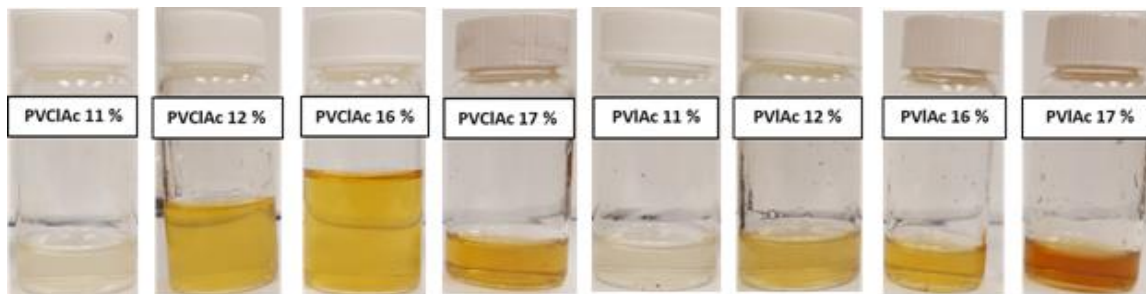


Figure 2.7. Electrospinning dope of PVA copolymers.

PVA and PVA co PVAc were spun into uniform round fibers with diameter of ~150 nm. Among PVA-*co*-PVClAc polymers, electrospun fiber morphology changed from continuous and round fibers to branched and flattened fibers with increase in % functionalization as shown in Figure 2.8. Fibers electrospun from PVA-*co*-PVlAc were similar in diameter to PVA-*co*-PVClAc polymers at 11 and 12% acetylation (see Table 2.4). Branching was observed among fibers produced from 16-17% of chloroacetylation. The copolymer started showing up the amphiphic behaviour and leads to micelles formation. The micelle formation also leads to nonuniformity (presence of lumps) of spinning dope and lead to large standard deviation of fiber diameter. These lumps were very clear and couldn't be observed from the naked eyes.

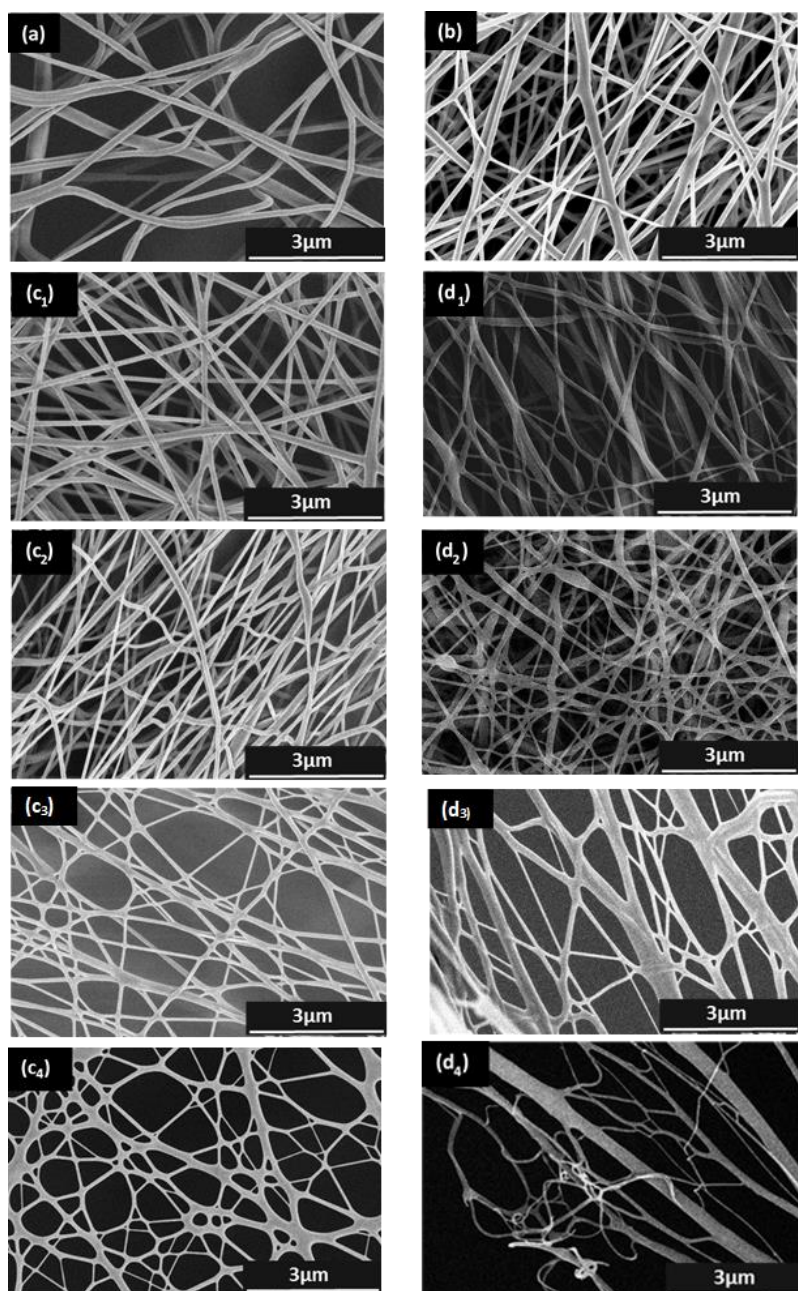
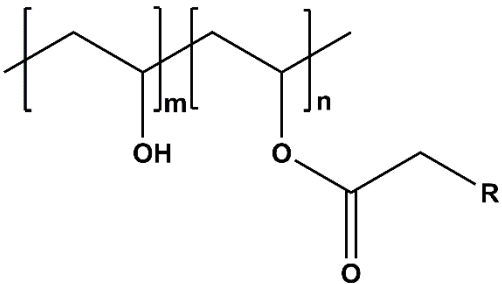


Figure 2.8. Fiber morphology of PVA and its copolymers. (a) Pure PVA, (b) PVA Co PVAc, (c1) PVClAc 11%, (c2) PVClAc 12%, (c3) PVClAc 16%, (C4) PVClAc 17% (d1) PVClAc 11%, (d2) PVlAc 12%, (d3) PVClAc 16% (d4) PVlAc 17.

Table 2.4. Solution Conductivity and electrospun fiber diameter of PVA and its copolymers.

| Sample # | <p style="text-align: center;">Polymer</p>  | Conductivity ($\mu\text{S}/\text{cm}$) | Fiber Diameter (nm) |
|----------|-------------------------------------------------------------------------------------------------------------------------------------|---------------------------------------------|------------------------|
| 1 | m=99, n=1, R=H | 521 \pm 6 | 149 \pm 50 |
| 2 | m=88, n=12, R=H | 371 \pm 3 | 138 \pm 61 |
| 3 | m=89, n=11, R=Cl | 775 \pm 6 | 114 \pm 19 |
| 4 | m=88, n=12, R=Cl | 776 \pm 6 | 93 \pm 30 |
| 5 | m=84, n=16, R=Cl | 962 \pm 3 | 114 \pm 51 |
| 6 | m=83, n=17, R=Cl | 1050 \pm 4 | 158 \pm 76 |
| 7 | m=89, n=11, R=I | 1078 \pm 4 | 100 \pm 50 |
| 8 | m=88, n=12, R=I | 1387 \pm 3 | 76 \pm 30 |
| 9 | m=84, n=16, R=I | 1654 \pm 5 | 151 \pm 82 |
| 10 | m=83, n=17, R=I | 1880 \pm 2 | 123 \pm 102 |

2.3.4 PVA Copolymer Conductivity

Conductivity values for PVA copolymers are given in Table 2.4. The dissolution of PVA in water resulted in a more electrically conductive solution than PVA dissolved in aprotic DMSO. Charge transfer between PVA -OH groups and water contributed to a greater release of charge into solution. Further, the solution conductivity of aqueous PVA was expected to be greater than that of aqueous PVA-*co*-PVAc, which has a lower percentage of electron donating -OH groups.

Conductivity values for PVA copolymers were influenced by the size of the acetate R-groups. In the following order, acetated R-groups of -H, -Cl, and -I increase in atomic and yielded higher values of solution conductivity at similar values of acetylation (Table 2.4). As

the degree of acetylation increased, electron withdrawing -Cl groups increased solution conductivity in water. Electron releasing -I groups resulted in even higher conductivity values than -Cl groups, as acetylation increased from 11 to 17%. Therefore, fiber diameters decreased as the percentage of haloacetate groups increased along the polymer chain. Fiber diameters did not continue to decrease over the entire range of conductivity values for chloro- and iodoacetylated copolymers of PVA. At higher percentage of chloroacetylated (17%) and iodoacetylated (16% and 17%) pendant groups phase separated into polymer rich and solvent rich domains.

The conductivity range of electrospinning dope was too narrow to show any significant effect on the reduction of fiber diameter. All the spinning solutions had conductivity values in the range of 0.5 to 1.8 mS/cm. Son et al. were able to reduce the fiber diameter of polyethylene oxide significantly from 380 microns to 150 microns by varying the solution conductivity in the range of 0.5-1.5 S/cm. Therefore, our solution conductivity was lower than Son et al.'s work by 3 orders of magnitude and did not show any significant effect of fiber size.

2.4 Conclusion

PVA blends and copolymers, having different acetate moieties, were successfully electrospun. These spinning dopes of blends and copolymers varied in their conductivity. However, conductivity ranges were too narrow to affect fiber size upon electrospinning. PVA/PVAc solutions in DMSO showed lower conductivity than PVA copolymers solutions that were spun in water- an aprotic solvent. The diameter of PVA/PVAc nanofibres was affected by intermolecular hydrogen bonding among polymers. PVA/PVAc fiber diameters from DMSO decreased with increases in % of acetate groups: from 1 μm to 730 μm . A higher polymer concentration were employed to optimize the solvent evaporation time of DMSO.

This leads to micron sized fibers with PVA/PVAc dissolved in DMSO. The fiber size was further optimized by dissolving PVA/PVAc blends in binary solvents of acetic acid/water (3:1,v/v). Fiber diameters varied from 63-164 nm using the acetic acid/water solvent systems. PVA was successfully modified with chloroacetate and iodoacetate groups. The solution conductivity of PVA and chloroacetylated PVA and iodoacetylated PVA increased with increasing percentages of chloro and iodoacetate groups along the polymer. At higher degrees of acetylation, aggregation occurred in aqueous spinning dopes. Fiber diameters in the range of 70-150 nm was successfully achieved. No significant change in fiber morphology was observed until 12 % acetylation. However, more than 16 % acetylation led to aggregation and causes irregularities among fiber morphology and branching.

Generally, higher degree of functionalization are desired to maximize the utility of functional nanofibers. However, functionalization led to incompatibility between polar -OH groups and nonpolar pendant -CO₂ CH₂X groups. Therefore, optimization is required for uniform nanofibers, having a narrow fiber diameter and distribution. Aggregation at higher percentages of modification can be avoided by using solvent mixtures to dissolve incompatible blends: Acetone or acetic acid in this case.

CHAPTER 3

MECHANISM OF PROTEIN ATTACHMENT ONTO PVA-PVIAC NANOFIBERS

3.1 Introduction

Functionalized nanofibers are gaining popularity in many applications; such as filtration^{41,107,42}, protective textiles¹⁰⁸, separation and purification^{109,47,84,110,49}. Nanofibers can be functionalized with inorganic particles, enzymes, biological moieties and chemical groups. The functionalization can be done in two ways- in bulk polymer or on the surface of polymer. Proteins are important in our day-to-day life; these are the naturally occurring, building block of human life. Protein separation and purification are important in several applications such as blood purification, toxin removal and biological separation. Protein separation/purification is based upon affinity; such as electrostatic attraction and ion exchange. Affinity by secondary bonding refers to comparatively weak interactions that result in ion exchange, hydrogen bonding, and electrostatic adsorption. This form of intermolecular interaction is a reversible form of binding. This mode of bonding is desired where captured molecules must be recovered, as in the case of blood purification.

On the contrary, primary bonding refers to ionic, covalent or coordination bonds between atoms; this gives irreversible binding between target molecules. This kind of bonding is required where the species for capture is not for toxin removal. In this research, we are focusing on protein attachment using functional nanofibers via covalent bonding. Alkylation of thioether and thiol residues with iodoacetate functionality is a popular chemistry for attaching peptides to polymeric surfaces⁶⁸. Iodoacetic acid is a toxic and highly reactive molecule. Immobilizing iodoacetate functionalities onto polymer backbones make this chemistry more useful.

In this research, we are testing the hypothesis that PVA immobilized iodoacetate groups will bond covalently with thiol and thioether groups along proteins. We have fabricated iodoacetate functionalized, electrospun membranes to achieve the covalent attachment of proteins. The research goal was achieved in three phases. First, PVA was functionalized with iodoacetate groups-^{100,101,88,102,103,104}. Secondly, we electrospun nanofibers and optimized the electrospinning of iodoacetylated PVA to achieve finer diameter fibers as it gives rise to high surface area for protein attachment. Finally, we have selected three target molecules that resembles amino acid residues- these contained thiol and thioether groups. Our target molecules were methionine, glutathione and mercaptoethanol.

3.2 Materials and Methods

3.2.1 Materials

Pure PVA (99% H , MW-89000-98000 g/mol), chloroacetic acid (ClCH_2COOH), L methionine, sodium phosphate buffer (pH 7, 0.1 M), and glutaraldehyde (50% aq. solution) and glutathione were purchased from Sigma Aldrich. Potassium iodide (KI) was purchased from Fisher Scientific. Sulfuric acid (2.5 N H_2SO_4) and isopropanol (>99% purity) were purchased from British Drug House, (BDH). Dimethyl sulfoxide (DMSO) and mercaptoethanol were purchased from Alfa Aesar. Sodium carbonate was purchased from Brenntag Inc. Acetone was purchased from VWR.

3.2.2 Methods

3.2.2.1 Synthesis of Functionalized Polyvinyl Alcohol

The functionalized nanofibers were prepared according to the reaction scheme (Figure 3.1), which was discussed in the previous chapter in detail. The functionalization was confirmed with FTIR spectroscopy and mass spectrometry. 12% iodoacetylation was found optimum for this capture study.

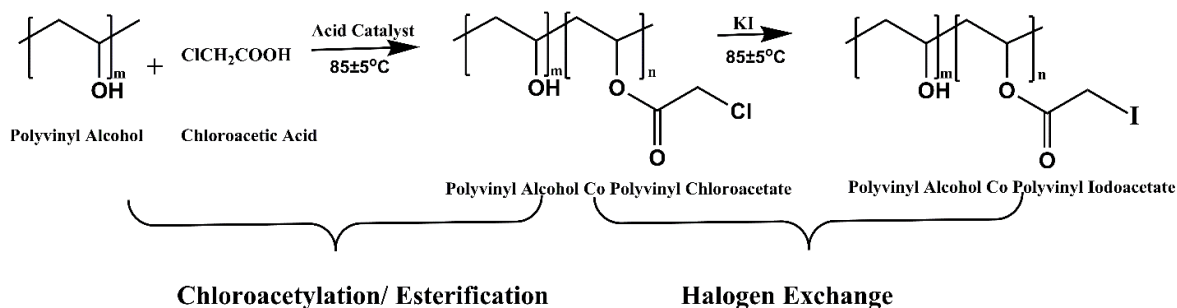


Figure 3.1. Functionalization of PVA for protein attachment.

3.2.2.2 Electrospinning of Functionalized PVA

PVA with 12% iodoacetate groups was electrospun. 11 wt. % polymer was spun using the horizontal electrospinning set up. The applied voltage and tip to collector distance was kept at 15 kV and 12 cm, respectively. Electrospinning was performed at ambient conditions.

The morphology of electrospun nanofibers were imaged with the Verios Field Emission Scanning Electron Microscope (FESEM) at an accelerating voltage of 2 kV and current of 13 mA. Nanofibers were sputter coated with 60/40 Au/Pd for 1 min at 0.7 nm/min before imaging. Image J software was used to measure the diameters of at least 25 fibers per sample.

3.2.2.3 Crosslinking of Nanofibers

Functionalized PVA nanofibers were crosslinked with GA to prevent its dissolution in aqueous environments, as shown in Figure 3.2. 50 mg of functionalized nanofiber was immersed in 2.8 ml of 50% GA solution (300 mM of GA) in 50 ml of acetone with 1 drop of

1N H₂SO₄ for 24 h. After crosslinking, nanofibers were rinsed with acetone three times to remove unreacted GA and then air dried for 24 h. The unreacted glutaraldehyde was further removed from the nanofibers by heating the nanofibers with water for 2 h at 70 °C. This process was repeated three times; then nanofibers were heated at 70 °C for 16 h. The crosslinking of PVA and iodoacetate functionalized nanofibers is shown in Figure 3.2.

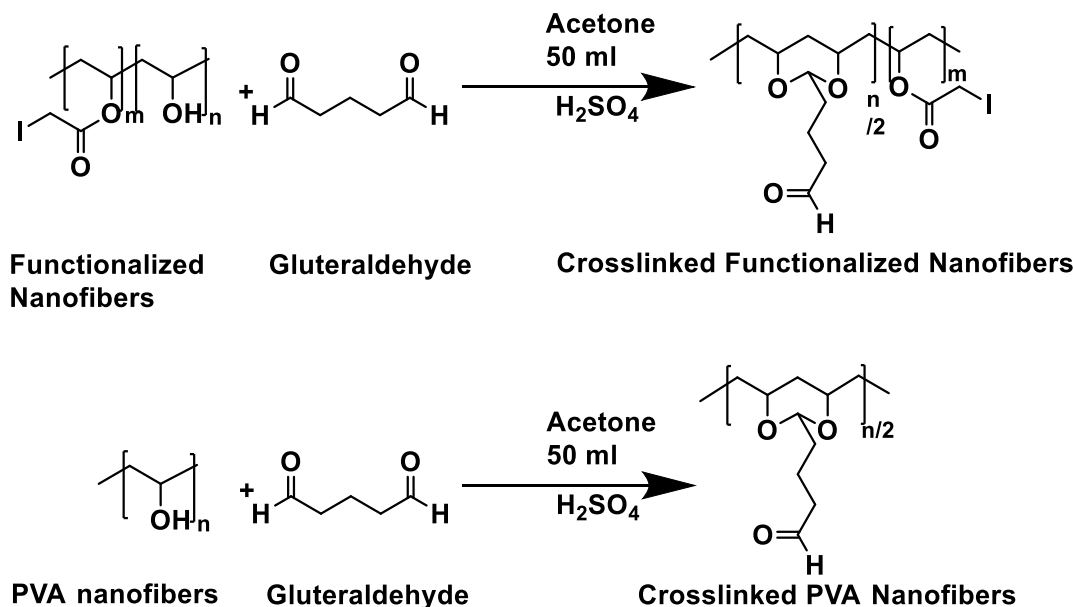


Figure 3.2. Crosslinking of functionalized nanofibers and PVA with GA.

3.2.3 Protein Attachment on Functionalized Nanofibers

Three target molecules (methionine, glutathione – the two amino acids- and mercaptoethanol- the thiol) were chosen for the covalent attachment to iodoacetylated nanofibers (Figure 3.3). To test the protein-attachment, 5 mg of iodoacetylated nanofiber were reacted under three pH values: acidic conditions at $\text{pH } 3.7 \pm 0.4$, neutral conditions at $\text{pH } 7.0 \pm 0.4$, and alkaline conditions at $\text{pH } 9.1 \pm 0.5$ at 37 ± 3 °C for 48 h. The molar ratio of iodoacetate group to thiol/thioether was maintained at 1:2. After reaction, the nanofibrous membrane was removed from solution and rinsed with 5 ml of water under strong agitation- to

remove any of the adsorbed target molecules from the nanofiber surface. This rinsing step was repeated twice with each sample.

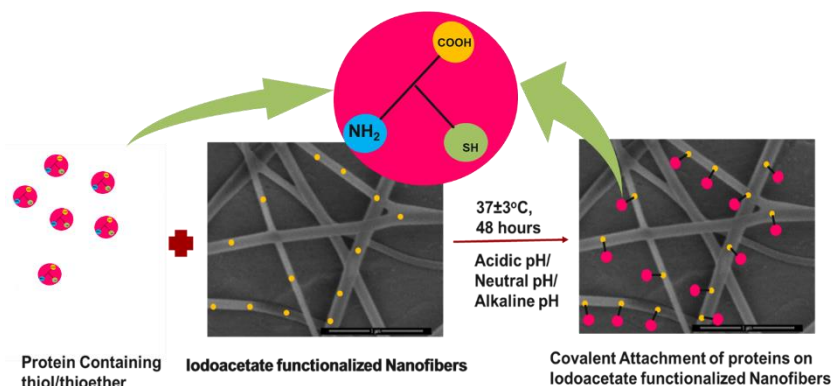


Figure 3.3. Protein attachment on Iodoacetate Functionalized nanofibers.

3.2.4 Characterization of Protein Attachment on Functionalized Nanofibers

The covalent attachment of target molecules onto nanofibers was assessed by two methods. First, the absorbance spectra of target molecule in control solutions- at each pH condition- was measured before reaction with nanofibers using the Varian Cary 3 UV-Vis Spectrophotometer. The absorbance of each target molecule- at each pH condition- after reaction with nanofibers was also measured. Reaction mechanisms were explored including any indication of side products; such as chemical decomposition. Any reduction in the concentration of a target molecule was attributed to the covalent attachment of target molecules onto nanofibers. Measurements were performed in triplicates. Spectra were recorded in the wavelength range of 200-280 nm. Water was used as the blank for all spectra. Additional controls were used to prepare subtraction spectra as further confirmation of reaction versus adsorption.

Secondly, the attachment of amino acids onto nanofibers were also analyzed by FTIR spectroscopy. The covalent attachment of target molecules onto nanofibers formed new chemicals that were measurable by FTIR spectroscopy. Three spectra for each sample were

collected. The spectra of PVA and PVIAC nanofibers were collected before and after their immersion in solutions containing target molecules. The spectra of nanofibers without target attachment was subtracted from the spectra of nanofibers with target attachment to see the effect of new bond formation. All spectra were normalized by the 1433 cm^{-1} peak for C-H bending.

3.3 Result and Discussion

3.3.1 Morphology of Functional Nanofibers

The morphology of functional nanofibers is shown in Figure 3.4. Average fiber diameter of PVA nanofibers was $148 \pm 50\text{ nm}$ and of PVIAC nanofibers was of $76 \pm 30\text{ nm}$. After crosslinking, the fiber diameter of PVA nanofibers was $98 \pm 26\text{ nm}$ and of PVIAC nanofibers was $87 \pm 18\text{ nm}$. Crosslinking PVA hydroxyl groups among functional nanofibers was successful and no significant change was observed in fiber size after crosslinking.

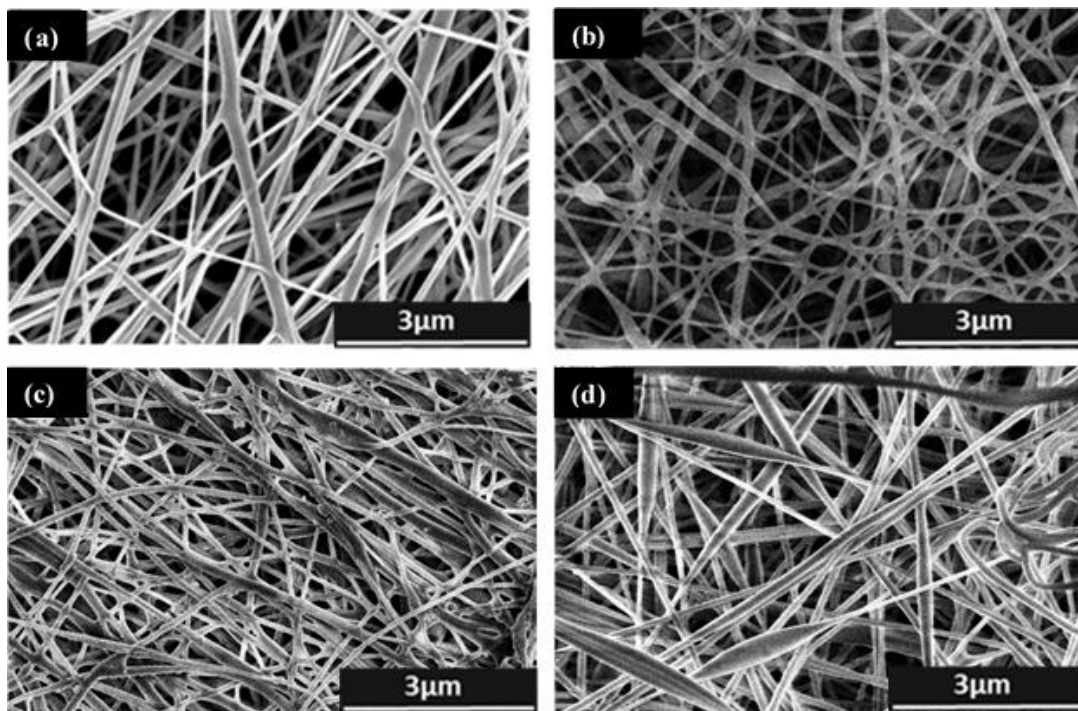


Figure 3.4. Morphology of functionalized nanofibers before crosslinking (a) PVA and (b) PVA-Co-PVIAC and (c) PVA and (d) PVA-Co-PVIAC after crosslinking

3.3.2 Methionine Attachment on Membranes

3.3.2.1 UV-Vis Study of Membranes after Methionine Attachment

UV Vis spectroscopy is a popular characterization technique for qualitative and quantitative analysis. UV-Vis study of methionine attachment to nanofiber is described below.

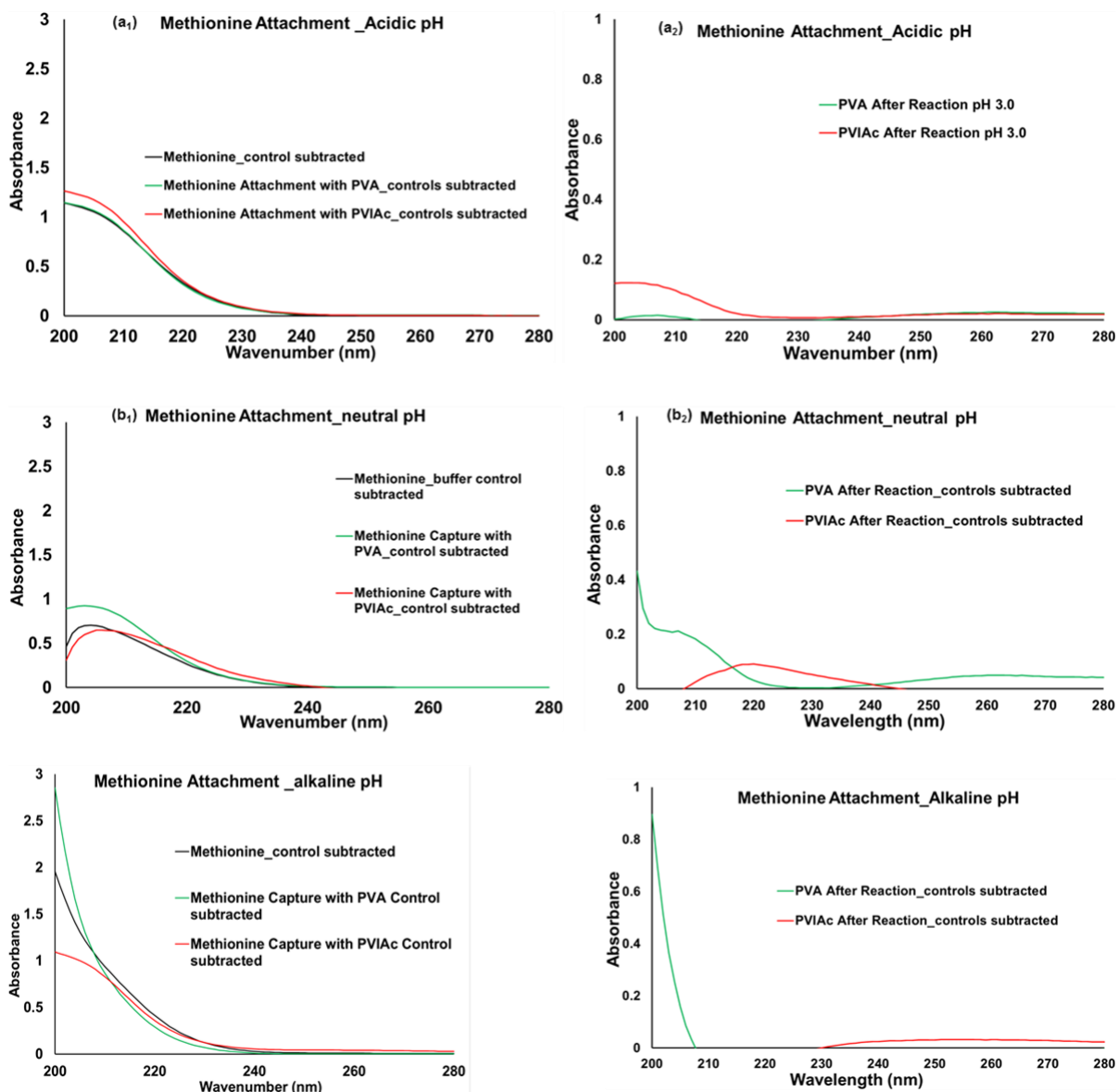


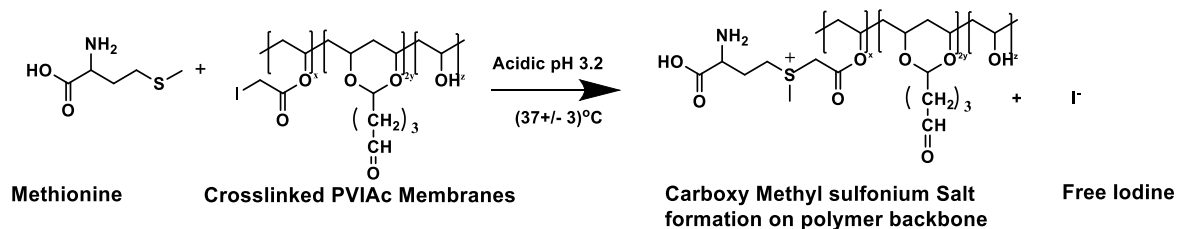
Figure 3.5. Capture of methionine with PVIAC membrane under acidic (a₁&a₂), neutral (b₁&b₂), and alkaline (c₁&c₂) condition.

UV-Vis spectra of methionine reaction with nanofibers are shown in Figure 3.5. The absorbance at 200 nm was used as a reference to comment on the reaction. Changes in absorbance (ΔA) under all pH conditions are shown in Table 3.1.

Table 3.1. Change in UV absorbance after Methionine attachment on membranes

| | ΔA at 200 nm (%) | |
|-----------------|--------------------------------------------|--------------|
| | PVA | PVIAc |
| Acidic | 0 | +9.5 |
| Neutral | +35 | -19 |
| Alkaline | +54 | -46 |

Under acidic condition, PVIAc led to 9.5% increase in absorbance intensity in comparison to the original methionine absorbance spectra- which indicated new reaction products had formed. When iodoacetate reacts with methionine under acidic condition and physiological pH (pH 7.37-7.4 in human blood), carboxymethyl-sulfonium salts form and free iodine releases into the reaction mixture,¹¹¹ as shown in Figure 3.6.

**Figure 3.6.** Methionine Attachment on PVIAc membranes under acidic conditions

The carboxymethyl sulfonium salt is highly unstable in nature and can thermally degrade over time. These reaction by-products could have increased absorbance in the region of interest. In 1959, Gundalch et al. reported the formation of homoserine- a decomposition product of carboxymethyl sulfonium salt⁶⁸ as shown in Figure 3.7-. The increased absorption intensity could also result from the formation of homoserine. In summary, methionine reacted with PVIAc membrane under acidic conditions.

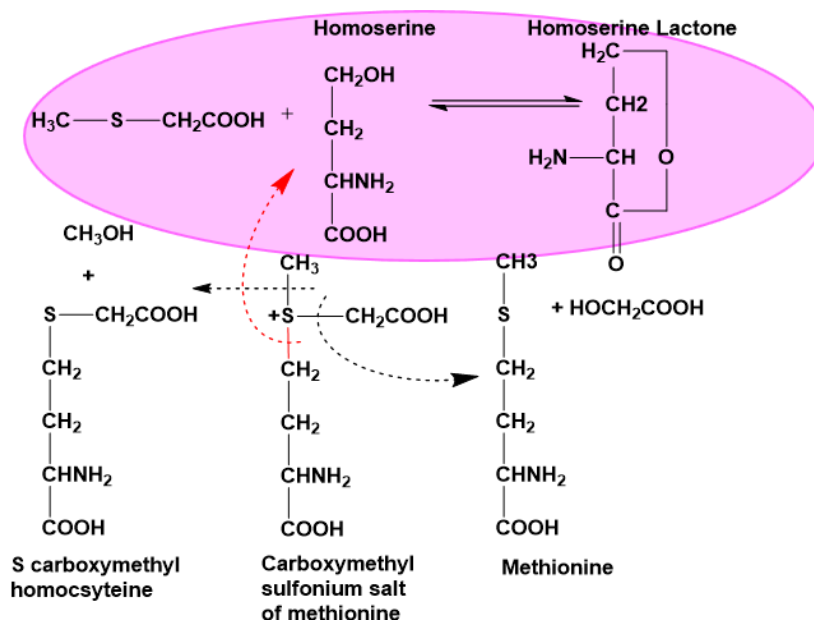


Figure 3.7. Decomposition product of carboxymethyl sulphonium salt⁶⁸.

No significant absorbance increase was observed when methionine was reacted with PVA nanofiber under acidic pH, as shown in Figure 3.5. 0.1 M Sodium phosphate buffer at pH 7.0 was used to analyze methionine reaction under neutral conditions. The absorbance of methionine changed significantly after reaction with both nanofibers: PVA (+35%) and PVIAC (-19%). PVIAC reaction with methionine under neutral and alkaline condition were the same, according to UV Vis results.

In case of PVA, absorbance intensity increased by 35% and 54% under neutral and alkaline conditions, respectively. This was indicative of new reaction products. Control PVA nanofibers contained significant amount of free aldehyde groups- due to GA crosslinking. Destaye et al. (2013) reported the presence of free aldehyde groups along PVA after crosslinking with GA¹¹². Aldehyde groups react with thiol groups at room temperature- under acidic, neutral and alkaline pH conditions- while forming hemithioacetals.^{113,114} Sprung (1939) also reported aldehyde reacted with primary and secondary amines at room temperature and under alkaline and acidic conditions, as shown in the reaction scheme of Figure 3.8.¹¹⁵

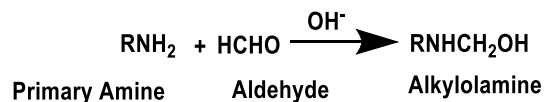


Figure 3.8. Reaction of amine and aldehyde under alkaline pH¹¹⁵.

Therefore, the possible mechanism of reaction- in the presence of PVA nanofibers is shown in Figure 3.9. Methionine Attachment on PVA membrane under neutral and alkaline condition. However, the reason for increased UV absorption of reaction mixture was unknown. Alkaline condition for methionine's covalent attachment with PVIAC membranes was found most suitable because maximum removal of methionine was observed under this condition

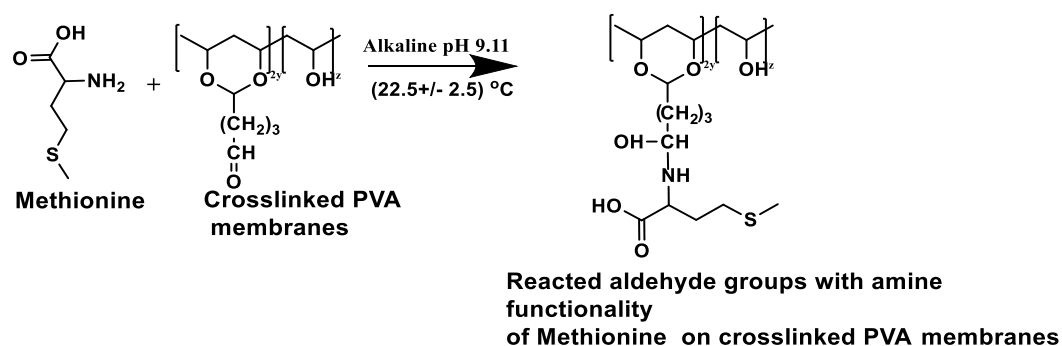


Figure 3.9. Methionine Attachment on PVA membrane under neutral and alkaline condition.

PVIAC membranes also contained significant amount of free aldehyde groups- since it was also crosslinked with GA-. Prior to iodoacetylation, the PVA polymer contained 88% OH groups.

The reaction occurred between the with aldehyde and iodoacetate functionalities of PVIAC with thioether functionality of methionine as shown in Figure 3.10

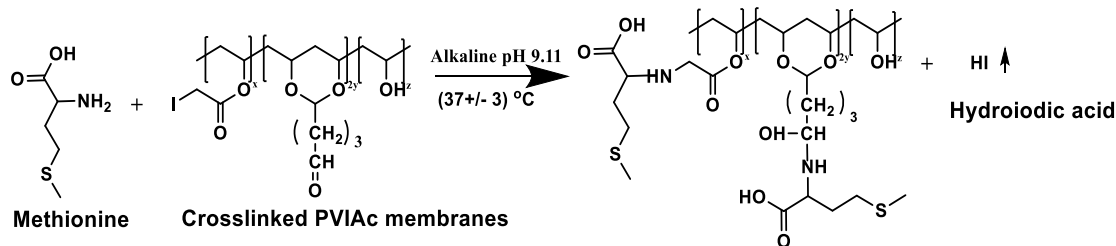


Figure 3.10. Methionine Attachment on PVIAC membrane under neutral and alkaline conditions.

The absorbance decreased by 19% and 46% under neutral and alkaline pH respectively, as shown in Table 3.1, an indication that the methionine was consumed and /removed from solution the reaction mixture after reaction. The alkaline conditions were found. Furthermore, pH reduced as hydroiodic acid (HI) was released upon reaction, see Figure 3.10. However, no reduction in pH was observed under alkaline conditions. UV Vis absorption intensity did not change because HI is a colorless gas.

3.3.2.2 FTIR study of membranes after methionine attachment

To confirm the attachment of methionine onto nanofibers, FTIR was performed before and after attachment to nanofibers. Methionine was reacted with the control PVA nanofibers and functional PVIAC nanofibers. Subtraction spectra were obtained by subtracting the spectra of neat nanofibers without methionine from featuring methionine attachment. Figure 3.11 (a) represents the change in membrane chemistry after methionine attachment under acidic conditions. The bottom curve (black line) is from methionine powder. The green line represents

the subtraction spectra from PVA reacted with methionine, and the pink line represents the subtraction spectra of PVIAC reacted with methionine.

With methionine powder, the peak at 3153 cm^{-1} represents the -NH and -OH stretch. 2914 and 2854 cm^{-1} was due to the increase in -CH stretch after methionine reaction, 2740 cm^{-1} was due to N-CH₃ stretch, 2575 and 1610 cm^{-1} represented the carboxylate ion, and 1425 cm^{-1} was due to the -CH₂ bending.

From the control PVA membrane, we see the peaks at 3426 cm^{-1} - due to -OH and -NH stretch, 2824 cm^{-1} due to the increase in -CH stretch, 1732 cm^{-1} due to -C=O stretch, and 1099 cm^{-1} due to -CN stretch. In the case of reacted PVA membranes, reaction is expected to occur via PVA aldehyde groups with the amine groups of methionine. Therefore, we looked for the formation of new C-N bonds- based on the reaction showed in Figure 3.9.

Under acidic pH, negligible C-N stretch absorbance was observed at $1080\text{-}1360\text{ cm}^{-1}$; however, it could result from the absorption of methionine onto nanofibers. The FTIR result of PVA-Met concurred with UV Vis results, which indicated covalent attachment did not occur under acidic conditions.

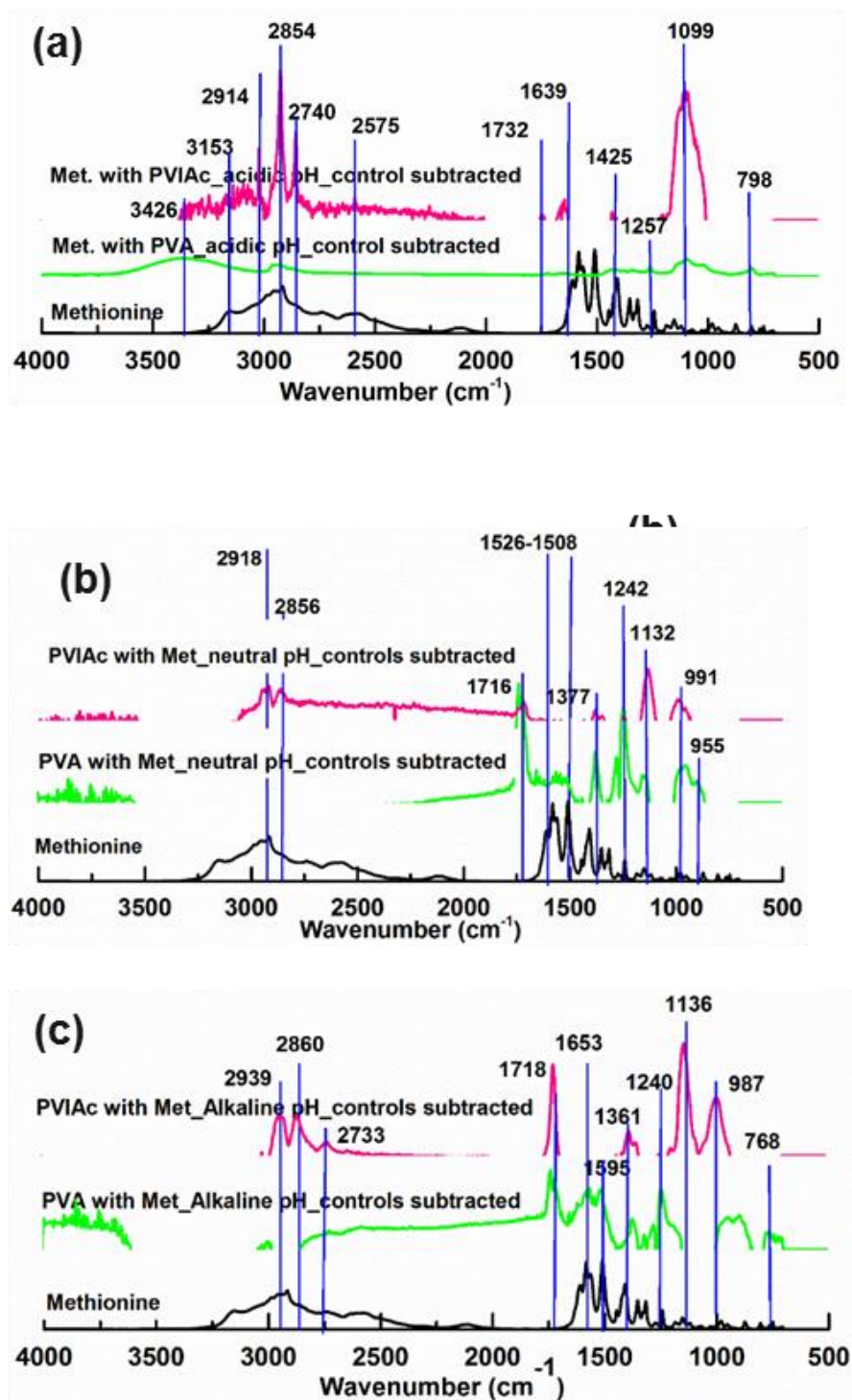


Figure 3.11. Study of change in PVIAC membrane chemistry after methionine attachment under (a) acidic pH, (b) neutral pH, and (c) alkaline pH

Under neutral pH (Figure 3.11), we have found the characteristic peaks for methionine on the nanofiber surface; this confirmed the presence of methionine on both control and functional nanofiber. Additionally, the peak intensity at 1242 cm^{-1} - which represents the C-N bond- increased significantly after exposure to neat PVA nanofibers. Aldehyde groups of crosslinked PVA membranes reacted with amine terminals of methionine and formed -CN bonds on the nanofibers. Under alkaline pH (Figure 3.11), similar results were found at 1240 and 1136 cm^{-1} with PVA and PVIAC respectively. Therefore, it was confirmed that the reaction mechanism of methionine attachment onto nanofibers was the same under neutral and alkaline pH. Under both cases, the reaction occurred via amine terminals, which disagrees with previous literature- that under physiological pH, methionine reacts via sulfur end groups and form carboxymethyl-sulfonium salts¹¹¹. Gundalch et al. have reported the formation of carboxy methyl sulfonium salt is pH independent when methionine reacts with iodoacetate⁶⁸. However, they have taken the iodoacetic acid in excess which formed the carboxymethyl sulfonium salt under alkaline pH. When all the amine groups react with iodoacetate functionality under alkaline condition, the remaining iodoacetate groups reacts with thioethers.

Among functional PVIAC membranes, peaks were observed in the $3426\text{-}3153\text{ cm}^{-1}$ region, which was due to -OH and -NH stretching. The peaks in the range of $2914\text{-}2854\text{ cm}^{-1}$ appeared because of an increase in -CH bonds after methionine attachment. Peaks at 1732 and 1639 cm^{-1} was due to -C=O stretch. The peak at 1425 cm^{-1} was due to increase -CH₂ groups and 1099 cm^{-1} was due to C-N stretch. No -C-S bond ($\sim 700\text{ cm}^{-1}$) was observed among either spectra of PVA and PVIAC nanofibers. -C-S absorbance appears in the finger print region, but its absorbance could be found among subtraction spectra.

Under neutral and alkaline pH reactions with PVIAC nanofibers, methionine amine groups reacted with aldehyde and iodoacetate groups of crosslinked PVIAC nanofibers, which contained free aldehyde groups. Because of the two reacting groups (aldehyde and iodoacetate) a strong peak appeared at 1136 cm^{-1} . Researchers proved -CN stretching occurs under a broad range: $1050\text{-}1250$.^{116,117} Therefore, FTIR results indicated the formation of new -C-N bonds and secondary amine -N-H bonds on nanofibers, as the result of aldehyde and iodoacetate reactions with amines.

In summary, traces of methionine were found on the surface of nanofibrous membranes by absorption, as in the case of PVA, or due to absorption and chemical attachment. The -C-N stretch from reacted PVIAC nanofibers was observed at 1099 cm^{-1} was significantly larger when compared to reacted PVA nanofibers; thus, more methionine was present on PVIAC than the control PVA nanofibers. No change in bonding occurred after reaction; it was hard to confirm the covalent attachment of methionine onto PVIAC. With the help of FTIR, reaction under acidic conditions were possible. Secondary amine peaks signaled the reaction between methionine and PVIA nanofibers under neutral and alkaline conditions.

3.3.3 Mercaptoethanol Attachment on Membranes

3.3.3.1 UV-Vis Study of Membranes after Mercaptoethanol Attachment

UV-Vis study of membranes after mercaptoethanol attachment was studied. Mercaptoethanol reacted with PVIAC functionalized nanofibers under acidic, neutral and alkaline pH. The change in UV-Vis absorbance at 200 nm was used to analyze the occurrence of reaction, as shown in Table 3.2.

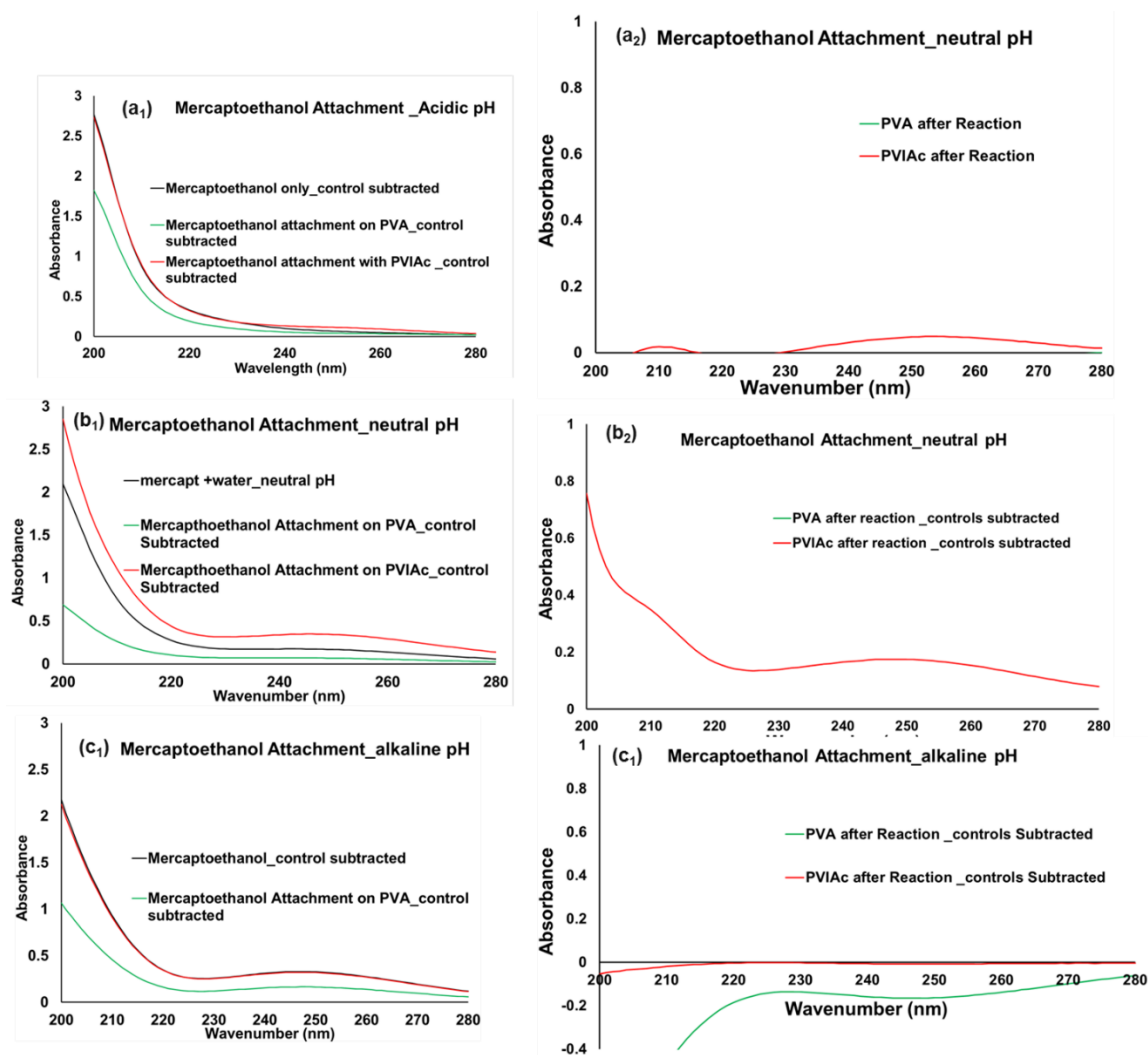


Figure 3.12. Mercaptoethanol capture with PVIAC membrane under acidic condition (a1&a2), neutral condition (b1&b2) and alkaline condition (c1&c2).

Table 3.2. Change in UV absorbance after Mercaptoethanol attachment on membranes

| | ΔA at 200 nm (%) | |
|-----------------|--------------------------|-------|
| | PVA | PVIAc |
| Acidic | -36 | +75 |
| Neutral | -60 | +104 |
| Alkaline | -50 | -2 |

PVA membranes showed decrease in absorbance after reaction under all conditions. See the possible reaction mechanism in Figure 3.15.

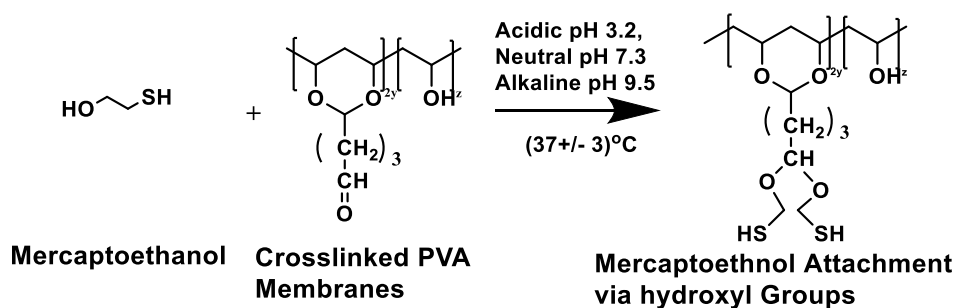


Figure 3.13. Mercaptoethanol attachment on PVA membranes.

Hydroxyl groups of mercaptoethanol reacted with the aldehyde groups of PVA membranes under all reaction conditions, as shown in Figure 3.15. Maximum attachment of mercaptoethanol was achieved under neutral condition.

When PVIAc membranes were reacted under acidic and neutral condition, the absorbance of reaction mixture increased by 75% and 104% respectively. This was indicative of reagent degradation or reaction by-products. One possible mechanism of reaction would

result from the autooxidation of mercaptoethanol into disulphanediylldimethanol, which is catalyzed by iodide ions as shown in Figure 3.14

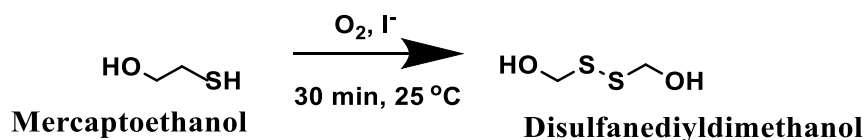


Figure 3.14. Mercaptoethanol oxidation in the presence of Iodide ion¹¹⁸.

Under alkaline pH, absorbance intensity lightly reduced by 2%. It seems two reactions were occurring simultaneously: oxidation of mercaptoethanol (as shown in Figure 3.14) which leads higher UV Vis absorbance, and the covalent attachment of mercaptoethanol onto PVIAC (shown in Figure 3.15), which leads to reduced absorbance. As a result, negligible or low intensity changes were noticed.

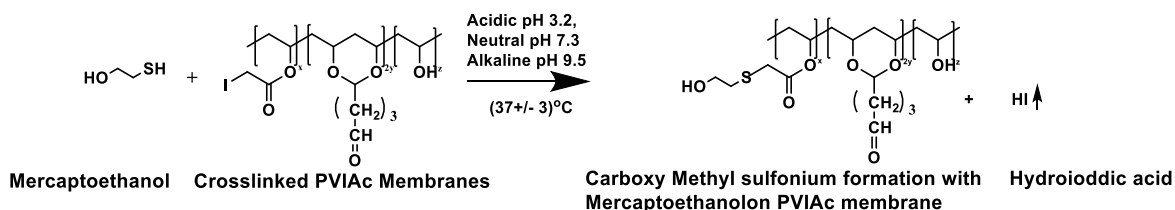


Figure 3.15. Mercaptoethanol attachment on PVIAC membranes.

3.3.3.2 FTIR Study of Membranes After Mercaptoethanol Attachment

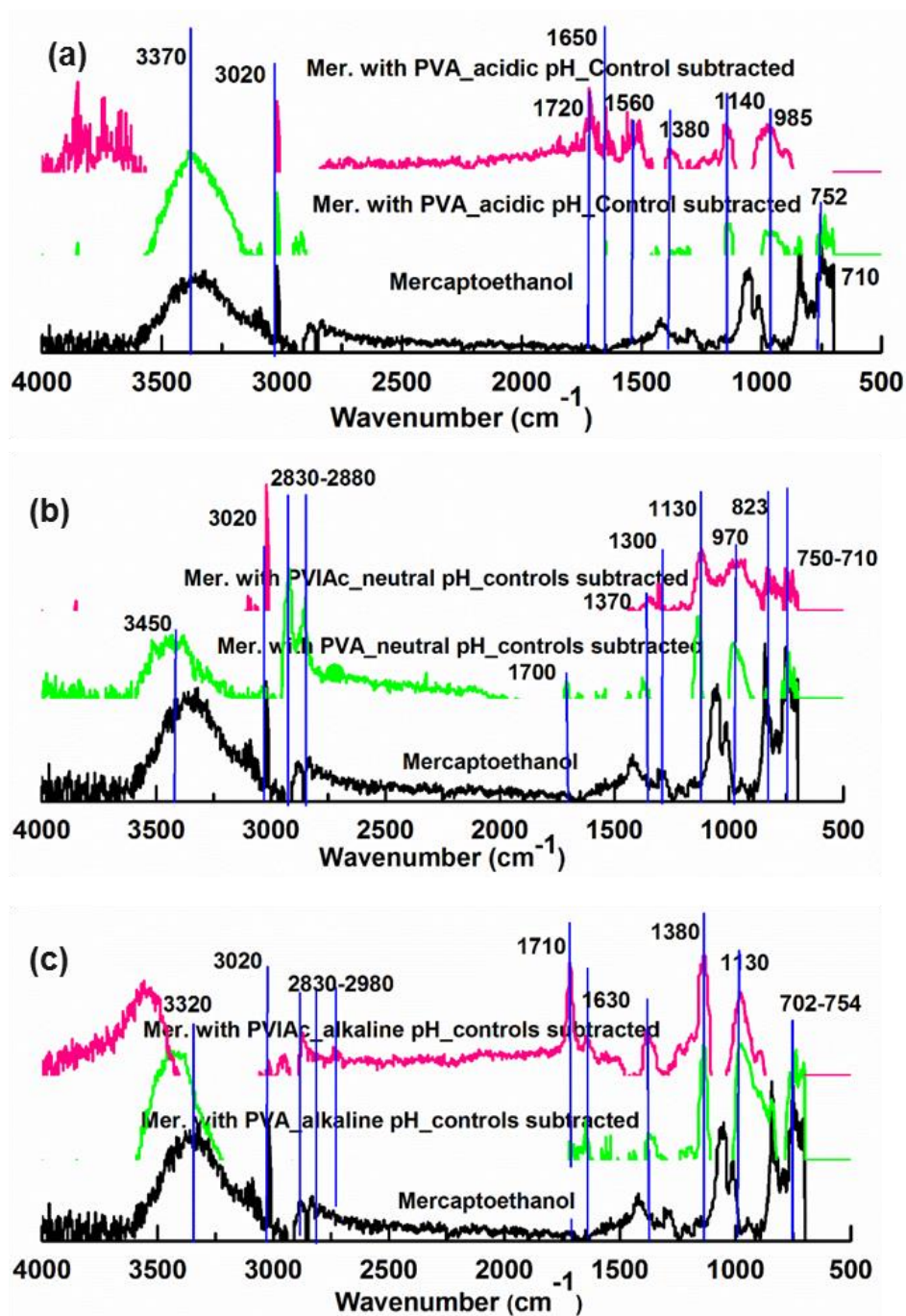


Figure 3.16. Study of change in PVIAC membrane chemistry after mercaptoethanol attachment under (a) acidic, (b) neutral, (c) alkaline conditions.

To evaluate mercaptoethanol attachment by functional nanofibers, FTIR spectra (in Figure 3.16) were analyzed. The characteristic peaks were found at 3320, 3090, and 3020 cm^{-1} .

¹ for -OH stretching; 2880 and 2830 cm⁻¹ for -C-H stretching, and 1420 cm⁻¹ for -CH₂ bending; 1300 and 1210 cm⁻¹ for -OH bending; 1160 cm⁻¹ for -CH₂ twisting; 1010 - 1050 cm⁻¹ for C-O stretching, 843 - 945 cm⁻¹ for -CH₂ rocking, 752 cm⁻¹ for -C-SH bending; and 710 cm⁻¹ for -C-S stretching. Absorbance peaks for -S-H were not visible in the region of 2555 cm⁻¹ due to noise. IR absorbance related to -C-SH bending and -C-S stretching were of interest to distinguish between mercaptoethanol adsorption to nanofibers versus its covalent attachment. If mercaptoethanol only absorbed only onto nanofibers, then the -C-SH bending peak should be present among IR spectra. However, if the reaction occurred between functional nanofibers and mercaptoethanol via thiol groups, then thiols should have converted to thioethers, as shown in Figure 3.15.

Under acidic condition, PVA nanofibers showed peaks at 3370, 3020, 2940, 985, 752 and 710 cm⁻¹ due to -C-S stretching. In this case, the peak at 752 cm⁻¹ corresponded to C-SH bending, which indicated mercaptoethanol did not attach covalently via thiol groups. In the case of PVIAC nanofibers, mercaptoethanol was present among nanofibers as confirmed by characteristic peaks at 3700, 3020, 1380, 1140 and 985 cm⁻¹ that are due to -OH stretching, -OH bending, -CH₂ twisting and rocking. No peaks were observed near ~750 cm⁻¹, which indicates the disappearance of -C-SH vibrations. This suggests the covalent attachment of mercaptoethanol onto PVIAC nanofibers may have occurred.

Under neutral condition (Figure 3.16), PVA as well as PVIAC nanofibers had shown only traces of mercaptoethanol, but covalent attachment was not confirmed as denoted by peaks intensities around ~750 cm⁻¹ for and-C-SH bending.

The results of reaction under acidic and alkaline conditions were similar. In both cases, mercaptoethanol was absorbed by PVA and it covalently attached to PVIAC. Since the ~750 cm⁻¹

¹ peak disappeared among PVIAC nanofibers, -SH bonds may have converted to -CSC bonds. However, C-S bonding was not visible around 710 cm⁻¹. In summary, the possibility of covalent attachment between mercaptoethanol and PVIAC was observed. Neat PVA nanofibers had shown the presence of mercaptoethanol after reaction, which was attributed to reactions between hydroxyl and aldehyde groups; C-SH absorption peaks near ~750 cm⁻¹ were present in all cases.

3.3.4 Glutathione Attachment on Membranes

3.3.4.1 UV-Vis Study of Membranes after Glutathione Attachment

Glutathione was reacted under acidic, neutral, and alkaline pH with nanofibers. Changes in UV Vis absorbance intensities as the result of reaction are shown in Table 3.3.

Table 3.3. Change in UV absorbance after Glutathione attachment on membranes

| | ΔA at 200 nm (%) | |
|-----------------|-------------------------|--------------|
| | PVA | PVIAC |
| Acidic | -11 | -13 |
| Neutral | +25 | +42 |
| Alkaline | +12 | +14 |

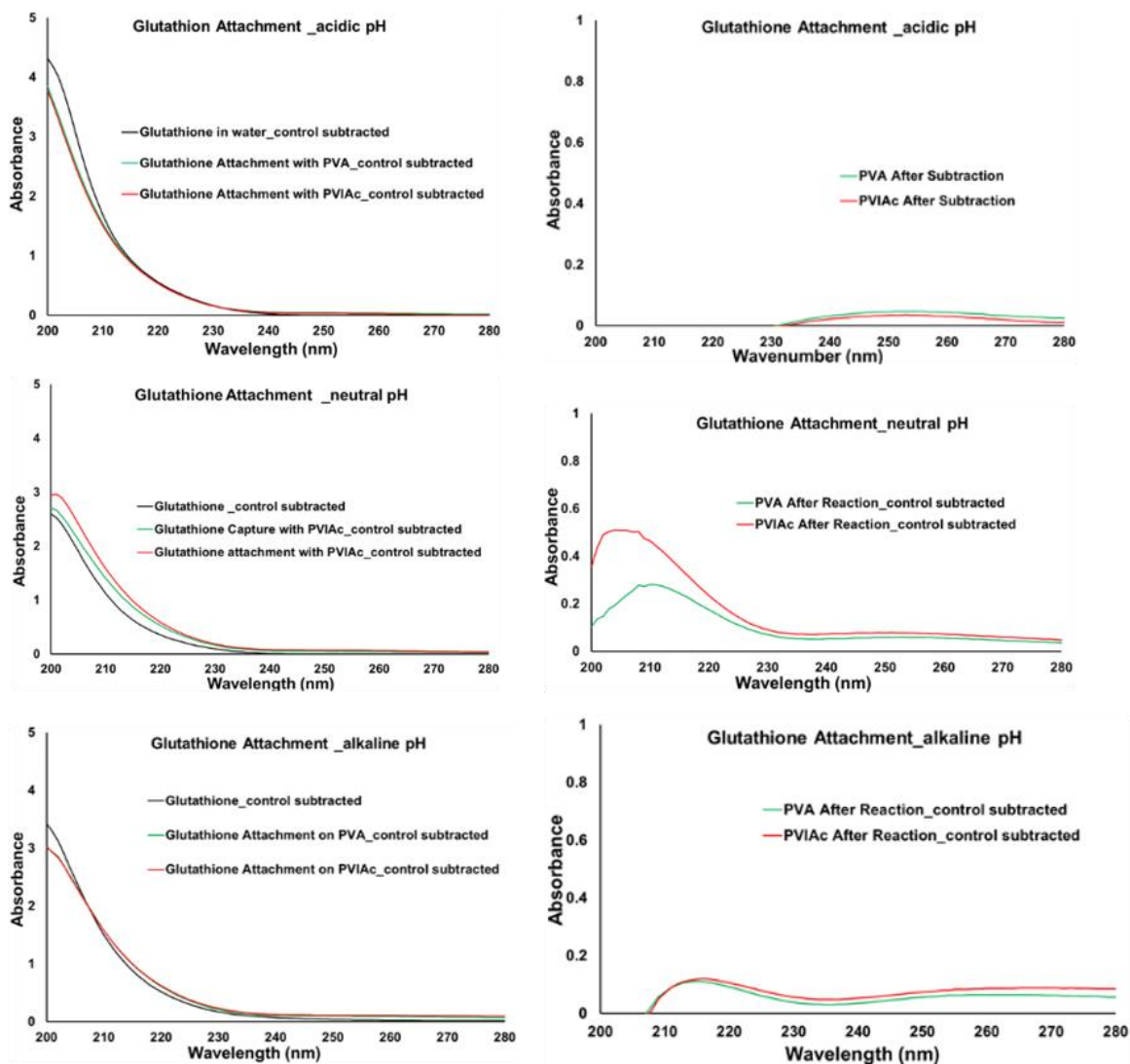


Figure 3.17. Glutathione Capture with PVIAC membrane under acidic (a1&a2), neutral and (b1&b2, and alkaline (c1&c2) condition.

Under acidic pH, absorbance due to glutathione reaction with PVA dropped by 11 %, as shown in Table 3.3

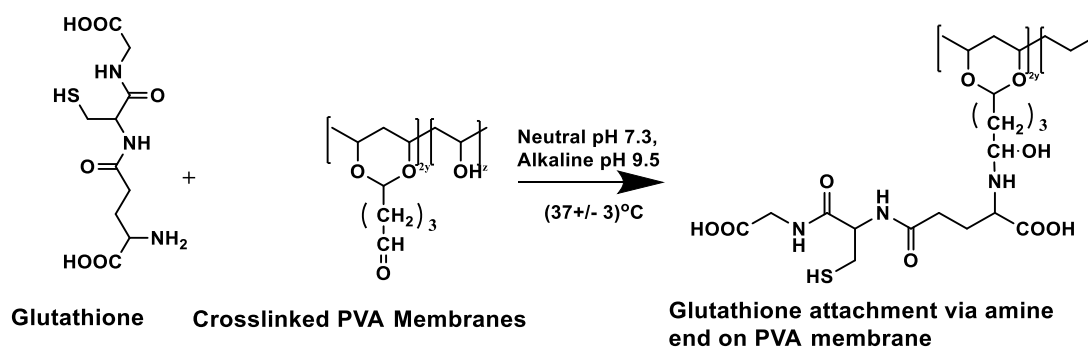


Figure 3.18. Glutathione attachment on PVA membranes under neutral and alkaline pH.

Under neutral and alkaline conditions, the UV Vis absorbance increased by 42% and 14% as the result of reaction. This behavior was indicative of side reactions. Glutathione can undergo oxidation in the presence of iodide ions, as shown in Figure 3.19.

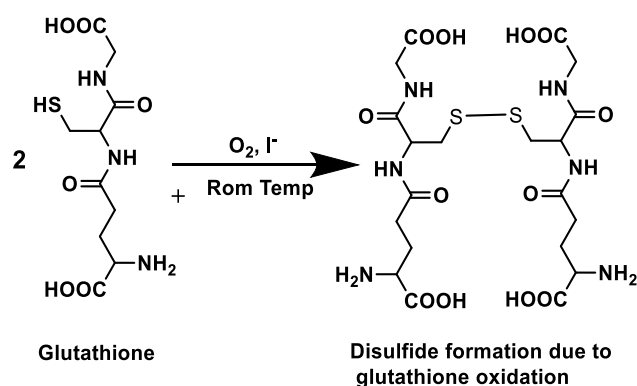


Figure 3.19. Glutathione oxidation under mild conditions

In the case of PVIAC nanofibers under acidic conditions, UV Vis absorbance dropped by 14% after reaction. The thiol group can react with iodoacetate functionalities, thus forming carboxymethyl-sulfonium salts on the backbone of PVIAC, as shown in Figure 3.20. Under neutral and alkaline conditions, the absorbance of increased by 42% and 14%, respectively after reaction. These results resembled those obtained for PVA-glutathione reaction. It seems glutathione was highly prone to oxidation under neutral and alkaline conditions; oxidized is described in the reaction scheme shown in Figure 3.19. The presence of iodide ions further catalyzed the reaction.¹¹⁹ Under alkaline conditions, glutathione oxidation and its covalent

attachment to PVIAC nanofibers occurred (Figure 3.21); this resulted in lower percentages of unreacted glutathione in solution.

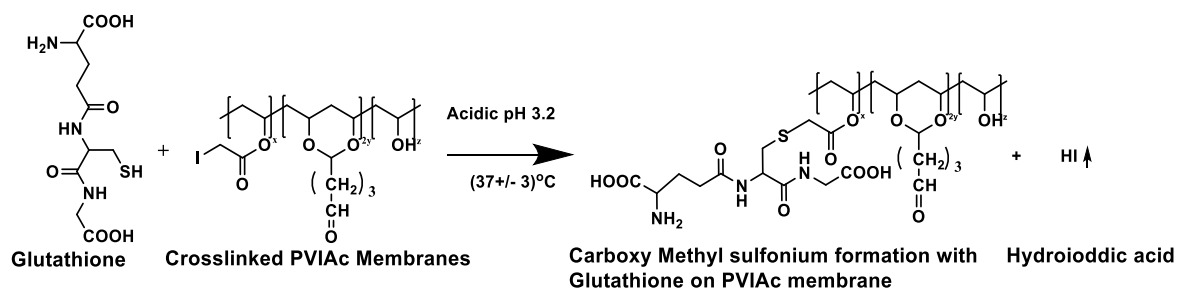


Figure 3.20. Glutathione attachment on PVIAC membranes under acidic pH.

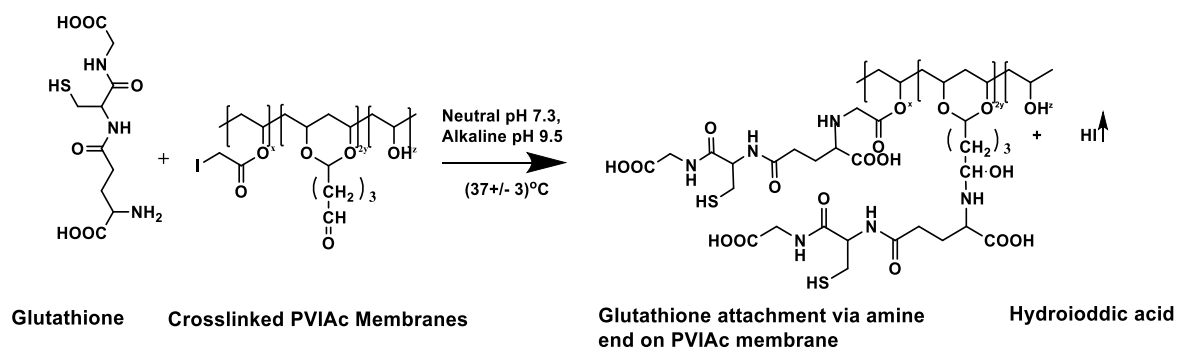


Figure 3.21. Glutathione attachment on PVIAC membranes under neutral and alkaline pH.

3.3.4.2 FTIR Study of Membranes after Glutathione Attachment

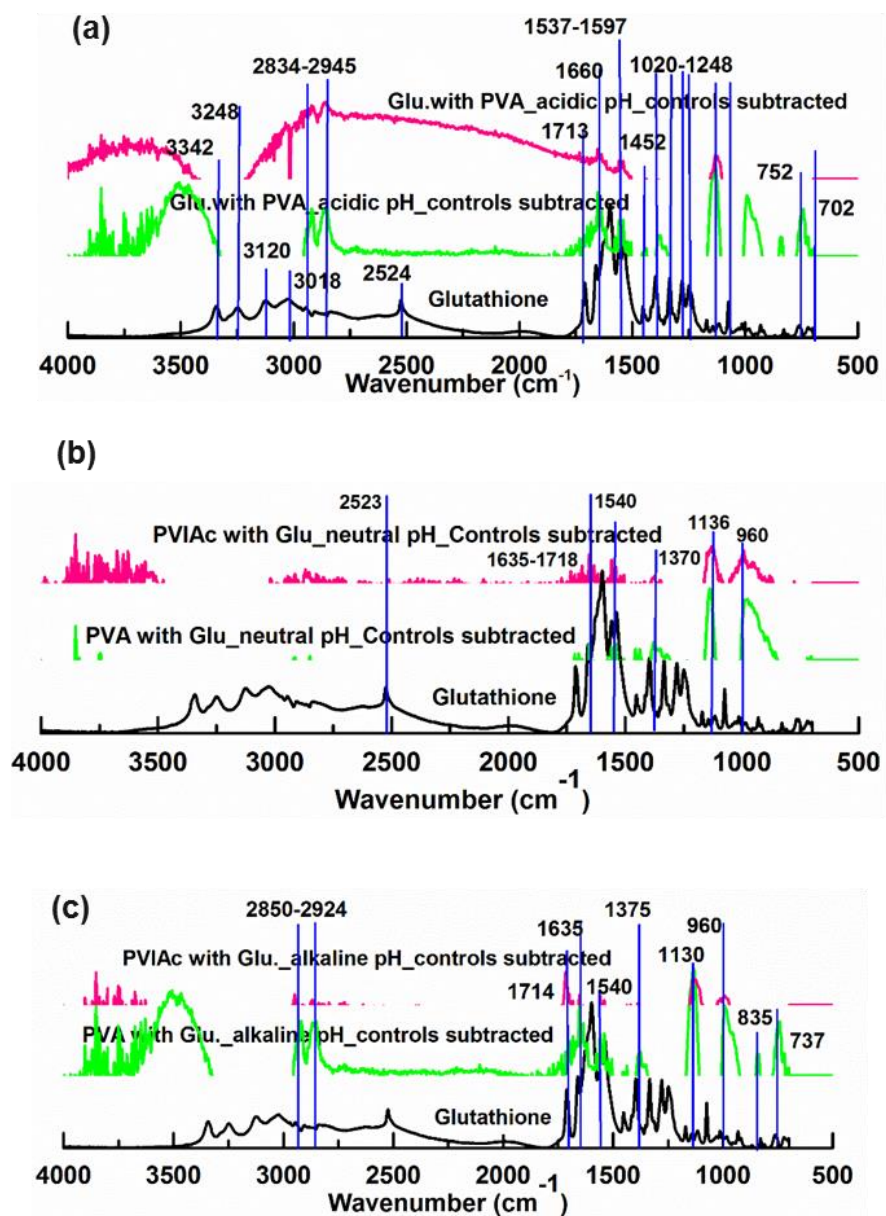


Figure 3.22. IR study of PVIAC reaction chemistries after glutathione attachment under (a) acidic, (b) neutral, and (c) alkaline conditions.

Figure 3.22 shows the FTIR spectra of PVA and PVIAC nanofibers after glutathione attachment under acidic, neutral and alkaline conditions. Glutathione had characteristic IR peaks at 3018 and 3248 cm^{-1} due to -NH and -OH stretching, respectively; 2834-2945 cm^{-1} due to -CH stretching; 2524 cm^{-1} due to -S-H stretching; 1713 and 1660 cm^{-1} due to C=O stretching; 1537 - 1597 cm^{-1} due to -NH bending; 1452 cm^{-1} due to -CH₂ bending; 1020-1248 cm^{-1} due to -C-N stretching; 752 cm^{-1} due to -C-SH bending; and 702 cm^{-1} due to C-S stretching. Among all these peaks, -C-SH bending and -C-N stretching peaks were used to understand mechanisms of glutathione attachment. If glutathione covalently attached to PVIAC via its thiol groups, then the thiol group should convert to thioether groups, as shown in Figure 3.22. Additionally, -S-H stretching should disappear from the IR spectra. If covalent attachment of glutathione to PVIAC nanofibers via the amine, then the intensity of the primary amine absorbance intensity should decrease as the secondary amine peak increases.

Under all pH values, the presence of glutathione on nanofibers was confirmed, as noted by the presence of glutathione's characteristic peaks. Under acidic pH, -S-H and -C-SH vibrations were not observed- where reaction would occur via the thiol. Additionally, the peak intensity at $\sim 1130 \text{ cm}^{-1}$ increased, which suggests -C-N bonds had formed. The C-N bond could result from glutathione absorption or its covalent bonding with nanofibers. C-N stretching among primary amines appear at 1050 cm^{-1} and secondary amines appear at $\sim 1140 \text{ cm}^{-1}$.¹²⁰ In the case of PVA and PVIAC, the strongest peaks appeared at $\sim 1130\text{-}1140 \text{ cm}^{-1}$, which is indicative of secondary amines along reacted nanofibers. Researches have reported amine groups can react with aldehyde and iodoacetate groups under alkaline condition. However, in this research, we also observe this reaction under acidic conditions. The steric preference of amine groups towards reaction may explain why this reaction was feasible under acidic

conditions as well. -SH vibrations around 2530 cm^{-1} were not observed among PVA or functionalized nanofibers. Thiol-aldehyde reactions as well as thiol-iodoacetate reactions, which are usually acid catalyzed, occur at room temperature. Reaction products are in the form of hemi-thioacetal intermediates and dithioacetal as the final product. Hemi-thioacetals are very unstable and readily dissociate into thiols and aldehydes.¹²¹ Upon reaction, thiol groups are converted to thioether groups. Therefore, vibrations related to -SH stretching and -C-SH bending should disappear if this reaction happens. The results from glutathione attachment were the same for both neutral and alkaline conditions. In all cases, the -SH vibration peak and -C-SH vibration peak disappeared, and -CN stretching appeared upon reaction. Thus, the reaction between nanofibers and glutathione were pH independent. Glutathione is a bulky molecule in comparison to methionine and mercaptoethanol; its reaction with nanofibers occurred over 48 hours and the steric preference of amine-iodoacetate and thiol-iodoacetate reactions occurred irrespective of pH. Additionally, amine groups also reacted with the aldehyde groups of both PVA and PVIAc nanofibers.

3.4 CONCLUSION

Protein immobilization onto surfaces is a popular technique for making functional materials that have use in many applications. Iodoacetate functional groups was successfully synthesized on PVA polymer via chloroacetylation and halogen exchange reaction. Protein attachment was performed on 12% iodoacetylated nanofibers, having diameters less than 100 nm. Crosslinked PVA-based nanofibers had free aldehyde groups. These aldehyde groups were reactive with amine and thiols groups, which are commonly among proteins. The confirmation of protein attachment was performed using two methods. First, changes in UV Vis absorbance were analyzed upon reaction. The covalent attachment of target molecules was expected to reduce

UV Vis absorbance intensities- as the concentration of target molecules reduced. In contrast, the absorbance intensities increased when methionine and glutathione reagents were used. The decomposition/oxidation of those reagents increased absorbance intensities.

Secondly, FTIR spectroscopy was used to confirm the covalent attachment of proteins onto nanofibers. FTIR was chosen because it would aid the identification of new covalent bonds between protein and nanofibers. As confirmed by IR spectroscopy, methionine as reacted with nanofibers under neutral and alkaline conditions. The amine-iodoacetate reaction that was associated with methionine attachment resulted in secondary amine peak among the IR spectra. Methionine reactions via thiol-iodoacetate groups were not confirmed, because both the reactant and product would have thioether bonds. In the case of mercaptoethanol, covalent attachment occurred under acidic and alkaline conditions. The absorbance peak due to C-SH disappeared as thiol groups were converted to thioether groups upon attachment. Glutathione attached to nanofibers via iodoacetate and aldehyde functional groups under all pH conditions. Glutathione is bulky and has a larger molar mass than methionine and mercaptoethanol. The steric positioning of amine groups causes reaction between amine-thiol groups under acidic conditions- although literature has noted amine-thiol reactions under alkaline pH. In summary, our hypothesis that the covalent attachment of proteins- containing thiol, thioether and amine groups- to nanofibers is possible when polymer is synthetically modified with iodoacetate groups.

CHAPTER 4

IMMOBLIZATION AND ENZYMATIC ACTIVITY OF GOX ON FUNCTIONAL PVA BASED NANOFIBERS

4.1 Introduction

The immobilization of enzymes onto polymeric surfaces is very popular; especially for applications in diagnostics, bio-affinity chromatography, and biosensors^{122,123,124}. Enzyme biocatalysts are active under mild conditions, are very specific in terms of their activity, and are sensitive to storage conditions. Denaturing among enzymes is a very serious problem because it inhibits activity that takes places in specific cavities of the enzyme. The isolation of active enzymes from inactive enzymes is very high; thus, it is very difficult to recover active enzymes from a mixture¹²⁵. A motivation for work on enzyme immobilization is to enhance enzyme activity and its resistance to denaturing through conjugation.^{125,126}

Researchers have tried to immobilize enzymes onto electrospun nanofibers. Glucose isomerase, amino acid acylase, nitrile hydratase, and glucose oxidase (GOx) have been used.^{122,127,128,129} GOx is catalyzes glucose oxidation into gluconic acid and hydrogen peroxide in the presence of molecular oxygen, i.e. an electron acceptor.¹³⁰ Chemically, GOx is made with two identical polypeptide units. Each unit has a molecular weight of 80 kDa, are linked together by disulphide bonds, and contain three moles of cysteine per mole of enzyme.^{130,131} GOx has been immobilized onto various surfaces; such as nanowires, nanotubes, and nanofibers^{123,124,127}. GOx attachment to surfaces has occurred via adsorption, blending, or adsorption which is followed by crosslinking^{128,129,132,133}. Less work has focused on the covalent attachment of GOx to a surface. Zhao et al. attached GOx to polyaniline nanofibers covalently by reacting its -NH₂ groups with nanofibers functionalized with -COOH groups.¹²⁷

Kim et al. also proved that immobilized GOx (covalently crosslinked to a surface) had improved activity.¹³³

The reaction of iodoacetate groups with amine and thiols groups are well-known chemistries for protein purification and separation.⁶⁸ Iodoacetate groups can react with thiol or amine functional groups covalently; it is just a matter of its pH dependence.^{134,111} Researchers have iodoacetic acids and iodoacetamides for protein reaction; however, these small molecules are highly toxic, corrosive, and contaminate protein residues after exposure.¹³⁵ One method of dealing offsetting the harmful effects of small molecule, alkylating reagents is to immobilize them on polymeric materials. To the best of our knowledge, iodoacetate functionalities have never been used to immobilize proteins onto nanofibers.

In this research, we have synthetically modified PVA polymers with iodoacetate groups and fabricated electrospun nanofibers from them. These functional nanofibers will be used to attach polypeptides or proteins covalently.

4.2 Materials and Methods

4.2.1 Materials

Pure PVA was purchased from Sigma Aldrich. Chloroacetic acid (ClCH_2COOH from Sigma Aldrich), potassium iodide (KI from Fisher Scientific), sulfuric acid (H_2SO_4 having normality of 2.5 N from British Drug House, BDH), and dimethyl sulfoxide (DMSO from Alfa Aesar) were employed in the synthetic functionalization of PVA. Sodium carbonate (from Brenntag Inc.), isopropanol (>99% purity from BDH) and deionized water were used to purify polymers. Glutaraldehyde (GA) solution 50 % in water was purchased from Sigma Aldrich, Acetone was purchased from VWR. GOx was purchased from Tokyo Chemical Industries (TCI). Acid blue 25 dye was purchased from Sandoz.

4.2.2 Methods

4.2.2.1 Functionalization of PVA for Enzyme Attachment

Functionalized nanofibers were synthesized according to the reaction scheme in Figure 4.1, which was discussed in Chapter 2. Chemical functionalization was confirmed by FTIR spectroscopy and mass spectrometry. 12% iodoacetylation was found to be optimum for the capture study.

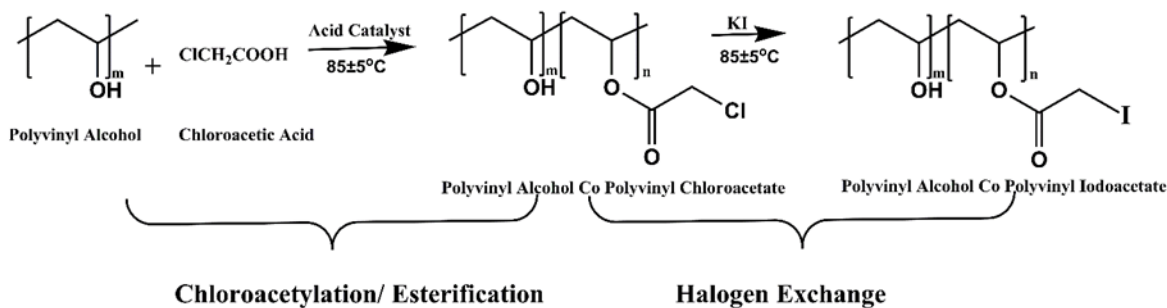


Figure 4.1. Reaction Scheme for PVA Functionalization with Iodoacetate Functionality.

4.2.2.2 Electrospinning of Functional Nanofibers

PVA, having 12% iodoacetylation, was electrospun at 11 wt. % polymer in solution and using the horizontal electrospinning set up. Applied voltage was kept at 15 kV, and tip to collector distance was 10 cm under atmospheric conditions.

4.2.2.3 Morphology of Electrospun Nanofibers

The morphology of electrospun nanofibers was imaged with the Verios Field Emission Scanning Electron Microscope (FESEM) at an accelerating voltage of 2 kV and operating current of 13 mA. Fibers were sputter coated with 60/40 Au/Pd for 1 min at 0.7 nm/min before imaging. Image J software was used to measure the diameters of at least 25 fibers per sample.

4.2.2.4 Crosslinking of Electrospun Nanofibers

Functionalized PVA-based nanofibers were crosslinked with GA to prevent its dissolution in aqueous solutions. 50 mg (14 mM of OH groups) of functionalized nanofibers

were immersed in 2.8 ml of 50% GA solution (300 mM of GA) in 50 ml of acetone and 1 droplet of 1N H₂SO₄ for 24 h. After crosslinking, nanofibers were rinsed with acetone 3 times to remove unreacted GA and then air dried for 24 h.

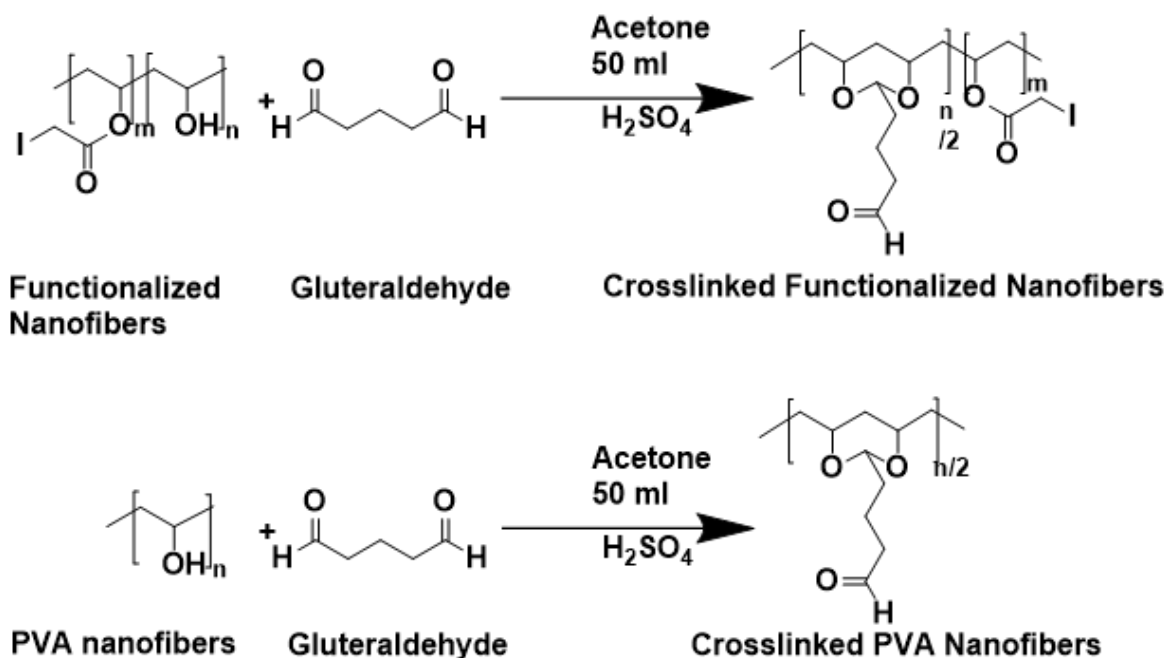


Figure 4.2. Crosslinking of functionalized nanofibers with glutaraldehyde solution.

4.2.2.5 Attachment of Glucose oxidase (GOx) on Iodoacetate Functionalized Nanofibers

GOx protein-attachment onto iodoacetylated nanofibers was tested with 5 mg of nanofibers under 3 different pH values: acidic ($\text{pH } 3.7 \pm 0.4$), neutral ($\text{pH } 7.0 \pm 0.4$), and alkaline (9.1 ± 0.5) conditions over 48 h at $37 \pm 3^\circ\text{C}$. 252 nM of GOx was stored in 25 ml of solution, having 1 mg of GOx, theoretically.

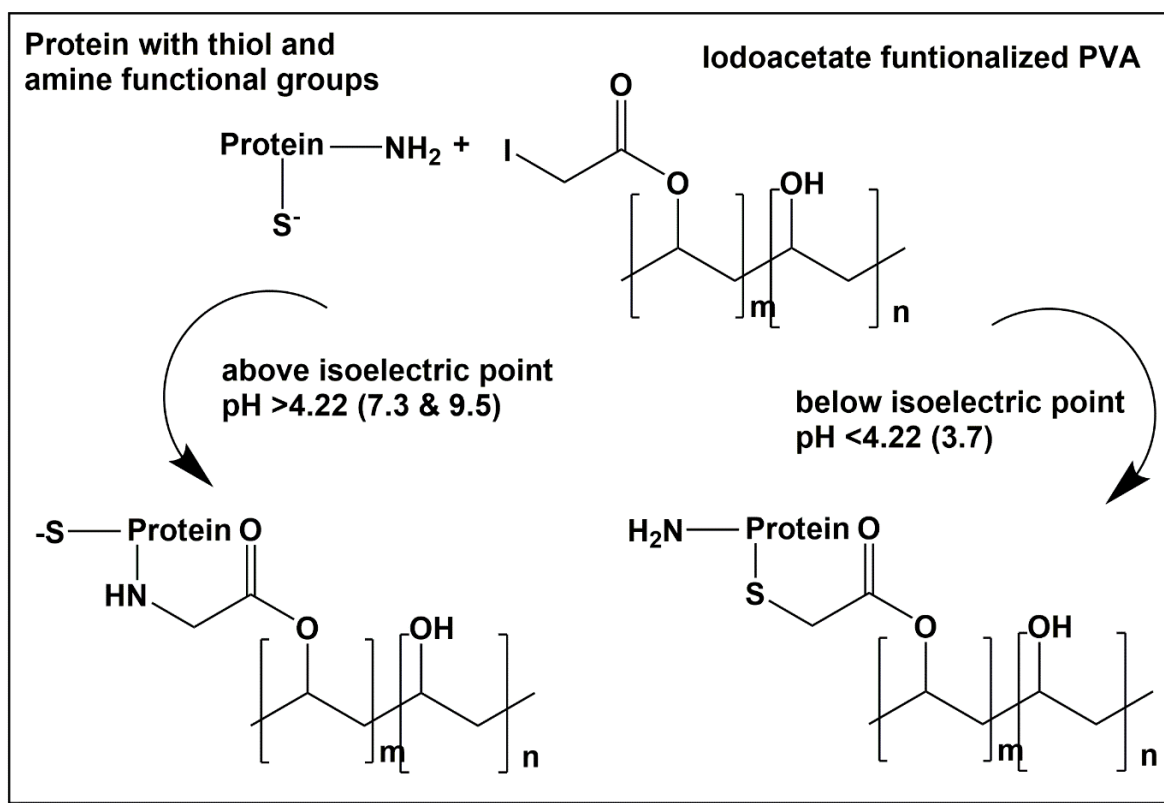


Figure 4.3. Protein Capture through functional nanofibers having iodoacetate functionality.

After reaction, membranes were removed from solution and rinsed with 5 ml of water with agitation- agitation was used to remove adsorbed protein from the nanofiber surface. Rinsing was twice repeated with each sample. The remaining concentration of unreacted GOx was quantified using UV -Vis spectroscopy.

4.2.2.6 GOx activity of enzyme immobilized functional membrane for dye decolorization

The enzymatic activity of GOx immobilized nanofibers against glucose oxidation were tested under acidic conditions, because GOx activity is optimum under acidic conditions of pH 5.0 ± 0.5

5 mg of GOx immobilized nanofibers were reacted with 10, 20, 30 and 50 mg/L of Acid Blue 25. The volume of dye solution was 25 ml and their pH 5.5 was maintained by adding a few drops of sulfuric acid. The reaction occurred over 24 h at 28 °C. Afterwards,

nanofibers were removed from solutions and dye solutions were analyzed by UV-vis spectroscopy

4.3 Result and Discussion

4.3.1 Morphology of Electrospun and Crosslinked Nanofibers

The morphology of functional fiber is shown in Figure 4.4. Crosslinking nanofibers did not show any significant changed in their fiber size after crosslinking. PVA nanofibers were 150 ± 60 nm in size, and PVIAC nanofibers were 80 ± 30 nm in size.

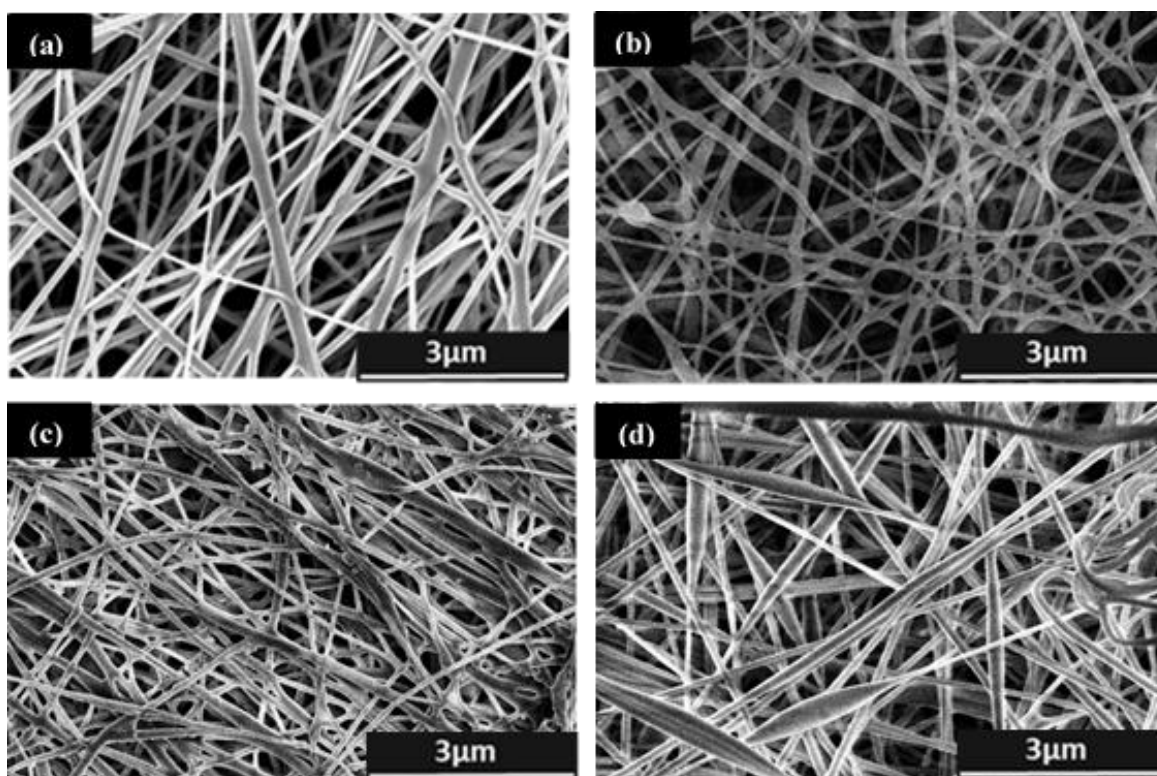


Figure 4.4. Morphology of functionalized nanofibers before crosslinking (a) PVA and (b) PVA-Co-PVIAC and after crosslinking (c) PVA and (d) PVA-Co-PVIAC.

4.3.2 Enzyme Attachment on Functional Nanofibers

GOx was attached to functional PVIAC nanofibers according to reaction schemes shown in Figure 4.3. Three different pH values were applied to represent acidic, neutral and basic conditions. The attachment of GOx onto PVIAC functionalized nanofibers was done

using two methods. First, the change in GOx concentration was measured by UV-Vis spectroscopy. GOx consumed by nanofiber attachment was calculated through a calibration curve. Secondly, FTIR spectra of PVIAC nanofibers were used to detect the formation of new bonds from covalent reaction.

4.3.3 UV-Vis study to Confirm Concentration Change After Reaction

GOx concentration was analyzed with UV-Vis spectroscopy before and after GOx attachment under three different pH values: acidic, neutral and alkaline conditions. The change in absorption at 200 nm was used to monitor changes in GOx concentration. Under acidic conditions, a slight reduction in GOx concentration was observed when control PVA and PVIAC nanofibers were used, as shown in Table 4.1. This reduction was attributed to the absorption of GOx inside the pores of nanofibrous membranes. Previously researchers reported iodoacetate functionalities react with thiols and thioethers under acidic pH.¹³⁴ Since, each mole of GOx contains only three moles of thiol, low yields for protein attachment are expected.

The isoelectric point (pI) of GOx is 4.22; thus, under neutral and alkaline (pH > 7.0) conditions, the enzyme has free amine groups and deprotonated carboxylic acid groups. In this case, amine groups would compete with thiol groups. The reaction is most likely to occur between amine and iodoacetate groups. We have observed a significant reduction in GOx enzymes after their reaction with PVIAC functionalized nanofibers under neutral and alkaline conditions. However, no significant difference in GOx concentration was observed under the three pH values. This indicates the reduction in GOx concentration upon exposure to PVA nanofibers was due to absorption. PVA nanofibers absorbed slightly more GOx (24%) under basic conditions in comparison to GOx absorption under acidic and neutral pH (17%). The

electrostatic adsorption of proteins onto nanofibers may have resulted from the deprotonated of PVA hydroxyl groups in the presence of the protein's nucleophilic amine groups.

Table 4.1. Glucose Oxidase attachment on PVIAC membrane.

| pH of reaction mixture | Initial Concentration of GOx in Solution (nM) | Final Concentration of GOx after PVA attachment (nM) | Final Concentration of GOx after PVIAC attachment (nM) |
|------------------------|-----------------------------------------------|------------------------------------------------------|--------------------------------------------------------|
| Acidic | 190 ± 9.3 | 156 ± 10 | 156 ± 11 |
| Neutral | 187 ± 9.8 | 155 ± 10 | 86 ± 11 |
| Alkaline | 198 ± 10 | 149 ± 8 | 63 ± 11 |

Therefore, changes in GOx concentration in the presence of PVIAC was attributed to absorption and the covalent attachment of enzymes onto PVAIc nanofibers. To isolate the effects covalent attachment from absorption, GOx absorption to PVA was subtracted values of GOx absorbed/reacted to PVIAC nanofibers. The results are shown in Table 4.2.

Table 4.2. Absorption vs covalent attachment of Glucose Oxidase on PVIAC membranes.

| | Absorbed on PVA % | Absorbed and Chemically Attached on PVIAC % | Chemically Attached on PVIAC % |
|----------|-------------------------|---------------------------------------------------|--------------------------------------|
| Acidic | 17 | 17 | 0 |
| Neutral | 17 | 54 | 37 |
| Alkaline | 24 | 68 | 44 |

Of the original GOx concentration, 37 and 44% of GOx in reaction mixture (0.27 mg and 0.34 mg, respectively) attached to PVIAC membranes under neutral and alkaline pH. Membranes having maximum attachment (0.34 mg of GOx) was used in dye oxidation studies.

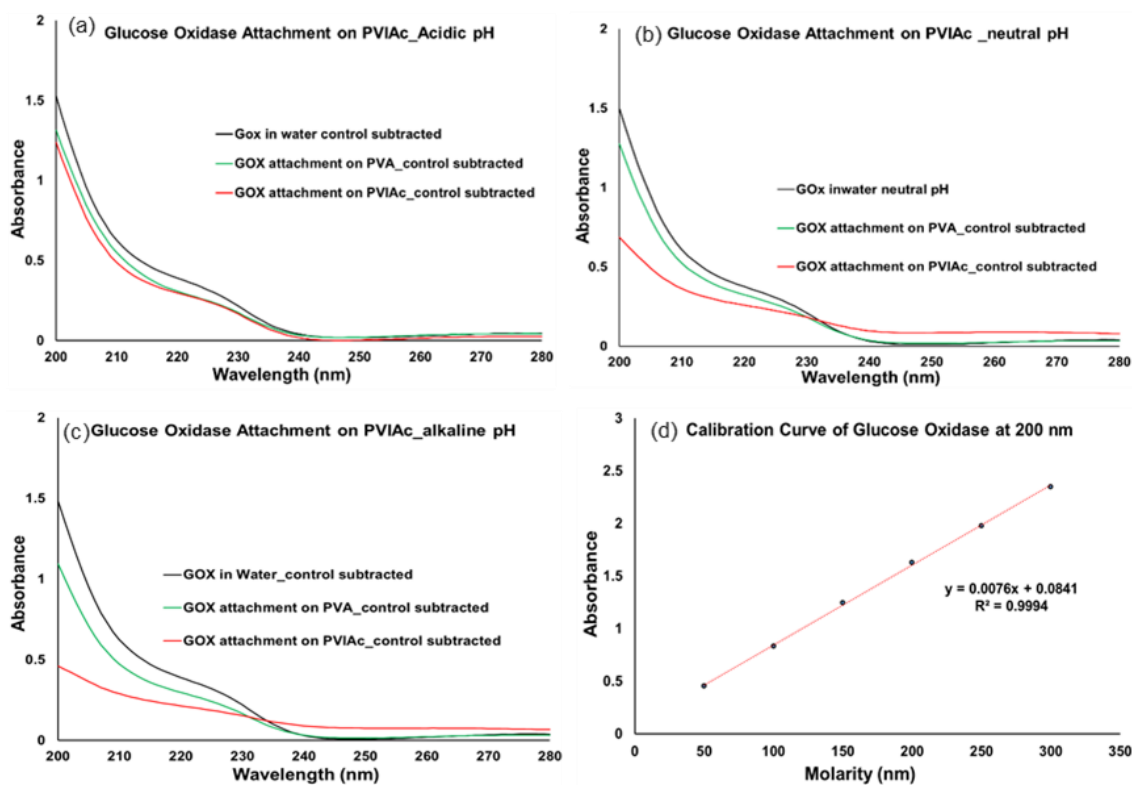


Figure 4.5. Glucose Oxidase attachment on PVIAC nanofibers (a) acidic, (b) neutral, (c) and alkaline conditions with the (d) calibration curve of glucose oxidase.

4.3.4 FTIR study to Confirm Glucose Oxidase Attachment on Functional Nanofibers Surface

Glucose oxidase attachment to PVIAC nanofibers was confirmed with FTIR spectroscopy. Spectra of GOx attached to PVA nanofibers is shown in Figure 4.5. Glucose Oxidase attachment on PVIAC nanofibers (a) acidic, (b) neutral, (c) and alkaline conditions with the (d) calibration curve of glucose oxidase. (a)- the subtraction spectra of PVA-GOx minus PVA nanofibers. Vibrations caused by -N-H stretching were not observed among control PVA nanofibers in the region of $3400 - 3000 \text{ cm}^{-1}$. Some peak vibrations appeared among subtraction spectra in the region of $1653 - 1734 \text{ cm}^{-1}$, as the result of carbonyl stretching at 1132 cm^{-1} . Absorbance peaks indicated the presence of GOx on PVA nanofibers, where GOx had absorbed into PVA pores.

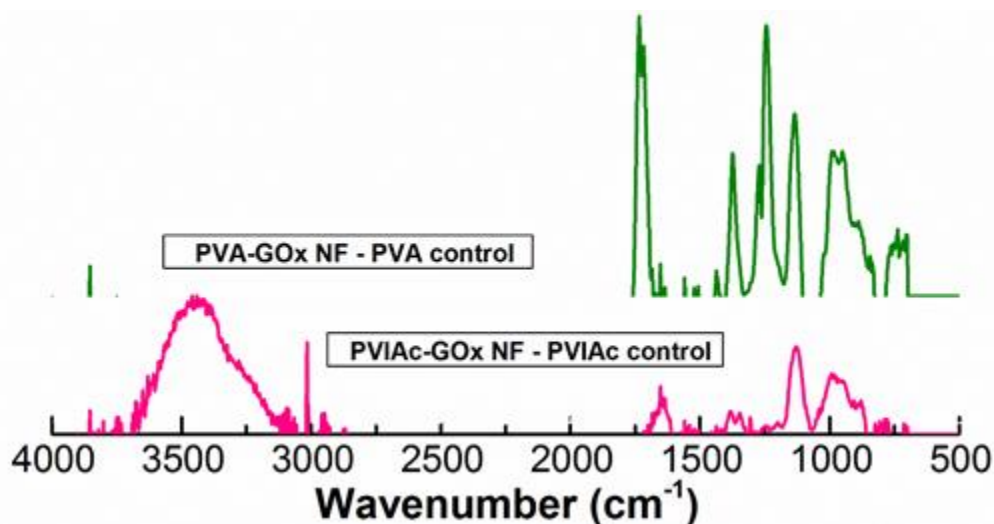


Figure 4.6. Spectra of GOx attached PVA and functionalized PVIAC after subtraction under alkaline pH.

The spectra of PVIAC nanofibers were obtained before and after GOx attachment. Since vibrational hydroxyl and amines groups superimposed upon each, subtraction spectra for PVIAC-GOx were observed. Spectra of PVIAC-GOx nanofibers showed an absorbance peak at 3422 cm^{-1} among its subtraction spectra representing the -N-H stretching. Interestingly, a

distinctive shoulder appeared in the PVIAC-GOx spectra at 3093 cm^{-1} : the overtone of -NH_2 bending at 1653 cm^{-1} was observed. This overtone was absent among PVA-GOx nanofibers. Another distinct peak appeared among PVIAC-GOx nanofibers at 3036 cm^{-1} , which is also present among GOx spectra (not shown) at the same vibrational frequency. Peaks at $2947 - 2866\text{ cm}^{-1}$ corresponded to -CH stretching among -CH_2 groups. -N-H bending and amide stretching peaks both appeared near 1655 cm^{-1} region. A peak also appeared at 1122 cm^{-1} representing C-N stretching. In summary, FTIR spectra confirmed the presence of GOx on PVIAC nanofibers as the result of chemical bonding with PVIAC and PVA absorption. These results confirmed measurements performed by UV-Vis spectroscopy..

4.3.4.1 Dye Decolorization with GOx without Immobilization

Glucose oxidase activity towards dye decolorization was evaluated in solution among dissolved (pure) enzymes- i.e. without immobilization- in Table 4.3. Concentrations of 0.2 - 1 mg in 25 ml of solution were used to evaluate dye decolorization under acidic conditions at pH 5.5 for 24 h at $28\text{ }^{\circ}\text{C}$.

Table 4.3. Dye Decolorization of GOx without Immobilization.

| GOx (mg/25ml) | Initial Dye Concentration (mg/L) | Final Dye Concentration (mg/L) | Dye Degradation (%) |
|--------------------------|-------------------------------------------------|-----------------------------------------------|----------------------------|
| 0.2 | 48.8 | 43.8 | 10 |
| 0.4 | 48.8 | 42.0 | 14 |
| 0.6 | 48.8 | 40.1 | 15 |
| 0.8 | 48.8 | 41.9 | 19 |
| 1.0 | 48.8 | 39.7 | 20 |

Enzymatic activity increased with enzyme concentration. A maximum of 20% dye decolorization was observed with 1mg of GOx per 25 ml of dye in solution. GOx immobilized nanofibers were used for dye decolorization studies; where nanofiber samples had ~0.34 mg of GOx. An equivalent amount of free GOx (0.34 mg) in 25 mL of water achieved 12.5% dye decolorization.

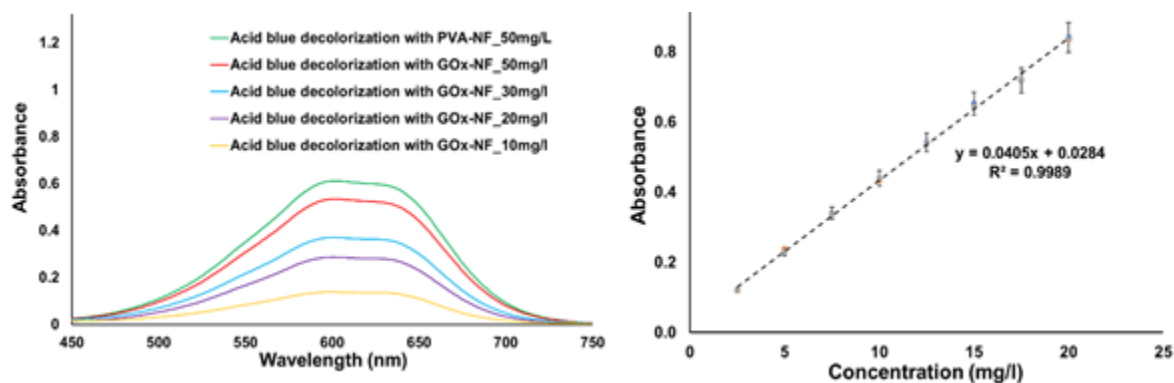
4.3.4.2 Dye Decolorization with GOx Immobilized Nanofibers

The enzymatic activity of GOx towards dye decolorization was evaluated after GOx immobilization onto nanofibers (Table 4.4). Four different dye concentrations were chosen: 10, 20, 30, & 50 mg/l. Control PVA and PVIAc fibers were also evaluated against dye concentrations of 50 mg/l. Sample details are provided in Table 4.4. A calibration curve was used to dye discoloration.

Table 4.4. Samples Used for Dye Decolorization.

| Sample No | Sample ID | GOx Attached on nanofibers (mg) | Mechanism of Attachment |
|-----------|-------------------|---------------------------------|-------------------------|
| 1 | PVA-Control NFs | N/A | N/A |
| 2 | GOx-PVA NFs | 0.2 | Absorbed |
| 3 | PVIAC-Control NFs | N/A | N/A |
| 4 | GOx-PVIAC NFs | 0.34 | Covalently Attached |

The spectra after dye decolorization and calibration curve is shown in Figure 4.7P. PVA and PVIAC control membranes were able to reduce the dye concentration by 18% and 21 % from the reaction mixture due to absorption. PVA nanofibers were tinted significantly after the reaction which confirmed the dye removal mechanism to be absorption. The reduction of 6, 4, 23& 29 of dye from the reaction mixture at concentrations 10, 20, 30 and 50 mg/l respectively were achieved with GOx attached PVIAC nanofibers as shown in Table 4.5.

**Figure 4.7.** Dye Decolorization with GOx-PVIAC nanofibers and calibration curve.

Maximum 29% dye discoloration was achieved at the concentration of 50 mg/l with immobilized GOx on PVIAC nanofibers. This number is more than double than that of dye decolorization by the same number of free enzymes (14% discoloration). It is possible that enzyme immobilization has improved the activity and stability of enzymes. At 10 and 20 mg/l

of dye, less decolorization was observed. Enzyme activity may be concentration dependent. The nonuniform attachment of enzymes over the nanofiber surface area may also lower the degree of decolorization. Interestingly, tinting of the nanofibers was only observed along PVIAC-GOx nanofibers, as shown in Figure 4.8. Thus, immobilized enzymes were responsible for dye degradation and significant reduction of dye concentration in solution.

Table 4.5. Dye decolorization of GOx-PVIAc nanofibers.

| Sample No | Sample Details | Initial Dye Concentration (mg/l) | Final Dye Concentration (mg/l) | Dye Removal (%) | Mechanism |
|------------------|-----------------------|-----------------------------------------|---------------------------------------|------------------------|------------------|
| 1 | PVA Control NFs | 48.7 | 39.8 | 18 | Absorption |
| 2 | GOx-PVA NFs | 48.7 | 37.3 | 24 | Absorption |
| 3 | PVIAc-Control NFs | 48.7 | 38.5 | 21 | Absorption |
| 4 | GOx-PVIAc NFs | 10.4 | 9.8 | 6 | Decolorization |
| 5 | GOx-PVIAc NFs | 20.2 | 19.4 | 4 | Decolorization |
| 6 | GOx-PVIAc NFs | 29.4 | 22.7 | 23 | Decolorization |
| 7 | GOx-PVIAc NFs | 48.7 | 34.9 | 29 | Decolorization |
| | | | | | |

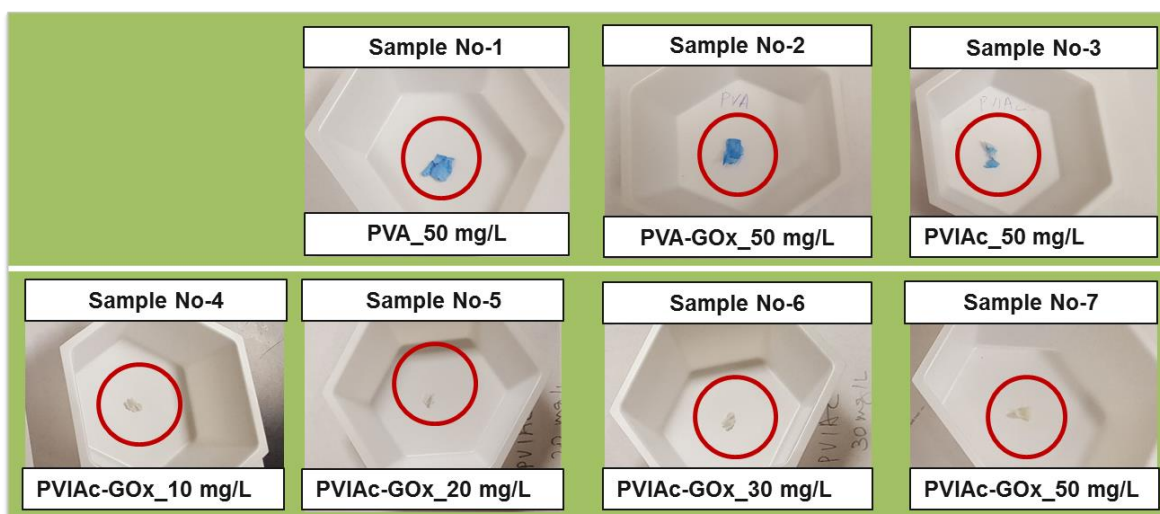


Figure 4.8. Dye decolorization of GOx-PVIAc nanofibers.

4.4 Conclusion

Enzyme immobilization via covalent bonding prevents the leaching of expensive enzymes during reaction. In this study, GOx was successfully attached to electrospun nanofibers, having iodoacetate functional groups. Up to 88% iodoacetate functionality were employed for enzyme attachment under alkaline conditions. Enzymatic activity was evaluated using Acid Blue 25 via dye decolorization studies. The enzymatic activity of GOx was enhanced upon immobilization. Up to 29% dye discoloration by immobilized enzyme occurred under acidic conditions. PVIAc nanofibers were not tinted by dye, because of the dye oxidizing enzymes along its surface. Dye absorption by PVA nanofibers result in nanofiber tinting.

CHAPTER 5

CONCLUSIONS AND RECOMMENDATIONS

5.1 Conclusions

In this research, novel functional electrospun membranes were developed with iodoacetylated polyvinyl alcohol for proteins attachment. The covalent attachment of protein/peptide functional groups was obtained via thiol-iodoacetate reaction and amine-iodoacetate reactions as a function of pH. The same mechanism was used to enhance enzyme activity by immobilizing glucose oxidase onto functional nanofibrous membranes. The major findings of this research are as follows:

5.1.1 Influence of Degree of Iodoacetylation on Polymer Solubility

The degree of polymer modification was found to influence polymer solubility in various solvents. The iodoacetylation of PVA converted hydrophilic hydroxyl groups to hydrophobic iodoacetate groups. When the percentage of hydrophobic groups are less, the hydrophilic groups cause polymer to remain water soluble. In this research, polymer having up to 12% iodoacetylation was found to be water soluble. When this number slightly increased from 12% to 16%, difficulties in polymer solubility started to occur, which can be observed by longer dissolving times and lumps in solution. Solution homogeneity is extremely important to produce uniform fibers during electrospinning. The change in polymer solubility demands an optimized solvent system for electrospinning. 16% iodoacetylated polymer was successfully spun with binary solvent system- containing 50:50 acetic acid: water-. Fiber morphology improved in comparison to fibers spun using water as a solvent. However, polymer with 16% functionalization still showed significant water solubility and so crosslinking was needed for nanofiber use in water-based application. We have also tried to increase the extent of

modification for more water insoluble polymer. Iodoacetylated PVA with 40% modification was synthesized. The water insoluble polymer was achieved. However, another challenge among polymer dissolution arises. We tried to dissolve the polymer in various solvents, which include polar and non-polar solvents and binary solvent systems that contain polar and nonpolar solvents. The dissolution of polymer was found extremely difficult. A very fine dispersion was obtained using a binary system of 3:1-acetic acid and water. By preparing a very dilute solution and then evaporating the excess solvent, the optimum concentration was achieved for electrospinning. However, fibers were not observed, due to the lack of polymer chain entanglements. Therefore, the optimum degree of iodoacetylation is of importance when fabricating electrospun nanofibers.

5.1.2 Influence of Crosslinking on PVA based Membranes with Glutaraldehyde

GA was used as a crosslinking agent for enhancing the water stability of PVA based membranes. The molar ratio of CHO:OH was very high (530), which resulted in plenty of free aldehyde groups on the nanofiber surface. In addition to that, significant amounts of unreacted GA were present on the surface after crosslinking, which can leach during protein attachment. This demanded glutaraldehyde removal prior to protein attachment. GA removal was achieved with multiple rinsings of the nanofibrous membranes at 70 °C with water. This created an additional step for glutaraldehyde use. The aldehyde groups are very reactive towards amines and thiols, which convoluted the characterization of protein attachment mechanisms. Therefore, GA was not a suitable cross-linker for this research.

5.1.3 Identification of Covalent Attachment vs Absorption of Proteins:

The identification of covalent attachment vs protein absorption onto nanofibrous membranes was performed using ATR-FTIR. When the target protein was just absorbed onto

the nanofibers, the same type of bonds was present on the controls and iodoacetylated nanofibers. However, when proteins were covalently attached with the nanofibers, this generated new bonds. For example: In the case of mercaptoethanol, when the thiol attached with iodoacetate functionalities covalently, thioether linkages formed, which eliminated the -C-SH bending peak from spectra. On the other hand, when the attachment occurred via amine functionalities the primary amine converted to secondary amines and the -C-N peak shifted from ~ 1200 to ~ 1100 cm^{-1} . Therefore, ATR-FTIR was found useful in distinguishing between covalent attachment vs absorption.

5.1.4 Immobilization and Activity of GOx towards Dye Decolorization

GOx was used as model protein for protein attachment onto iodoacetylated nanofibers. Maximum attachment of GOx occurred under alkaline pH as evidenced by UV-Vis spectroscopy. Enzyme immobilization on nanofibers enhanced their stability and activity. We have tested enzyme activity towards dye decolorization of anthraquinone dye. The decolorizing ability of immobilized enzymes was double that of free enzymes without immobilization.

5.2 Recommendation for Future Work

We recommend the following to enhance protein attachment onto iodoacetylated nanofibers.

- Increase the functional sites on the nanofibers by increasing the degree of modification. However, 40 % modification will make the polymer insoluble in almost every solvent- both polar and nonpolar-. Therefore, it is recommended that polymer modification start with very low concentration (w/v) of reactants in the reaction mixture. Aliquots could be used to check the water solubility of polymer after every 4 h. The key is to look for signs of polymer

precipitation and polymer redissolution in water until a hydrophobic polymer is obtained. In this way, we can enhance protein attachment and eliminate the crosslinking step.

- The effect of time on the protein attachment could also be optimized so that the reaction product does not degrade. This is most desirable in the case of evaluating the enzyme's activity. In this research, we have achieved 30% dye decolorization, which is low in comparison to existing literature. Therefore, optimizing the time for protein attachment and enzyme activity may enhance the results.

APPENDICES

Appendix A

XPS Study of Covalent Capturing of Methionine through Functional PVIAC Nanofibrous Membrane

Functional nanofibers were studied using XPS before and after the reaction. The objective of using this technique was to detect sulphur and nitrogen after the reaction and differentiating covalent attachment from physical adsorption onto functional surfaces. For that the attachment was performed on functional and non-functional nanofibers (PVA control). More oxygen (15800 CPS) than carbon (11800 CPS) was detected, which indicated the presence of functional groups on the surface. This confirmed, that positive bias was appropriate polarity for creating functional surfaces with our polymer system. The presence of sulphur and nitrogen was very less as compared to carbon and oxygen. This was because of low degrees of functionality. Therefore, for 12% iodoacetylated PVA, it contains only 4.2% of iodine. Out of this number, 2.8% of the functional groups (302 CPS) reacted, which indicates 66% utilization of functional groups. Nitrogen was higher than expectation for given degrees of functionality, which could be due to physical adsorption.

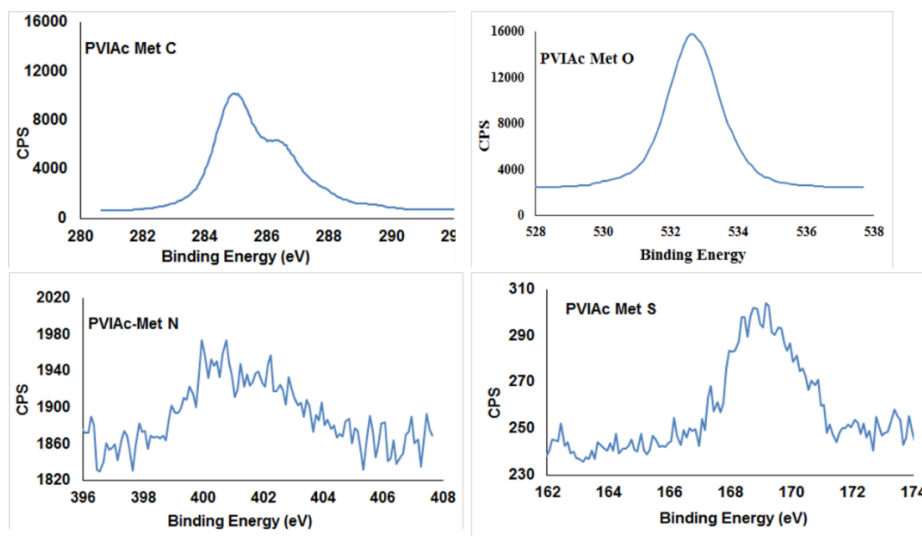


Figure. A.1. XPS curves of methionine attachment on PVIAC nanofibers

A.1.1 XPS Result Analysis-

Functional PVIAC contained 12% iodoacetylated groups and 88% hydroxyl groups along polymer chains having 2125 degree of polymerization (DP):

Number of Carbon Atom in Polymer/membrane after Methionine Attachment

$$= 2 \times 0.88 \times 2125 + 9 \times 0.12 \times 2125 = 6035$$

Number of sulfur atom in polymer after methionine attachment

= Number of Iodine atom present in the polymer/membrane

$$= 0.12 \times 2125 = 255$$

Number of Nitrogen atom in polymer after methionine attachment

= Number of Iodine atom present in the polymer/membrane

$$= 0.12 \times 2125 = 255$$

$$\% \text{ of nitrogen} = \% \text{ of sulfur with respect to carbon (theoretical)} = 255/6035 \times 100 = 4.2\%$$

$$\% \text{ of sulfur with respect to carbon} = 302/10500 \times 100 \text{ (practical)} = 2.8\%$$

$$\% \text{ Yield} = \text{Practical Attachment} / \text{Theoretical Attachment} = 2.8/4.2 = 66.7\%$$

Appendix B

Enzymatic Activity of Nanofibers towards Glucose Oxidation

To evaluate the enzymatic activity of GOx-attached PVIAC nanofibers, glucose oxidation was performed under acidic pH (pH=5.3) which is the optimum pH for GOx activity. The absorption of aqueous glucose solutions under acidic pH showed maximum absorption of 0.05 at 200 nm. No leaching was observed with PVIAC membranes under acidic conditions, but after the reaction gluconic acid formed as represented by the 226 nm peak, as shown in Figure 7. Gluconic acid is active under the UV- region of the spectrum. Previously Escandar et al. showed spectra of copper ions complexing gluconic acid, whose λ_{max} depended upon the pH of the solution. They observed λ_{max} at 200 nm at pH 3.39 and the peak absorbance shifted towards higher wavelengths upon increasing pH¹³⁶

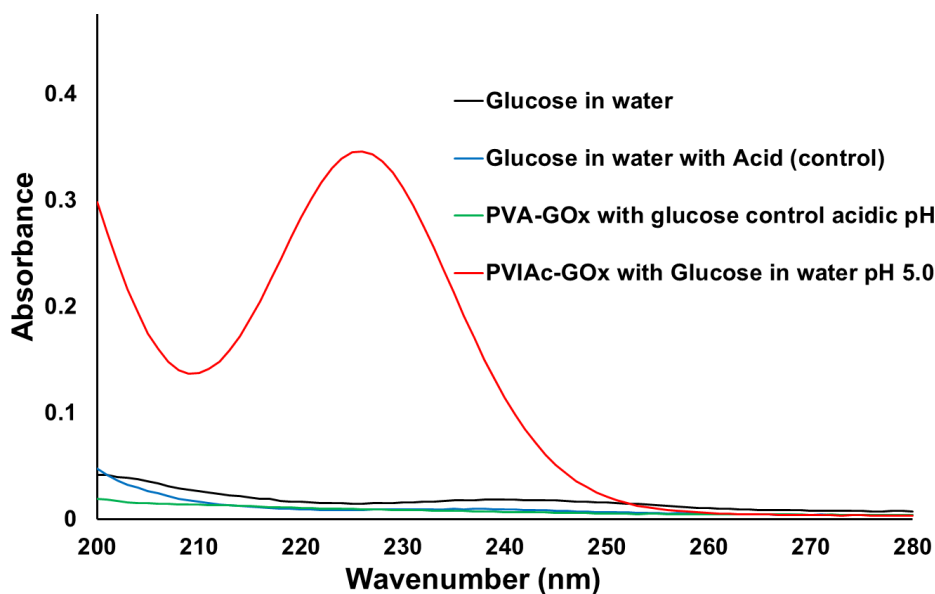


Figure B.1. Glucose oxidation with GOx-PVIAC nanofibers

REFERENCES

- (1) Nanofibers Market Size | Industry Research Report, 2024
<http://www.grandviewresearch.com/industry-analysis/nanofibers-market>.
- (2) Kiyak, Y.; Cakmak, E. Nanofiber Production Methods *. *Electron. J. Text. Technol.* **2014**, *2014* (3), 49–60.
- (3) Nayak, R.; Padhye, R.; Kyratzis, I. L.; Truong, Y. B.; Arnold, L. Recent Advances in Nanofibre Fabrication Techniques. *Text. Res. J.* **2012**, *82* (2), 129–147.
- (4) Bhardwaj, N.; Kundu, S. C. Electrospinning: A Fascinating Fiber Fabrication Technique. *Biotechnol. Adv.* **2010**, *28* (3), 325–347.
- (5) Nanofibers: Technologies and Developing Markets - NAN043B
<http://www.bccresearch.com/market-research/nanotechnology/nanofibers-technology-market-nan043b.html>.
- (6) Global Markets and Technologies for Nanofibers <http://www.prnewswire.com/news-releases/global-markets-and-technologies-for-nanofibers-210858631.html>.
- (7) Richard W. Baker. *Membranae Technology*; 2010; Vol. 3.
- (8) Yoon, K.; Kim, K.; Wang, X.; Fang, D.; Hsiao, B. S.; Chu, B. High Flux Ultrafiltration Membranes Based on Electrospun Nanofibrous PAN Scaffolds and Chitosan Coating. *Polymer (Guildf)*. **2006**, *47* (7), 2434–2441.
- (9) Liu, T.; Zhang, D.; Xu, S.; Sourirajan, S. Solution-Spun Hollow Fiber Polysulfone and Polyethersulfone Ultrafiltration Membranes. *Sep. Sci. Technol.* **1992**, *27* (2), 161–172.

- (10) Huang, Q.; Seibig, B.; Paul, D. Polycarbonate Hollow Fiber Membranes by Melt Extrusion. *J. Memb. Sci.* **1999**, *161* (1–2), 287–291.
- (11) Unger, R. E.; Huang, Q.; Peters, K.; Protzer, D.; Paul, D.; Kirkpatrick, C. J. Growth of Human Cells on Polyethersulfone (PES) Hollow Fiber Membranes. *Biomaterials* **2005**, *26* (14), 1877–1884.
- (12) Forester, T. E.; Sherman, L. R. Melt-Blown Material with Depth Fiber Size Gradient. 4,714,647, 1990.
- (13) Wang, X.; Chen, X.; Yoon, K.; Fang, D.; Hsiao, B. S.; Chu, B. High Flux Filtration Medium Based on Nanofibrous Substrate with Hydrophilic Nanocomposite Coating. *Environ. Sci. Technol.* **2005**, *39* (19), 7684–7691.
- (14) Gautam, A. K.; Lai, C.; Fong, H.; Menkhaus, T. J. Electrospun Polyimide Nanofiber Membranes for High Flux and Low Fouling Microfiltration Applications. *J. Memb. Sci.* **2014**, *466*, 142–150.
- (15) Hong, S. K.; Elimelech, M. Chemical and Physical Aspects of Natural Organic Matter (NOM) Fouling of Nanofiltration Membranes. *J. Memb. Sci.* **1997**, *132* (2), 159–181.
- (16) Gopal, R.; Kaur, S.; Ma, Z.; Chan, C.; Ramakrishna, S.; Matsuura, T. Electrospun Nanofibrous Filtration Membrane. *J. Memb. Sci.* **2006**, *281* (1–2), 581–586.
- (17) Tattersall, J.; Canaud, B.; Heimbürger, O.; Pedrini, L.; Schneditz, D.; Van Biesen, W. High-Flux or Low-Flux Dialysis: A Position Statement Following Publication of the Membrane Permeability Outcome Study. *Nephrol. Dial. Transplant.* **2010**, *25* (4),

1230–1232.

- (18) Choi, Y.-J. CRITICAL FLUX, RESISTANCE, AND REMOVAL OF CONTAMINANTS IN ULTRAFILTRATION (UF) OF NATURAL ORGANIC MATERIALS, The Pennsylvania State University, 2003.
- (19) Niu, H.; Wang, X.; Lin, T. *Needleless Electrospinning: Developments and Performances*; 2011.
- (20) Doshi, J.; Reneker, D. H. Electrospinning Process and Applications of Electrospun Fibers. *J. Electrostat.* **1995**, *35*, 151–160.
- (21) Ramakrishna, S.; Fujihara, K.; Teo, W. E.; Yong, T.; Ma, Z.; Ramaseshan, R. Electrospun Nanofibers: Solving Global Issues. *Mater. Today* **2006**, *9* (3), 40–50.
- (22) Teo, W. E.; Ramakrishna, S. A Review on Electrospinning Design and Nanofibre Assemblies. *Nanotechnology* **2006**, *17* (14), R89–R106.
- (23) Tonelli Alan, S. M. *Polymers From Inside Out*; A John Wiley & Sons, Inc., Publication: Newyork, 2001.
- (24) Won, J. J.; Nirmala, R.; Navamathavan, R.; Kim, H. Y. Electrospun Core-Shell Nanofibers from Homogeneous Solution of Poly(vinyl Alcohol)/bovine Serum Albumin. *Int. J. Biol. Macromol.* **2012**, *50* (5), 1292–1298.
- (25) Stachewicz, U.; Stone, C. A.; Willis, C. R.; Barber, A. H. Charge Assisted Tailoring of Chemical Functionality at Electrospun Nanofiber Surfaces. *J. Mater. Chem.* **2012**, *22* (43), 22935–22941.

- (26) Tang, C.; Ozcam, A. E.; Stout, B.; Khan, S. A. Effect of pH on Protein Distribution in Electrospun PVA/BSA Composite Nano Fibers. **2012**.
- (27) Ford, E. N. J.; Suthiwangcharoen, N.; D'Angelo, P. a.; Nagarajan, R. Role of Single-Walled Carbon Nanotubes on Ester Hydrolysis and Topography of Electrospun Bovine Serum Albumin/poly(vinyl Alcohol) Membranes. *ACS Appl. Mater. Interfaces* **2014**, 6 (14), 11741–11748.
- (28) Ding, B.; Wang, M.; Yu, J.; Sun, G. Gas Sensors Based on Electrospun Nanofibers. *Sensors (Basel)*. **2009**, 9 (3), 1609–1624.
- (29) Wang, X.; Drew, C.; Lee, S. H.; Senecal, K. J.; Kumar, J.; Samuelson, L. a. Electrospun Nanofibrous Membranes for Highly Sensitive Optical Sensors. *Nano Lett.* **2002**, 2 (11), 1273–1275.
- (30) Wang, X.; Drew, C.; Lee, S.-H.; Senecal, K.; Kumar, J.; Samuelson, L. Electrospinning Technology: A Novel Approach To Sensor Application. *J. Macromol. Sci. Part A* **2002**, 39 (10), 1251–1258.
- (31) Wang, W.; Huang, H.; Li, Z.; Zhang, H.; Wang, Y.; Zheng, W.; Wang, C. Zinc Oxide Nanofiber Gas Sensors Via Electrospinning. *J. Am. Ceram. Soc.* **2008**, 91 (11), 3817–3819.
- (32) Senecal, A.; Magnone, J.; Marek, P.; Senecal, K. Development of Functional Nanofibrous Membrane Assemblies towards Biological Sensing. *React. Funct. Polym.* **2008**, 68 (10), 1429–1434.

- (33) Jeong, E. H.; Yang, J.; Youk, J. H. Preparation of Polyurethane Cationomer Nanofiber Mats for Use in Antimicrobial Nanofilter Applications. *Mater. Lett.* **2007**, *61* (18), 3991–3994.
- (34) Lala, N. L.; Ramaseshan, R.; Bojun, L.; Sundarrajan, S.; Barhate, R. S.; Liu, Y. J.; Ramakrishna, S. Fabrication of Nanofibers with Antimicrobial Functionality Used as Filters: Protection against Bacterial Contaminants. *Biotechnology and Bioengineering*. 2007, pp 1357–1365.
- (35) Huang, T.; Zhang, M.; Cheng, L.; Zhang, L.; Huang, M.; Xu, Q.; Chen, H. A Novel Polysulfone-Based Affinity Membrane with High Hemocompatibility: Preparation and Endotoxin Elimination Performance. *RSC Adv.* **2013**, *3* (48), 25982.
- (36) Filtration Methods.
<http://www.chem.ucalgary.ca/courses/351/laboratory/filtration.pdf>.
- (37) George Kellie. *Advances in Technical Nonwovens*; Kellie, G., Ed.; Elsevier Science & Technology, 2016.
- (38) Membrane Filtration Systems - Pacific Water Technology
<http://www.pacificwater.com.au/applications/membrane-filtration/>.
- (39) Wang, R.; Liu, Y.; Li, B.; Hsiao, B. S.; Chu, B. Electrospun Nanofibrous Membranes for High Flux Microfiltration. *J. Memb. Sci.* **2012**, *392–393*, 167–174.
- (40) Gopal, R.; Kaur, S.; Feng, C. Y.; Chan, C.; Ramakrishna, S.; Tabe, S.; Matsuura, T. Electrospun Nanofibrous Polysulfone Membranes as Pre-Filters: Particulate Removal.

J. Memb. Sci. **2007**, 289 (1–2), 210–219.

- (41) Huang, L.; Arena, J. T.; Manickam, S. S.; Jiang, X.; Willis, B. G.; Mccutcheon, J. R. Improved Mechanical Properties and Hydrophilicity of Electrospun Nano Fiber Membranes for Filtration Applications by Dopamine Modification. **2014**, 460, 241–249.
- (42) Kaur, S.; Rana, D.; Matsuura, T.; Sundarrajan, S.; Ramakrishna, S. Preparation and Characterization of Surface Modified Electrospun Membranes for Higher Filtration Flux. *J. Memb. Sci.* **2012**, 390–391, 235–242.
- (43) Tanaka, Y. *Preparation of Ion Exchange Membranes 1.1*; 2015.
- (44) Ran, J.; Wu, L.; He, Y.; Yang, Z.; Wang, Y.; Jiang, C.; Ge, L.; Bakangura, E.; Xu, T. Ion Exchange Membranes : New Developments and Applications. **2017**, 522, 267–291.
- (45) Chakrabarty, T.; Kumar, M.; Rajesh, K. P.; Shahi, V. K.; Natarajan, T. S. Nano-Fibrous Sulfonated Poly (Ether Ether Ketone) Membrane for Selective Electro-Transport of Ions. *Sep. Purif. Technol.* **2010**, 75 (2), 174–182.
- (46) Wu, J. S.; Liu, C. H.; Chu, K. H.; Suen, S. Y. Removal of Cationic Dye Methyl Violet 2B from Water by Cation Exchange Membranes. *J. Memb. Sci.* **2008**, 309 (1–2), 239–245.
- (47) Zhang, W.; Chen, M.; Diao, G. Electrospinning β Cyclodextrin/poly(vinyl Alcohol) Nanofibrous Membrane for Molecular Capture. *Carbohydr. Polym.* **2011**, 86 (3),

1410–1416.

- (48) Bessbousse, H.; Rhlalou, T.; Verchère, J. F.; Lebrun, L. Removal of Heavy Metal Ions from Aqueous Solutions by Filtration with a Novel Complexing Membrane Containing Poly(ethyleneimine) in a Poly(vinyl Alcohol) Matrix. *J. Memb. Sci.* **2008**, *307* (2), 249–259.
- (49) Bessbousse, H.; Rhlalou, T.; Verchère, J.-F.; Lebrun, L. Sorption and Filtration of Hg(II) Ions from Aqueous Solutions with a Membrane Containing Poly(ethyleneimine) as a Complexing Polymer . *J. Memb. Sci.* **2008**, *325* (2), 997–1006.
- (50) Huang, Y.; Miao, Y. E.; Liu, T. Electrospun Fibrous Membranes for Efficient Heavy Metal Removal. *J. Appl. Polym. Sci.* **2014**, *131* (19), 1–12.
- (51) Charcosset, C. Review Purification of Proteins B Y Membrane Chromatograph Y. *J. Chem. Technol. Biotechnol.* **1998**, *71*, 95–110.
- (52) Gaeta, S. N.; Predosa, Z. Affinity Membranes: A Tool to Remove Pathogens. *Eur. Med. Device Technol.* **2010**, No. February, 24–26.
- (53) Ma, Z.; Ramakrishna, S. Electrospun Regenerated Cellulose Nanofiber Affinity Membrane Functionalized with Protein A/G for IgG Purification. *J. Memb. Sci.* **2008**, *319* (1–2), 23–28.
- (54) Ma, Z.; Kotaki, M.; Ramakrishna, S. Electrospun Cellulose Nanofiber as Affinity Membrane. *J. Memb. Sci.* **2005**, *265* (1–2), 115–123.

- (55) Ma, Z.; Masaya, K.; Ramakrishna, S. Immobilization of Cibacron Blue F3GA on Electrospun Polysulphone Ultra-Fine Fiber Surfaces towards Developing an Affinity Membrane for Albumin Adsorption. *J. Memb. Sci.* **2006**, 282 (1–2), 237–244.
- (56) Ma, Z.; Lan, Z.; Matsuura, T.; Ramakrishna, S. Electrospun Polyethersulfone Affinity Membrane: Membrane Preparation and Performance Evaluation. *J. Chromatogr. B Anal. Technol. Biomed. Life Sci.* **2009**, 877 (29), 3686–3694.
- (57) Herigstad, M. O.; Gurgel, P. V.; Carbonell, R. G. Transport and Binding Characterization of a Novel Hybrid Particle Impregnated Membrane Material for Bioseparations. *Biotechnol. Prog.* **2011**, 27 (1), 129–139.
- (58) Liu, H.; Gurgel, P. V.; Carbonell, R. G. Preparation and Characterization of Anion Exchange Adsorptive Nonwoven Membranes with High Protein Binding Capacity. *J. Memb. Sci.* **2015**, 493, 349–359.
- (59) Liu, H.; Zheng, Y.; Gurgel, P. V.; Carbonell, R. G. Affinity Membrane Development from PBT Nonwoven by Photo-Induced Graft Polymerization, Hydrophilization and Ligand Attachment. *J. Memb. Sci.* **2013**, 428, 562–575.
- (60) Zhang, Y.; Carbonell, R. G.; Rojas, O. J. Bioactive Cellulose Nano Fibrils for Specific Human IgG Binding. *Biomacromolecules* **2013**, 14, 4161–4168.
- (61) Wang, S.; Kaltashov, I. A. A New Strategy of Using o18-Labeled Iodoacetic Acid for Mass Spectrometry-Based Protein Quantitation. *J. Am. Soc. Mass Spectrom.* **2012**, 23 (7), 1293–1297.

- (62) Chu, F. un S.; Bergdoll, M. S. Studies on the Chemical Modification of Staphylococcal Enterotoxin B I. Alkylation and Oxidation of Methionine Residues. *Biochim. Biophys. Acta* - **1969**, *194*, 279–286.
- (63) Anderson, G. P.; Legler, P. M.; Zabetakis, D.; Goldman, E. R. Comparison of Immunoreactivity of Staphylococcal Enterotoxin B Mutants for Use as Toxin Surrogates. *Anal. Chem.* **2012**, *84* (12), 5198–5203.
- (64) Ahanotu, E.; Alvelo-ceron, D.; Ravita, T.; Gaunt, E. Staphylococcal Enterotoxin B as a Biological Weapon : Recognition , Management , and Surveillance of Staphylococcal Enterotoxin. **2006**, *11* (3), 120–126.
- (65) Balaban, N.; Avraham, R. Staphylococcal Enterotoxins. *Int. J. Food Microbiol.* **2000**, *61* (1), 1–10.
- (66) Palanivelan, V. Analysis of Staphylococcal Enterotoxin B (SEB) Using Bioinformatics Tools. *Internet J. Genomics Proteomics* **2010**, *6* (1).
- (67) Ina, M.; Hudson, S.; Krause, W. The Sysnthesis of Poly N-Acetyl Iodo Glucosamine and Its Gelation of Blood, 2013.
- (68) Gundlach, H Gerd, Moore, Stanford, H. Stein, W. The Reaction of Iodoacetate with Methionine. *J. Biol. Chem.* **1959**, *234* (7), 1761–1765.
- (69) Juzeliūnas, E. Quartz Crystal Microgravimetry – Fifty Years of Application and New Challenges. **2009**, *20* (4), 218–225.
- (70) Smith, P. K.; Krohn, R. I.; Hermanson, G. T.; Mallia, A. K.; Gartner, F. H.;

Provenzano, M. D.; Fujimoto, E. K.; Goeke, N. M.; Olson, B. J.; Klenk, D. C.

Measurement of Protein Using Bicinchoninic Acid. *Anal. Biochem.* **1985**, *150* (1), 76–85.

- (71) Olson, B. J. S. C.; Markwell, J. Assays for Determination of Protein Concentration. *Curr. Protoc. Protein Sci.* **2007**, Chapter 3, Unit 3.4.
- (72) Watts, J.; Wolstenholme, J. Electron Spectroscopy: Some Basic Concepts. In *An introduction to surface analysis by XPS and AES*; 2003; pp 1–15.
- (73) Min, M.; Shen, L.; Hong, G.; Zhu, M.; Zhang, Y.; Wang, X.; Chen, Y.; Hsiao, B. S. Micro-Nano Structure Poly (Ether Sulfones)/ Poly (Ethyleneimine) Nanofibrous Affinity Membranes for Adsorption of Anionic Dyes and Heavy Metal Ions in Aqueous Solution. *Chem. Eng. J.* **2012**, *197*, 88–100.
- (74) Rockley, N. L.; Rockley, M. G.; Halley, B. a; Nelson, E. C. Fourier Transform Infrared Spectroscopy of Polymers. *Methods Enzymol.* **1986**, *123*, 92–101.
- (75) Maria, C. *Application of FTIR Spectroscopy in Environmental Studies*; 2012.
- (76) Mansur, H. S.; Sadahira, C. M.; Souza, A. N.; Mansur, a. a P. FTIR Spectroscopy Characterization of Poly (Vinyl Alcohol) Hydrogel with Different Hydrolysis Degree and Chemically Crosslinked with Glutaraldehyde. *Mater. Sci. Eng. C* **2008**, *28* (4), 539–548.
- (77) Mansur, H. S.; Sadahira, C. M.; Souza, A. N.; Mansur, A. A. P. FTIR Spectroscopy Characterization of Poly (Vinyl Alcohol) Hydrogel with Different Hydrolysis Degree

- and Chemically Crosslinked with Glutaraldehyde. *Mater. Sci. Eng. C* **2008**, 28 (4), 539–548.
- (78) Kubo, S.; Kadla, J. F. The Formation of Strong Intermolecular Interactions in Immiscible Blends of Poly (Vinyl alcohol)(PVA) and Lignin. *Biomacromolecules* **2003**, 4 (3), 561–567.
- (79) Hendrick, E.; Frey, M. Increasing Surface Hydrophilicity in Poly (Lactic Acid) Electrospun Fibers by Addition of Pla-B-Peg Co-Polymers. *J. Eng. Fabr. Fibers* **2014**, 9 (2), 153–164.
- (80) Li, H. Z.; Chen, S. C.; Wang, Y. Z. Thermoplastic PVA/PLA Blends with Improved Processability and Hydrophobicity. *Ind. Eng. Chem. Res.* **2014**, 53 (44), 17355–17361.
- (81) Al-Itry, R.; Lamnawar, K.; Maazouz, A. Improvement of Thermal Stability, Rheological and Mechanical Properties of PLA, PBAT and Their Blends by Reactive Extrusion with Functionalized Epoxy. *Polym. Degrad. Stab.* **2012**, 97 (10), 1898–1914.
- (82) Fernandes, D. M.; Winkler Hechenleitner, A. A.; Job, A. E.; Radovanovic, E.; Pineda, E. A. G. Thermal and Photochemical Stability of Poly(vinyl Alcohol)/modified Lignin Blends. *Polym. Degrad. Stab.* **2006**, 91 (5), 1192–1201.
- (83) Rodriguez-Gonzalez, F. J.; Ramsay, B. A.; Favis, B. D. High Performance LDPE/thermoplastic Starch Blends: A Sustainable Alternative to Pure Polyethylene. *Polymer (Guildf)*. **2003**, 44 (5), 1517–1526.

- (84) Min, M.; Shen, L.; Hong, G.; Zhu, M.; Zhang, Y.; Wang, X.; Chen, Y.; Hsiao, B. S. Micro-Nano Structure Poly(ether Sulfones)/poly(ethyleneimine) Nanofibrous Affinity Membranes for Adsorption of Anionic Dyes and Heavy Metal Ions in Aqueous Solution. *Chem. Eng. J.* **2012**, *197*, 88–100.
- (85) Mazor L. *Analytical Chemistry of Organic Halogen Compounds.pdf*, First Edit.; Freiser, R. B. & H., Ed.; Elsevier: Budapest, 1975.
- (86) Anirudhan, T. S.; Jalajamony, S.; Sreekumari, S. S. Adsorption of Heavy Metal Ions from Aqueous Solutions by Amine and Carboxylate Functionalised Bentonites. *Appl. Clay Sci.* **2012**, *65–66*, 67–71.
- (87) Wang, X.; Min, M.; Liu, Z.; Yang, Y.; Zhou, Z.; Zhu, M.; Chen, Y.; Hsiao, B. S. Poly(ethyleneimine) Nanofibrous Affinity Membrane Fabricated via One Step Wet-Electrospinning from Poly(vinyl Alcohol)-Doped Poly(ethyleneimine) Solution System and Its Application. *J. Memb. Sci.* **2011**, *379* (1–2), 191–199.
- (88) Kenawy, E. R.; El-Newehy, M. H.; Abdel-Hay, F. I.; El-Shanshoury, A. E. R. R. Synthesis and Biocidal Activity of Modified Poly(vinyl Alcohol). *Arab. J. Chem.* **2014**, *7* (3), 355–361.
- (89) Reneker, D. H.; Chun, I. Nanometre Diameter Fibres of Polymer, Produced by Electrospinning. *Nanotechnology* **1999**, *7* (3), 216–223.
- (90) Leach, M. K.; Feng, Z.-Q.; Tuck, S. J.; Corey, J. M. Electrospinning Fundamentals: Optimizing Solution and Apparatus Parameters. *J. Vis. Exp.* **2011**, No. 47, 1–5.

- (91) Deitzel, J. .; Kleinmeyer, J.; Harris, D.; Beck Tan, N. . The Effect of Processing Variables on the Morphology of Electrospun Nanofibers and Textiles. *Polymer (Guildf)*. **2001**, *42* (1), 261–272.
- (92) Kim, Y.-J.; Ebara, M.; Aoyagi, T. Temperature-Responsive Electrospun Nanofibers for “on–off” Switchable Release of Dextran. *Sci. Technol. Adv. Mater.* **2012**, *13* (6), 64203.
- (93) Kalaoglu-Altan, O. I.; Sanyal, R.; Sanyal, A. “Clickable” polymeric Nanofibers through Hydrophilic-Hydrophobic Balance: Fabrication of Robust Biomolecular Immobilization Platforms. *Biomacromolecules* **2015**, *16* (5), 1590–1597.
- (94) Zhang, C.; Yuan, X.; Wu, L.; Han, Y.; Sheng, J. Study on Morphology of Electrospun Poly(vinyl Alcohol) Mats. *Eur. Polym. J.* **2005**, *41* (3), 423–432.
- (95) Pitt Supaphol, S. C. On the Electrospinning of Poly(vinyl alcohol)Nanofiber Mats: A Revisit. *J. Appl. Polym. Sci.* **2008**, *108* (7), 969–978.
- (96) Koski, A.; Yim, K.; Shivkumar, S. Effect of Molecular Weight on Fibrous PVA Produced by Electrospinning. *Mater. Lett.* **2004**, *58* (3–4), 493–497.
- (97) Son, W. K.; Youk, J. H.; Lee, T. S.; Park, W. H. The Effects of Solution Properties and Polyelectrolyte on Electrospinning of Ultrafine Poly(ethylene Oxide) Fibers. *Polymer (Guildf)*. **2004**, *45* (9), 2959–2966.
- (98) Park, J.-C.; Ito, T.; Kim, K.-O.; Kim, K.-W.; Kim, B.-S.; Khil, M.-S.; Kim, H.-Y.; Kim, I.-S. Electrospun Poly(vinyl Alcohol) Nanofibers: Effects of Degree of

- Hydrolysis and Enhanced Water Stability. *Polym. J.* **2010**, 42 (3), 273–276.
- (99) Son, W. K.; Ho Youk, J.; Seung Lee, T.; Park, W. H. Effect of pH on Electrospinning of Poly(vinyl Alcohol). *Mater. Lett.* **2005**, 59 (12), 1571–1575.
- (100) Davaran, S.; Entezami, a. Synthesis and Hydrolysis of Polyurethanes Containing Ibuprofen Pendant Groups. *J. Bioact. Compat. Polym.* **1997**, 12 (3), 47–58.
- (101) Arranz, F.; Bejarano, E. M.; Sanchez-Chaves, M. Poly(vinyl Alcohol) Functionalized by Chloroacetate Groups. Coupling of Bioactive Carboxylic Acids. *Macromol. Chem. Phys.* **1994**, 195 (12), 3789–3798.
- (102) Jin, B.; Shen, J.; Peng, R.; Shu, Y.; Tan, B.; Chu, S.; Dong, H. Synthesis, Characterization, Thermal Stability and Sensitivity Properties of the New Energetic Polymer through the Azidoacetylation of Poly(vinyl Alcohol). *Polym. Degrad. Stab.* **2012**, 97 (4), 473–480.
- (103) Iordanov, S. Use of Vinyl Alcohol Copolymers as Polymeric Carriers for Peptide Synthesis. II. Preproduction and Reactivity of Crosslinked Iodine -Containing Copolymers. *Godishnik na Visshiya Khimikotekhnologicheski Institut, Sofiya*. 1979, pp 168–170.
- (104) Jantas, R.; Draczyński, Z.; Herczyńska, L.; Stawski, D. Poly(vinyl Alcohol)-Salicylic Acid Conjugate: Synthesis and Characterization. *Am. J. Polym. Sci.* **2012**, 2 (5), 79–84.
- (105) Ping, Z. H.; Nguyen, Q. T.; Chen, S. M.; Zhou, J. Q.; Ding, Y. D. States of Water in

- Different Hydrophilic Polymers - DSC and FTIR Studies. *Polymer (Guildf)*. **2001**, 42 (20), 8461–8467.
- (106) Baschetti, M. G.; Piccinini, E.; Barbari, T. A.; Sarti, G. C. Quantitative Analysis of Polymer Dilation during Sorption Using FTIR-ATR Spectroscopy. *Macromolecules* **2003**, 36 (25), 9574–9584.
- (107) Ji, Y. L.; An, Q. F.; Zhao, Q.; Sun, W. D.; Lee, K. R.; Chen, H. L.; Gao, C. J. Novel Composite Nanofiltration Membranes Containing Zwitterions with High Permeate Flux and Improved Anti-Fouling Performance. *J. Memb. Sci.* **2012**, 390–391, 243–253.
- (108) Ramaseshan, R.; Sundarrajan, S.; Liu, Y.; Barhate, R. S.; Lala, N. L.; Ramakrishna, S. Functionalized Polymer Nanofibre Membranes for Protection from Chemical Warfare Stimulants. *Nanotechnology* **2006**, 17 (12), 2947–2953.
- (109) Gurgel, L. V. A.; Freitas, R. P. de; Gil, L. F. Adsorption of Cu(II), Cd(II), and Pb(II) from Aqueous Single Metal Solutions by Sugarcane Bagasse and Mercerized Sugarcane Bagasse Chemically Modified with Succinic Anhydride. *Carbohydr. Polym.* **2008**, 74 (4), 922–929.
- (110) Wang, X.; Min, M.; Liu, Z.; Yang, Y.; Zhou, Z.; Zhu, M.; Chen, Y.; Hsiao, B. S. Poly(ethyleneimine) Nanofibrous Affinity Membrane Fabricated via One Step Wet-Electrospinning from Poly(vinyl Alcohol)-Doped Poly(ethyleneimine) Solution System and Its Application. *J. Memb. Sci.* **2011**, 379 (1–2), 191–199.
- (111) Smythe, C. V. The Reaction of Iodoacetate and of Iodoacetamide with Various

- Sulphydeyl Groups, with Urease, and with Yeast Preparations. *J. Biol. Chem.* **1936**, *114*, 601–612.
- (112) Destaye, A. G.; Lin, C. K.; Lee, C. K. Glutaraldehyde Vapor Cross-Linked Nanofibrous PVA Mat with in Situ Formed Silver Nanoparticles. *ACS Appl. Mater. Interfaces* **2013**, *5* (11), 4745–4752.
- (113) Esterbauer, H.; Ertl, A.; Scholz, N. The Reaction of Cysteine with α,β -Unsaturated Aldehydes. *Tetrahedron* **1976**, *32* (2), 285–289.
- (114) Jencks, W. P.; Lienhard, G. E. Thiol Addition to the Carbonyl Group. Equilibria and Kinetics. *J. Am. Chem. Soc.* **1966**, *88* (17), 3982–3995.
- (115) Sprung, M. M. A Summary of the Reactions of Aldehydes with Amines. *Chem. Rev.* **1940**, *26* (3), 297–338.
- (116) Coates, J.; Ed, R. A. M.; Coates, J. Interpretation of Infrared Spectra , A Practical Approach. *Encyclopedia Anal. Chem.* **2000**, 10815–10837.
- (117) Ramanathan, T.; Fisher, F. T.; Ruoff, R. S.; Brinson, L. C. Amino-Functionalized Carbon Nanotubes for Binding to Polymers and Biological Systems. *Chem. Mater.* **2005**, *17* (6), 1290–1295.
- (118) Kirihaara, M.; Hatano, A. A Mild and Environmentally Benign Oxidation of Thiols to Disulfides SHORT PAPER A Mild and Environmentally Benign Oxidation of Thiols to Disulfides. *Synthesis (Stuttg.)*. **2007**, No. November 2007.
- (119) Fialaire, A.; Postaire, E.; Prognon, P.; Pradier, F.; Pradeau, D. Thermal Decomposition

of Reduced Glutathione in Solution for Organ Preservation. *J. Pharm. Biomed. Anal.* **1992**, *10* (6), 457–460.

- (120) Coates, J.; Ed, R. A. M.; Coates, J. Interpretation of Infrared Spectra , A Practical Approach Interpretation of Infrared Spectra , A Practical Approach. *Encyclopedia Anal. Chem.* **2000**, 10815–10837.
- (121) Barnett, R. E.; Jencks, W. P. Diffusion-Controlled and Concerted Base Catalysis in the Decomposition of Hemithioacetals. *J. Am. Chem. Soc.* **1969**, *91* (24), 6758–6765.
- (122) Brena, B.; González-Pombo, P.; Batista-Viera, F. Immobilization of Enzymes: A Literature Survey. *Methods Mol. Biol.* **2013**, *1051*, 15–31.
- (123) Wang, Z.; Liu, S.; Wu, P.; Cai, C. Detection of Glucose Based on Direct Electron Transfer Reaction of Glucose Oxidase Immobilized on Highly Ordered Polyaniline Nanotubes Detection of Glucose Based on Direct Electron Transfer Reaction of Glucose Oxidase Immobilized on Highly Ordered Polyani. *Anal. Chem.* **2009**, *81* (4), 16385–16392.
- (124) Wang, H.; Wang, X.; Zhang, X.; Qin, X.; Zhao, Z.; Miao, Z.; Huang, N.; Chen, Q. A Novel Glucose Biosensor Based on the Immobilization of Glucose Oxidase onto Gold Nanoparticles-Modified Pb Nanowires. *Biosens. Bioelectron.* **2009**, *25* (1), 142–146.
- (125) Iyer, P. V.; Ananthanarayan, L. Enzyme Stability and Stabilization-Aqueous and Non-Aqueous Environment. *Process Biochem.* **2008**, *43* (10), 1019–1032.
- (126) Mateo, C.; Palomo, J. M.; Fernandez-Lorente, G.; Guisan, J. M.; Fernandez-Lafuente,

- R. Improvement of Enzyme Activity, Stability and Selectivity via Immobilization Techniques. *Enzyme Microb. Technol.* **2007**, 40 (6), 1451–1463.
- (127) Zhao, M.; Wu, X.; Cai, C. Polyaniline Nanofibers : Synthesis , Characterization , and Application to Direct Electron Transfer of Glucose Oxidase. **2009**, 4987–4996.
- (128) Ge, L.; Zhao, Y. S.; Mo, T.; Li, J. R.; Li, P. Immobilization of Glucose Oxidase in Electrospun Nanofibrous Membranes for Food Preservation. *Food Control* **2012**, 26 (1), 188–193.
- (129) Ren, G.; Xu, X.; Liu, Q.; Cheng, J.; Yuan, X.; Wu, L.; Wan, Y. Electrospun Poly(vinyl Alcohol)/glucose Oxidase Biocomposite Membranes for Biosensor Applications. *React. Funct. Polym.* **2006**, 66 (12), 1559–1564.
- (130) Bankar, S. B.; Bule, M. V; Singhal, R. S.; Ananthanarayan, L. Glucose Oxidase — An Overview. *Biotechnol. Adv.* **2009**, 27 (4), 489–501.
- (131) Raba, J.; Mottola, H. A. Glucose Oxidase as an Analytical Reagent. *Crit. Rev. Anal. Chem.* **1995**, 25 (1), 1–42.
- (132) Vamvakaki, V.; Tsagaraki, K.; Chaniotakis, N. Carbon Nanofiber-Based Glucose Biosensor. *Anal. Chem.* **2006**, 78 (15), 5538–5542.
- (133) Kim, H.; Lee, I.; Kwon, Y.; Kim, B. C.; Ha, S.; Lee, J. heon; Kim, J. Immobilization of Glucose Oxidase into Polyaniline Nanofiber Matrix for Biofuel Cell Applications. *Biosensors and Bioelectronics*. 2011, pp 3908–3913.
- (134) Michaelis, L.; Schubert, M. P. Reaction of Iodoacetic Acid on Mercaptans and

Amines. *J. Biol. Chem.* **1934**, *106*, 331–341.

- (135) Wei, X.; Wang, S.; Zheng, W.; Wang, X.; Liu, X.; Jiang, S.; Pi, J.; Zheng, Y.; He, G.; Qu, W. Drinking Water Disinfection Byproduct Iodoacetic Acid Induces Tumorigenic Transformation of NIH3T3 Cells. *Environ. Sci. Technol.* **2013**, *47* (11), 5913–5920.
- (136) Escandar, G. M.; Peregrin, J. M. S.; Sierra, M. G.; Santoro, M.; Frutos, A. A.; Garci, S. I.; Labadie, G.; Sala, L. F. Interaction of Divalent Metal Ions Withd-Gluconic Acid in the Solid Phase and Aqueous Solution. *Polyhedron* **1996**, *15* (13), 2251–2261.